DETERMINATION OF PASSIVE VIBRATION ISOLATION CHARACTERISTICS OF JET AIRCRAFT AVIONICS

A THESIS SUBMITTED TO
THE GRADUATE SCHOOL OF NATURAL AND APPLIED SCIENCES
OF
MIDDLE EAST TECHNICAL UNIVERSITY

BY

ZAFER EKER

IN PARTIAL FULFILLMENT OF THE REQUIREMENTS
FOR
THE DEGREE OF MASTER OF SCIENCE
IN
AEROSPACE ENGINEERING

AUGUST 2019

Approval of the thesis:

DETERMINATION OF PASSIVE VIBRATION ISOLATION CHARACTERISTICS OF JET AIRCRAFT AVIONICS

submitted by **ZAFER EKER** in partial fulfillment of the requirements for the degree of **Master of Science in Aerospace Engineering Department, Middle East Technical University** by,

Prof. Dr. Halil Kalıpçılar
Dean, Graduate School of **Natural and Applied Sciences** _____

Prof. Dr. İsmail Hakkı Tuncer
Head of Department, **Aerospace Engineering** _____

Prof. Dr. Yavuz Yaman
Supervisor, **Aerospace Engineering, METU** _____

Examining Committee Members:

Assoc. Prof. Dr. Ercan Gürses
Aerospace Engineering Dept., METU _____

Prof. Dr. Yavuz Yaman
Aerospace Engineering, METU _____

Assist. Prof. Dr. Gökhan Özgen
Mechanical Engineering Dept., METU _____

Dr. Mustafa Kaya
Aerospace Engineering Dept., Ankara Yıldırım Beyazıt Uni. _____

Dr. Munir Elfarra
Aerospace Engineering Dept., Ankara Yıldırım Beyazıt Uni. _____

Date: 29.08.2019

I hereby declare that all information in this document has been obtained and presented in accordance with academic rules and ethical conduct. I also declare that, as required by these rules and conduct, I have fully cited and referenced all material and results that are not original to this work.

Name, Surname: Zafer Eker

Signature:

ABSTRACT

DETERMINATION OF PASSIVE VIBRATION ISOLATION CHARACTERISTICS OF JET AIRCRAFT AVIONICS

Eker, Zafer
Master of Science, Aerospace Engineering
Supervisor: Prof. Dr. Yavuz Yaman

August 2019, 123 pages

Airborne electronics are subjected to adverse effects of vibration exposure that is defined by military standards to be used in the design stage. It is important to ensure the sustainability of such equipment through vibration isolation. Passive isolation mechanism distinguishes as the simplest practice for this purpose, which is applied in this study.

In this thesis, a complete design of the isolation system is achieved by creating the representative mathematical model, implementing the vibration analysis followed by the optimization analysis and simulating the possible deviations of system properties. Rigid body connected to the rigid base through resilient elements is modeled with six degrees-of-freedom. Viscous damper is considered in the formulation as the damping mechanism to represent realistic conditions. It is allowed for describing the system by resilient element stiffness, damping, position and orientation of installation beside the body mass. Following the definition of spatial properties in the theoretical model, normal modes and response analysis based on random excitation are carried out. Thereafter, system of optimum stiffness and damping is searched by aiming the minimum acceleration response under pre-determined constraints in the optimization problem. Eventually, Monte Carlo simulation is performed to consider possible deviations of the system spatial properties from their nominal values during the actual

application. Though the employed techniques herein are general, they are demonstrated through the application on jet aircraft avionics.

Entire analysis process is applied by the developed computer code in the open software Python environment. It is also brought into use via a GUI.

Keywords: Passive Vibration Isolation, MDOF Isolation System, Modal Property Optimization, Monte Carlo Simulation, Python.

ÖZ

JET UÇAK AVİYONİKLERİNİN PASİF TİTREŞİM YALITIM ÖZELLİKLERİNİN BELİRLENMESİ

Eker, Zafer
Yüksek Lisans, Havacılık ve Uzay Mühendisliği
Tez Danışmanı: Prof. Dr. Yavuz Yaman

Ağustos 2019, 123 sayfa

Havacılık elektronik ekipmanları maruz kaldığı titreşimden dolayı olumsuz etkilere konu olmaktadır. Operasyonel titreşim karakteristiği askeri standartlar tarafından belirlenmektedir. Bu ekipmanların titreşim yalıtımıyla sürekliliğini sağlamak gerekmektedir. Bu çalışmada başvurulan pasif yalıtım mekanizması bu amaca yönelik olarak kullanılabilecek en basit yöntemdir.

Bu bitirme tezinde, bütün yönleriyle düşünülmüş bir yalıtım sistemi tasarımı ele alınmaktadır. Temsili matematiksel modelin kurulması, titreşim analizinin ifası, ardı sıra en-iyileme analizi ve sistem değişkenlerindeki olası sapmaların benzetim analizinin gerçekleştirilmesi bahsedilen tasarımın aşamalarını ifade eder. Temel elemana esnek elemanlarla bağlı elektronik ekipman altı serbestlik derecesiyle modellenir. Hem temel eleman hem de ekipman rijit farz edilirken ara bağlantı elemanları esnek olarak ele alınır. Formulasyonda, gerçeğe uygun olması adına sönümleme mekanizması olarak viskoz sönümleyici kullanılır. Sistemin tanımlanması boyunca, ekipmanın kütle ve atalet değerlerinin yanı sıra esnek elemanların katılık ve sönüm ile bağlantı konum ve yönelim değişkenlerine yer verilmesi mümkündür. Kuramsal modelin uzamsal özelliklerinin belirlenmesini takiben serbest titreşim analizi ve rastgele uyarıma bağlı olarak zorlamalı titreşim analizi yerine getirilir.

Sonrasında, en-iyileme probleminin hâlihazırda belirlenmiş olan tasarım kısıtları gözetilerek katılık ve sönüm değişkenleri üzerinden sistemin ivmelenme tepkisi asgariye indirilir. Nihai olarak, uzamsal değişkenlerin fiili uygulama boyunca teoride tanımlanmış değerlerinden sapmasını hesaba katmak adına Monte Carlo benzetimi gerçekleştirilir. Çalışmada başvurulan teknikler her ne kadar genel geçer olsa da jet uçakların elektronik ekipmanlarına uygulanarak gösterilir.

Bütün analiz süreci, açık-kaynak yazılım olan Python ortamında geliştirilen bilgisayar kodu ile yürütülür. Geliştirilen bilgisayar kodu grafik kullanıcı ara yüzü maharetiyle kullanıma sunulur.

Anahtar Kelimeler: Pasif Titreşim Yalıtımı, Çok Serbestlik Dereceli Yalıtım Sistemi, Modal Özellik En-İyilemesi, Monte Carlo Benzetimi, Python.

This study is wholeheartedly dedicated to my grandmother and my older brother; true owners of freedom.

ACKNOWLEDGEMENTS

I would first like to thank my supervisor, Prof. Dr. Yavuz Yaman, for guiding me in the direction of clear, concise, complete and correct study with his invaluable expertise.

I would like to acknowledge my family for their immense support for love.

TABLE OF CONTENTS

LIST OF TABLES

TABLES

LIST OF FIGURES

FIGURES

LIST OF ABBREVIATIONS

ABBREVIATIONS

ANSYS	Analysis System
CI	Confidence Interval
DCC	Developed Computer Code
DOE	Design of Experiment
DOF	Degree-of-Freedom
FBFE	Flexible Base Flexible Equipment
FE	Finite Element
FEMAP	Finite Element Modeling and Post-processing
FRF	Frequency Response Function
GRG	Generalized Reduced Gradient
GRMS	Root Mean Square Value of Gravitational Acceleration
GUI	Graphical User Interface
LB	Lower Bound
LQG	Linear-Quadratic-Gaussian
LRU	Line-Replaceable Unit
MCMC	Markov Chain Monte Carlo
MDOF	Multiple-Degree-of-Freedom
MFD	Method of Feasible Directions
MR	Magneto-Rheological
NASA	National Aeronautics and Space Administration
NASTRAN	NASA Structural Analysis
OFRF	Output Frequency Response Function
PDF	Probability Density Function
PSD	Power Spectral Density
RBM	Rigid Body Motion
RMS	Root-Mean-Square
SD	Standard Deviation
SE	Standard Error
SESAM	Software Engineering Simulation by Animated Models
SI	Statistical Interval
SLP	Sequential Linear Programming
SQP	Sequential Quadratic Programming
PZT	Piezoelectric
SDOF	Single-Degree-of-Freedom
TFS	Transfer Function Synthesis
UB	Upper Bound

LIST OF SYMBOLS

SYMBOLS

A	Mass-Proportional Damping Coefficient
B	Stiffness-Proportional Damping Coefficient
G	Equivalent Viscous Damping Value
H	Frequency Response Function
Q	Amplification Factor
S	Spectral Response
T	Transmissibility
a	Distance of Elastic Center of Resilient Element to Mass Center
c	Viscous Damping Matrix of Resilient Element
f	Frequency in Hz
f(x)	Design Objective
g_j	Design Inequality Constraint
h_i	Design Equality Constraint
I	Rigid Body Mass Moment of Inertia
k	Stiffness Matrix of Resilient Element
m	Rigid Body Mass
n	Number of Resilient Elements in a System
p	Limit Value of Uncertainty Simulation Input Parameter
x	Design Variable
[C]	Global Damping Matrix
[M]	Global Mass Matrix
[K]	Global Stiffness Matrix
{L}	Load Vector
{X}	Displacement Vector
Φ	Mass-Normalized Eigenvector
δ	Static Deflection
ζ	Viscous Damping Ratio
λ	Eigenvalue
σ	Mean-Square of Spectral Response
φ	Eigenvector
ω	Frequency in rad/s

CHAPTER 1

INTRODUCTION

1.1. Airborne Electronics

Avionics are defined as the electronic systems used in the air and space vehicles. In the modern aerospace industry, it is inevitable to utilize electronic systems that ensure the control of the air vehicles.

Avionics are referred during the entire flight mission of the aircraft from power-on to power-off. They serve a wide variety of tasks such as flight control, instrumentation to communication and surveillance in military operation etc. Military avionics can be basically classified into navigation, communications, sensors, mission systems, displays and controls.

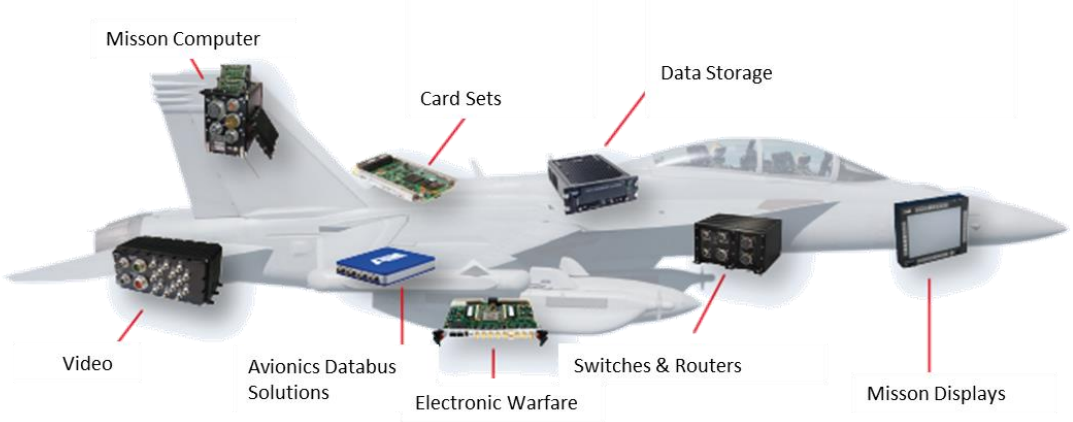

Figure 1.1. Example of Avionics across Aircraft [54]

The protection of electronic systems to maintain their structural integrity and functional capacity is important. Otherwise, it might result in a disaster in the vehicle.

According to the failure history of electronic equipment hardware, which is observed and investigated by United States Air Force for about two decades, failures due to the operating environments are graded by percentage weight. Thus, high temperature and cycling through extreme temperatures get a percentage of 55, humidity get a percentage of 20, and vibration and shock get a percentage of 20 [46].

1.2. Vibration Isolation

Vibration isolation in order to reduce vibratory loads transmitted from the base structure, which acts as the vibration source, to the equipment through resilient mountings has been a much-discussed issue over years because of the fact that vibratory loads may eventually lead to fatigue failure on relevant parts of aircraft.

Avionics equipment are subjected to a wide variety of vibration. A broad frequency spectrum is swept in aircraft applications. As an unwanted condition, it must be handled by a proper treatment. This brings about the necessity of protection of the equipment from the damaging vibration sources.

Vibration control of the equipment includes the force reduction, mass addition, tuning, isolation and damping. Isolation is applicable to prevent the airborne electronic boxes from malfunction due to the vibration sources.

Isolation relies on the separation of the equipment and excitation forces in phase by decoupling them through resilient supports. In this way, transmitted forces are reduced by resisting the motion or opposing the input excitation by inertia.

Vibration isolation may be provided by either passive or active systems. Active systems require external input unlike the passive systems. Passive systems are appealing through being simpler. The complexity of active isolation systems enables high performance in the expense of cost and impracticability. Semi-active isolation systems are also considered as an intermediate form between the active and passive systems. System properties can be changed in response to the input forces in semi-

active systems. In general, passive isolation systems are mostly preferred unless severe limitations arise [1].

1.3. Thesis Objective

In this thesis study, it is aimed to achieve a complete theoretical design of passive vibration isolation system for jet aircraft avionics to isolate them from harsh vibration environment. For this purpose, vibration analysis on the representative mathematical model concerning the search for optimum and risks of uncertainties is conducted. The issue which appears as implementing the whole process in a sophisticated manner is accomplished by developing a computer code in an open software environment Python, which is promoted by a GUI for the ease of use.

1.4. Thesis Organization

This thesis study basically comprises of eight main topics. The present chapter is the introductory chapter that imparts the thesis subject, thesis objective and organizational layout.

In the second chapter, literature survey is included. Different types of isolation practices such as the passive isolation, semi-active isolation and active isolation are reviewed. Superiority and inferiority over others are also touched on. Beside the classification of the isolation mechanisms, general considerations such as the nonlinearity effect are also mentioned briefly. Subsequently, review of the isolation system design is inclusively given place.

In the third chapter, build-up of the theoretical model is included. Coordinate frames used in the model are elucidated at the very beginning. Representation of the resilient element is referred by touching on the fundamental representative elastic element models e.g. Maxwell model. 6-DOF system equations of motion are given explicitly. Immediately after, matrix form is presented for simultaneous solution of these equations. In addition, commonly applied mounting configurations and vibrational symmetry that reduces the coupling in degrees-of-freedom are mentioned briefly.

In the fourth chapter, vibration analysis is included in two basic stages, namely the normal modes analysis and frequency response analysis. The orthogonality property of the multiple-degree-of-freedom system is utilized to obtain the modal model. Frequency response analysis is implemented based on the modal model. Random excitation is generated referring to the military standards. Equations of vibration analysis regarding the random vibration phenomenon are fully presented.

In the fifth chapter, theoretical model subjected to the vibration analysis is verified. Literature is reviewed to find an isolation system model with shared natural frequency results. This model is generated in the FE environment. Once the natural frequencies of the FE model and referred model are shown to agree, then the FE model is available to be employed in the verification of the theoretical model. Thereby, modal properties e.g. natural frequencies, mode shapes and response values e.g. acceleration root mean square value (rms), velocity rms and displacement rms obtained from the mathematical model and FE model are compared.

In the sixth chapter, optimization analysis and uncertainty simulation details are included. At the first stage of this chapter, the definition of the optimization problem being specific to this study is explained after mentioning the optimization approach in general. Design variables considered in the optimization process concerning the capability of the developed computer code are imparted. Design constraints to be considered in the design of an isolation system are illustrated. Design objective to increase the system performance is determined. At the second stage of this chapter, probabilistic base of the simulation to take uncertainties into account is mentioned. The procedure of the used approach Markov Chain Monte Carlo simulation is presented. Input parameters selected among the spatial properties and output parameters selected among the system response parameters for simulation are pointed out.

In the seventh chapter, a case study is included. In this case study, a mathematical model is created with given spatial properties. All the previously mentioned analyses

are performed to achieve a complete isolation system design. Hereby, optimum system parameters are obtained, and violated limits of the response parameters according to the uncertainty analysis are revealed.

In the eight chapter, the summary and conclusions of the thesis study are included. Besides, possible improvements are imparted as future studies.

CHAPTER 2

LITERATURE SURVEY

A literature review for vibration isolation is carried out. There exist good many matters in the vibration isolation problem of aircraft equipment through mountings. The problem is inherently of interest in many other industries as well as in aerospace e.g. automotive, marine, etc. Basic solutions for vibration isolation are commonly seen to be used in different fields of application. With this fact in mind, a wide range of studies that address the problem of vibration isolation are investigated.

This study is concerned with the isolation system design that implies a whole of isolated device, vibration source and isolators. The focus will be on the varied approaches to the isolation system design following the touch on the different types of isolation practices.

2.1. Passive Isolation

[17] realizes a study on circular steel ring to measure the effectiveness of passive isolator to protect avionics equipment from base excitation. The system is modeled with SDOF. At first, an experiment is executed to obtain natural frequencies and modal damping of the ring and to demonstrate the agreement with analytical results. Afterwards, a concentrated mass attached to circular rings is evaluated in terms of acceleration response spectra. Finally, it is said that a properly designed circular ring comes with an effective protection of avionics equipment from possible damages of base excitation.

[40] considered the system flexibility in his work for vibration isolation without any approximations to avoid truncation errors. The Yang's transfer function synthesis (TFS) method is applied, which analytically models any flexible system of one-dimension. It is also touched on the importance of designation of mount frequency

and its placement in the flexible base, flexible equipment (FBFE) system. These two must be evaluated simultaneously because first several modes of the system shift to some extent depending on the isolator placement, which may lead to coupling of isolator modes with equipment and/or base modes. A unique technique is deliberated to observe a 2-DOF isolation system's transmissibility. In this unique method, transmissibility plot is obtained by freeing four non-dimensional parameters among five so that number of plots are reduced significantly to clarify the understanding of the isolation system's performance quality.

[50] studied on the determination of rubber isolator properties based on some major factors e.g. frequency, amplitude, temperature, and preload (finite deformation). The nonlinear behavior of rubber is investigated by considering its dependency to dynamic amplitude. The change of dynamic amplitude dependence based on excitation type e.g. random and sine is also brought forward. Describing the dependence of isolator to the temperature and frequency by an equation gives the possibility of determining the frequency dependent characteristic properties of rubber at very high frequencies at which it is very challenging to obtain the knowledge of those properties experimentally. This is called the method of reduced variables. Descriptive models are created by including some of those mentioned factors simultaneously. Fractional derivatives are addressed to decrease the number of model parameters to be used in the representation of frequency dependence. Because, the number of model parameters increases as the representative model gets more complex e.g. Wiechert model.

[33] discussed nonlinearity effects of passive engine isolator on the frequency response. A novel approach of "Output Frequency Response Function" (OFRF) is proposed to represent the output frequency response of systems with nonlinearity. An algorithm is developed to find out parameters included in this representation. The new approach put forward is based on Volterra series that is claimed to unambiguously explain a wide range of nonlinear effects.

2.2. Semi-Active Isolation

[25] discussed the vibration isolation employing soft mountings. However, soft mountings lead to large static and dynamic deflections during the start and stop in taxi. A control device, an elastomer with viscous fluid content, to limit these large dynamic motions without changing the damping characteristic properties of isolation during cruise is employed.

[53] studied on the designation of characteristics, and design of magnetorheological engine mounts. After designing three different MR mount models and implementing magnetostatic analysis of electromagnet to control the flow of the MR fluid in the mount, those models are manufactured. Those MR mounts manufactured are with slot, 8 holes, and 16 holes, separately. Tests are conducted with conventional hydraulic mounts and elastomeric mounts besides for those MR mounts, for the purpose of characterization of MR fluid-elastic mounts and comparing them with other mentioned types of mounts. Another comparison is performed between different models of MR mounts used in this study in the sense of characterization.

[2] discussed how parameters related to magneto-rheological (MR) mount affect the performance of vibration isolation. Fluid mounts and tuned vibration absorbers are said to have a drawback of that a peak in transmissibility existed in frequencies higher than notch frequency because of resonance frequency due to the reciprocating motion of the fluid in the mount. MR fluid is employed in the MR mount to open and close the inertia track to prevent the existence of transmissibility peak in those frequencies. Parameters considered during this study are stiffness of rubber, area of piston, volumetric stiffness, inertia track and resistance of fluid. After evaluation, it is claimed that first three exhibit the most remarkable effect on transmissibility.

[16] ascertained the significance of including internal resonances which came of the inertia of vibration isolator itself. Besides involving the mass of the isolator, he also uses a 3-DOF model in keeping with his focus on improving the representation of practical systems. In this study both vibration and noise radiation are considered to

analyze the problem of internal resonances. Both passive and hybrid dynamic vibration absorbers are studied to absorb the internal resonances of the vibration isolator itself.

[44] studied on determination of characteristic properties of tunable magnetorheological hydraulic mounts and their design. Increasing the efficiency of magnetic circuitry is the paramount goal of this study. Characterization of magnetorheological fluid-elastic mount for varying current amplitude is implemented through several tests. In this way, stiffness and damping properties are presented for different values of current amplitude considering the frequency dependence of mount. Furthermore, dynamics of force transmitted from vibration source is represented by using a transfer function model dependent on the current on the mount.

2.3. Active Isolation

[48] discussed the effect of active engine mounts of vehicles on vibration and noise reduction. Their superiority, in the sense of reducing vibration and noise transmitted from engine to the structure, over passive engine mounts is demonstrated. Both active hydraulic and active elastomeric mount models are investigated. The superior property of active mounts is that they become stiff at low frequencies while they are soft at high frequencies. This prevents engine from going under large deflections at low frequencies. In brief, this study includes comparison of passive and active engine mounts and explains how passive and active isolation models are constructed.

[28] modeled an experimental adaptive vibration isolator and observed its performance. An electromagnetic actuator is used to reduce the dynamic stiffness of fluid mount at the disturbance frequencies of engine vibration. A bond graph to increase the insight into the system behavior is employed to obtain translation functions to be used in the active control. A simple controller is used for only a certain frequency range in which there exist significant vibration disturbances. In the control range of frequency, many times smaller dynamic stiffness than the dynamic stiffness of passive isolator is accomplished. The force and displacement capacity of active

isolator are degraded at high frequencies; therefore, mount design parameters must be conformed to the operation requirements accordingly. It is worth mentioning that power requirement of an actuator, which is a problem in active vibration control for it needs an amplifier system to reach the desired power, can be decreased if the notch frequency is set to be near the vibration disturbance frequency; that is, facilitating actuator's work.

[57] studied on active vibration control of a transport aircraft engine by employing an engine mount system enhanced by pre-stressed piezoelectric (PZT) stack actuators. PZT stack actuators are placed on strut members attached to the Yoke ring on which the engine is mounted. Thus, vibration can be controlled when being transferred from engine to the aircraft structure through struts. Controller is generated based on the model design. Subsequently, required system matrices of the engine mount system that consists of active strut members are obtained. To find out the optimum value of gain parameter to be used in the designed controller, Linear-quadratic-Gaussian (LQG) control technique of MATLAB® is employed in accordance with the problem. The numerical model created in ANSYS® is used to simulate the active control mechanism in MATLAB®. After validating the controller based on the model design, a test can be conducted.

[11] discussed a repetitive control approach for active vibration suppression via a smart spring. There is no need for a feedforward concept when using this approach that can be applied in systems with periodic behavior. Because a learning transaction is performed during operation by means of that the information from previous periods is utilized to enhance the current isolation capacity of the system.

Mount to which body is attached may be designed as passive, semi-active, or active (adaptive). Passive engine mounts provide vibration reduction for only one specific notch frequency. On the other hand, semi-active and active isolation systems enable to reduce vibration for a wide range of frequency. Semi-active systems find favor

through considerable performance improvement compared to passive engine mounts and being more affordable and having simpler design than active systems.

Besides the general classification of isolation systems, each one can be differentiated such that the nonlinearity effects may be considered to represent the engine mount system more closely. Moreover, the involvement of the flexibility of the supporting structure that engages to engine via mountings may be provided to enable the representative model to resemble the actual system much better. While engine is modeled as a rigid body, mountings may be represented with many existing mathematical models such as a simple Linear Kelvin-Voigt model or a complicated Bouc-Wen model. Another issue that must be considered to represent a model more closely is that material parameters required for designing a model may need to be decided specifically for that material of interest. In addition, those parameters may vary depending on other parameters, and including this fact may be essential for representation e.g. elastomeric mounts' material parameters depend on frequency, temperature, etc.

2.4. Isolation System Design

[55] discussed the application of resilient mountings installed on shipboard equipment. Different mounting arrangements are worked through. Numerical calculations are included beside the methods of natural frequency calculation.

[24] touched upon the issue of theoretical model of resilient support itself. In conventional approach, linear isolators are employed in the isolator system design. Instead, a bilinear isolator is integrated to the system. Therefore, isolator with nonlinear softening and hardening property can cater for the high static loads or shock exposures.

[4] discussed design optimization of aircraft engine mount vibration isolator. He uses a rigid body and flexible base to represent the engine and the nacelle, respectively. Mounts are formed of spring in three dimensions and damping with hysteresis. In this study, orientation angles of each single mount are considered as optimization variables

as well as stiffness coefficients of isolators. A constraint is established to limit the static deflections of engine. This optimization problem is set for several engine speeds and solved employing recursive quadratic programming technique based on variable metric methods for constrained nonlinear optimization.

[19] addresses the design and analysis of both shock and vibration isolation of hard disk drives. Several tests are conducted to determine the acceptable response limits that the device can withstand. Thus, isolation system can be designed with known requirements and given harsh environment profiles that are described in MIL-STD-810E.

[56] studied on the design of vibration isolation of electronic equipment. During the adjustment of the isolator properties, internal components of the electronic equipment are considered in the system model beside its enclosure. It is claimed that the effectiveness of the isolation system increases according to the analytical and experimental results with the proposed novel design approach.

[43] proposed a vibration analysis and design optimization program for vibration isolation system. 6-DOF and 16-DOF engine mount systems can be analyzed through vibration analysis program that is based on MSC.ADAMS®. Design optimization is applied through design of experiment (DOE). Mount stiffness and location are considered as the design variables in the optimization problem.

[47] developed an interactive program for the design of isolation system which mounts aircraft engine to the nacelle. Aircraft engine is modeled as rigid as well as the nacelle that represents the base in the system. Optimization problem is solved to minimize the transmitted forces. Design variables are considered as the stiffness and installation orientation for each single isolator.

[3] studied on the vibration isolation of a motorcycle by mounting the powertrain on the frame by resilient supports. Mathematical modeling of mounts involves a variety of complexity levels. Simple Voigt model is employed beside the complex Voigt model that comprises the nonlinearity in stiffness, snubbing and hysteresis effect. Both

6-DOF and 12-DOF models are investigated through the mathematical representation of the system. Optimization problem is solved by adjusting the mount stiffness, orientation and location as the design variables. Method of Sequential Quadratic Programming (SQP) is applied to calculate the optimum design parameters. An attention is also given to modes decoupling. Off-diagonal elements of the overall stiffness matrix are manipulated through the optimization study to minimize their Frobenius norm.

[8] worked on the formulation of an optimization problem of the powertrain mounting system design. Modal properties are obtained by providing the modeled system to the finite element solver of MSC/NASTRAN®. Installation coordinates and stiffness properties of the mounts are considered as design variables. Natural frequencies are used as design constraints. Method of feasible directions (MFD) is the basis of the optimization program. MFD relies on gradient-based optimization method and requires gradient information. It is attained by employing the central difference method.

[49] worked on the minimization of transmitted forces to a cylinder engine. Following the construction of the mathematical model of the system to identify the engine motion, an optimization algorithm developed by Snyman is used. It relies on the gradient information of the objective function. It can handle inexact gradients due to the noise in the function.

[51] studied on the control of vibration from marine engine to the base floor. Both engine and floor are considered as rigid, and engine is placed to the floor by elastomeric mounts. Mounts are modeled as three mutually orthogonal spring and hysteresis damping elements. Transmitted forces from engine to the floor are aimed to be minimized by satisfying pre-defined constraints. Maximum static and dynamic deflection beside the minimum difference between the natural frequency and the engine excitation frequency are defined as the constraints in the optimization problem.

Design variables are selected as mount stiffness and orientations. Optimization algorithm used in the problem is the Sequential Quadratic Programming.

[39] studied on the optimization of mounting systems with nonlinearity unlike the typical approach of linear systems. He claimed that nonlinear modeling brings about improved performance on the isolation of vibratory forces. Both passive and active isolation are considered in the system design. The Galerkin method is used to solve nonlinear algebraic equations.

[7] mentioned the necessity of vibration isolator between the spacecraft and the launch vehicle. During the vibration control, the probabilistic reliability analysis is also considered by implying the uncertainties in isolator parameters. Reliability is calculated by perturbation method. The effect of natural frequency control on the system is identified by taking the uncertain parameters into account. Reliability sensitivity analysis is also implemented to investigate the extent of the effect of the parameters on the system.

[60] studied on the vibration isolation of whole spacecraft. The whole spacecraft platform is investigated by deriving the system equations of motion. Uncertain parameters are also investigated to identify the dynamic characteristics of the platform by utilizing non-probabilistic reliability theory. Zhang claimed that there is no need to a specific sample distribution from in the non-probabilistic reliability approach.

[5] developed a computer program to design and analyze mounting system for passive vibration isolation. A six degrees-of-freedom system is constructed mathematically with spring and structural damping elements on three mutually orthogonal axes. Base and the isolated structure are assumed rigid body and connected with resilient mounts. In the optimization problem, design variables are determined as stiffness, location and orientation of each single mount. Monte Carlo simulation is also implemented for reliability analysis. The different types of analyses are integrated in the MATLAB based computer program.

[10] studied on the vibration isolation of inertial measurement unit in the aircraft. Passive vibration isolation is applied on the elastically attached rigid base and mass. Optimization problem includes many constraints such as sway, angular dynamic displacement, maximum acceleration, static displacement, maximum isolation frequency, constraints of isolator stiffness ratio etc. Only the stiffness parameter is varied during the optimization analysis. Applied optimization techniques are based on MATLAB, which are Fmincon, Patternsearch and Genetic Algorithm. To account for the uncertainties in isolator parameters, a reliability analysis is implemented by applying Monte Carlo simulation.

In this thesis study, a six degrees-of-freedom rigid body is considered to be isolated from base excitation by means of resilient elements. It is easy to derive the equations of motion for six degrees-of-freedom system; besides, they can be easily found in literature. Resilient elements are represented by three mutually orthogonal spring and damper pairs as in Voigt model. More complex models are not attempted because of the difficulty to determine the required model parameters. The dependence of the stiffness on frequency, temperature and pre-load is not accounted for, and linear stiffness properties are used. Viscous damping is applied in order to represent the realistic conditions more closely instead of structural damping that is frequently employed in literature but only valid for harmonic motions whereas the current study actually attempts to bring solutions to random vibrations. Modal coordinate transformation method is used leading the equations of motion to be solved by the approach as in the single degree-of-freedom. On that account, a common viscous damping ratio is defined to the system instead of each single isolator and each single mode. In the optimization problem, the axial stiffness, radial stiffness and damping ratio are defined as the design variables, and mount installation position and orientation are not varied during the optimization process. Monte Carlo simulation is implemented by including all the system input parameters with normal distribution of 1000 samples for each. Python environment is used to perform the entire analysis

process. It is convenient as an open software. A friendly graphical-user-interface is also developed for the ease of use.

CHAPTER 3

MATHEMATICAL MODEL

3.1. Coordinate Frames

Three axis systems are primarily defined to construct the mathematical model with reference to them. The first system is the global axis system with the set of axes x, y, z. It is the basic frame in the space and fixed arbitrarily. The second coordinate system is the inertial axis system with the set of axes $\overline{X}$, $\overline{Y}$, $\overline{Z}$. Its origin is placed at the mass center of the isolated rigid boy at rest, and it is aligned with the basic frame. The last axis system with the set of axes X, Y, Z is fixed at the mass center of the isolated rigid body and it is coincident with the inertial frame when there is no motion. Primary coordinate frames are shown in *Figure 3.1*.

Each resilient element in the isolation system has its own coordinate frame. An isolator coordinate frame is defined such that its x-axis is coincident with the axial direction of the isolator. Therefore, the axes y and z refer to the transverse directions of the isolator. Attachment point matches with the elastic center of the isolator, which also corresponds to the origin of the related set of axes. These coordinate systems will be called the secondary frames. Each set of axes is named according to the corresponding resilient element e.g. First resilient element will have the set of axes X1, Y1, Z1, second resilient element will have the set of axes X2, Y2, Z2 and so on. Secondary coordinate frames are exemplified in *Figure 3.2*.

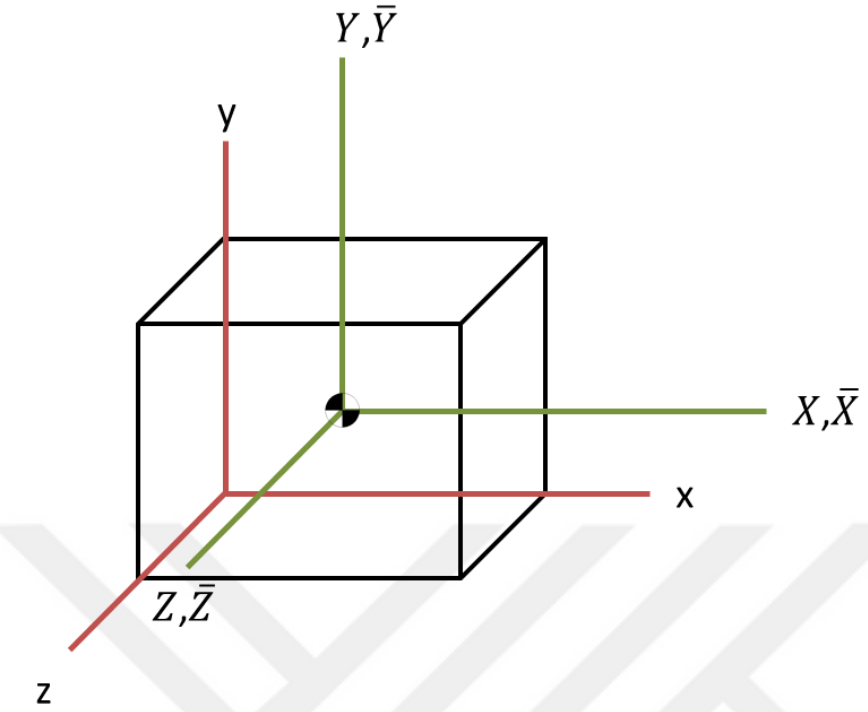

Figure 3.1. Primary Coordinate Frames

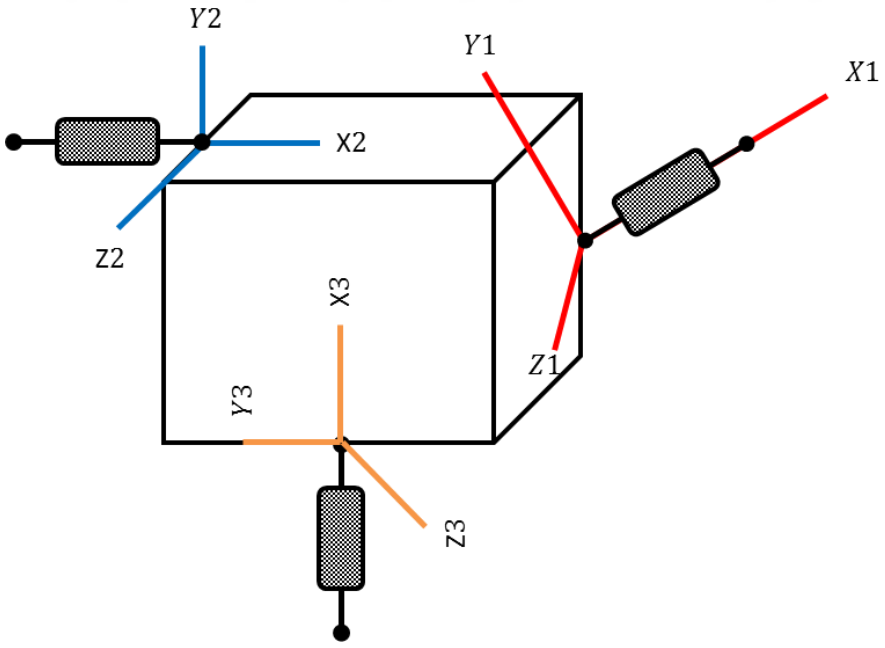

Figure 3.2. Secondary Coordinate Frames

3.2. Resilient Element Representation

Mount design is of primary importance in the design of an isolation system. The performance of the system is immediately based on the resilient element parameters. Therefore, the designation of stiffness and damping of the resilient element is critical to introduce a proper isolation system. There are a wide variety of models that are used to represent the mounting system. The most commonly used one is the *Linear Kelvin-Voigt Model* [52]. This model comprises parallel spring and damper. Another basic model is the *Maxwell Model* which refers to a system with a spring and damper that are connected in series. The Bouc-Wen element as a nonlinear member may be employed to capture hysteresis effects [3]. These models can be combined to create plenty of viscoelastic models. For example, a Linear Maxwell arm is connected with a spring in parallel to give *Standard Linear Solid Model*. Moreover, *Wiechert Model* is obtained by generalizing the Maxwell model by means of Prony series [38].

3.2.1. Linear Kelvin-Voigt Model

Linear Kelvin-Voigt model comprises a spring and a dashpot, which are connected in parallel as shown in *Figure 3.3*.This model is adequate to represent for creep compliance but not for stress relaxation. Furthermore, immediate loads cannot be accommodated. The only spring in the model continues to compress until just before the dashpot yields [27].

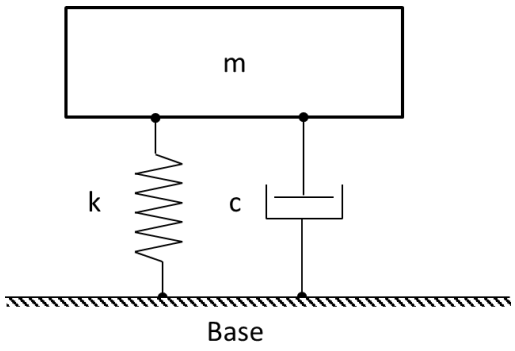

Figure 3.3. Voigt Model

3.2.2. Maxwell Model

Maxwell model comprises a spring and a dashpot, which are connected in series as shown in *Figure 3.4*. This model is adequate to represent for stress relaxation but not for creep compliance. However, a single stress relaxation is considered in this model through the only linear Maxwell arm [27].

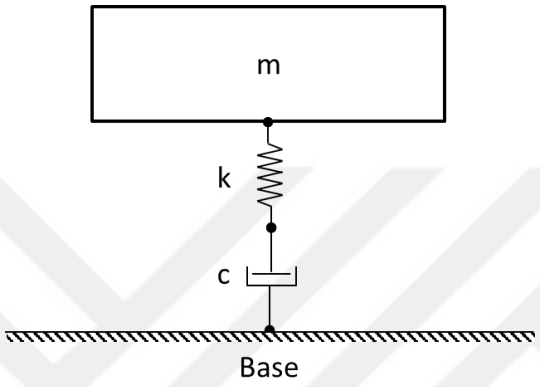

Figure 3.4. Maxwell Model

3.2.3. Standard Linear Solid Model

Standard linear solid model comprises a spring and a linear Maxwell arm, which are connected in parallel as shown in *Figure 3.5*. This model is adequate to capture both stress relaxation and creep compliance, which are the basic time-dependent properties of viscoelastic surfaces. It cannot reproduce multiple relaxation times like the Maxwell model [38].

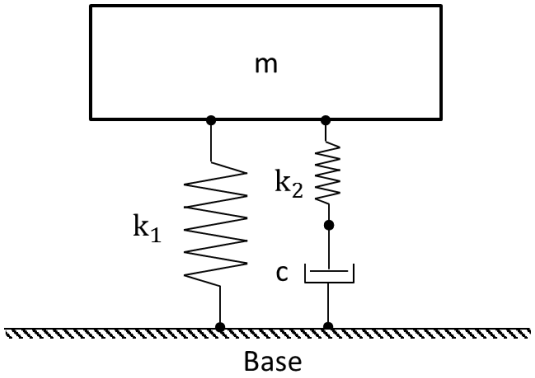

Figure 3.5. Standard Solid Linear Model

3.2.4. Wiechert Model

Wiechert model comprises a spring and multiple linear Maxwell arms, which are connected in parallel as shown in *Figure 3.6*. This model is highly representative for viscoelastic surfaces by the advantage of capturing multiple relaxation times. Many commercial FE codes employ this model to simulate the viscoelastic behavior [38].

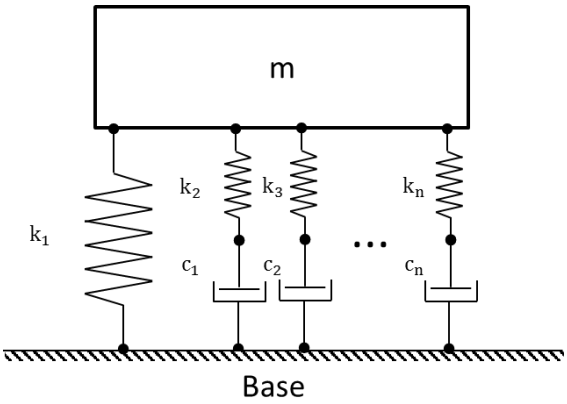

Figure 3.6. Wiechert Model

In this study, resilient elements are represented with the Voigt model. Because, it is frequently adopted to model the elastomeric mounts on account of that mount

parameters can be easily determined, and the analysis is much simpler [59]. Furthermore, it is sufficient for most practical considerations [12].

3.3. Isolation System Representation

Representation of the isolation system is mainly based on [34]. Besides, [36] is referred throughout this study for mathematical modeling. The isolated body is considered as a six degrees-of-freedom rigid body. Degrees of freedom comprise three translational and three rotational displacements. It rests on rigidly connected resilient elements which are fixed on the rigid base structure. Thereby, a six degrees-of freedom mathematical model is created. For this purpose, system equations of motion are defined for the mass **m** and mass moment of inertia **I** of the isolated body, stiffness **k** and viscous damping **c** of resilient element and distance of the elastic center of the resilient element to the mass center **a**.

Resilient support is represented as having linear spring and viscous damping elements. The elastic center of the support is indicated as the intersection point of the principal elastic axes. This parameter is important because of that it determines the magnitude of the stiffness by being used in the equations of motion. The torsional elements are neglected since the torsional stiffness is much smaller than the translational stiffness in general case. Therefore, there are no torsional springs and dampers to apply coupling to the isolated body.

Resilient element is represented by three mutually perpendicular members of Voigt model as shown in *Figure 3.7*. These members are oriented in axial and radial directions of principal axes of the resilient support. Principal elastic axes refer to the axes of symmetry. If the resilient element is deflected collinearly with the force exerted on it in a certain axis, then this axis is called the principal elastic axis. On this basis, spring constant **k** has two subscripts such that one denotes the direction of the applied force and other denotes the direction of the deflection on the element. Furthermore, the stiffness has reciprocal property.

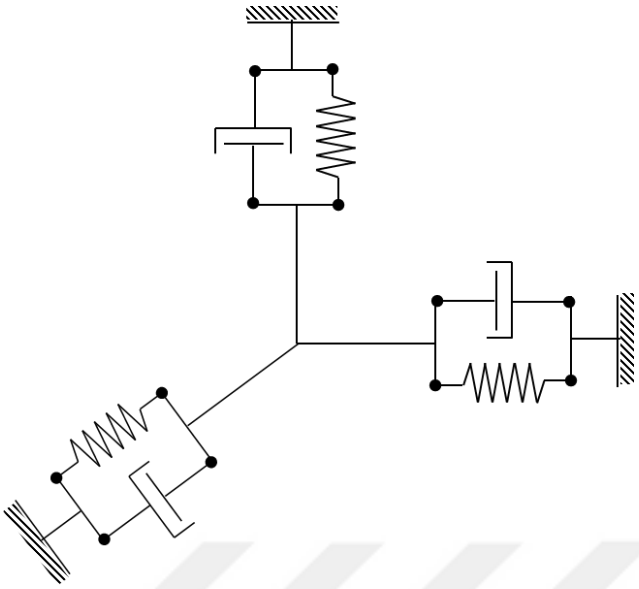

Figure 3.7. Resilient Element of Three Mutually Perpendicular Members

The displacements of the center of gravity of the rigid body are indicated by x_g, y_g and z_g in $\overline{X}$, $\overline{Y}$ and $\overline{Z}$ directions of the inertial frame, respectively. Besides, the rotations of the rigid body about these axes are denoted by α, β and γ, respectively. In the same manner, the displacements of the center of gravity of the foundation are indicated by u, v and w in $\overline{X}$, $\overline{Y}$ and $\overline{Z}$ directions of the inertial frame, respectively. Besides, the rotations of the rigid body about these axes are denoted by $\boldsymbol{\alpha}$, $\boldsymbol{\beta}$ and $\boldsymbol{\gamma}$, respectively.

The basic diagram of the system is presented in *Figure 3.8*. Coordinate frames with set of axes X, Y, Z and $\overline{X}$, $\overline{Y}$, $\overline{Z}$ are originated at the center of gravity of the rigid body as mentioned in *§3.1*. The distance of the center-of-gravity of the rigid body to the resilient element mounting position in $\overline{X}$, $\overline{Y}$ and $\overline{Z}$ directions are given as a_x, a_y, and a_z, respectively. Resilient element of three mutually perpendicular members of Voigt model is also illustrated at a single attachment point. Forces applied on the body are represented as forces in $\overline{X}$, $\overline{Y}$ and $\overline{Z}$directions by F_x, F_y, F_z, respectively. Moments applied on the body are represented about in $\overline{X}$, $\overline{Y}$ and $\overline{Z}$directions by M_x, M_y, M_z, respectively.

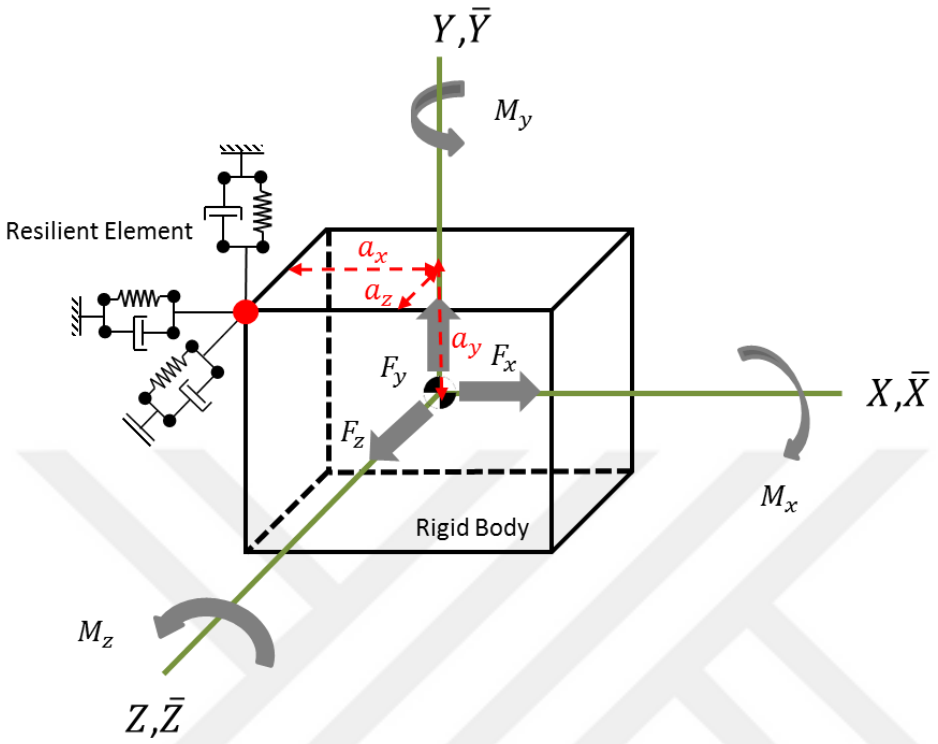

Figure 3.8. Basic System Diagram

System equation of motion for undamped system in compact form is given by *Equation 3.1*.

$$[M]\{\ddot{X}\} + [C]\{\dot{X}\} + [K]\{X\} = \{L\} \qquad 3.1$$

Equations of motion for six degree-of freedom system are given explicitly in *Equation 3.2* [34]. Damping forces applied on the rigid body by resilient members are not involved in these equations for convenience. They are to be included in each equation by appropriately adding damping terms analogous to corresponding stiffness terms.

$$m\ddot{x}_g + \sum k_{xx}(x_g - u) + \sum k_{xy}(y_g - v) + \sum k_{xz}(z_g - w) + \sum\sum (k_{xz}a_y - k_{xy}a_z)(\alpha - \boldsymbol{\alpha}) + \sum\sum (k_{xx}a_z - k_{xz}a_x)(\beta - \boldsymbol{\beta}) + \sum\sum (k_{xy}a_x - k_{xx}a_y)(\gamma - \boldsymbol{\gamma}) = F_x$$

$$I_{xx}\ddot{\alpha} - I_{xy}\ddot{\beta} - I_{xz}\ddot{\gamma} + \sum (k_{xz}a_y - k_{xy}a_z)(x_g - u) + \sum (k_{yz}a_y - k_{yy}a_z)(y_g - v) + \sum (k_{zz}a_y - k_{yz}a_z)(z_g - w) + \sum (k_{yy}{a_z}^2 + k_{zz}{a_y}^2 - 2k_{yz}a_y a_z)(\alpha - \boldsymbol{\alpha}) + \sum (k_{xz}a_y a_z + k_{yz}a_x a_z - k_{zz}a_x a_y - k_{xy}{a_z}^2)(\beta - \boldsymbol{\beta}) + \sum (k_{xy}a_y a_z + k_{yz}a_x a_y - k_{yy}a_x a_z - k_{xz}{a_y}^2)(\gamma - \boldsymbol{\gamma}) = M_x \quad 3.2$$

$$m\ddot{y}_g + \sum k_{xy}(x_g - u) + \sum k_{yy}(y_g - v) + \sum k_{yz}(z_g - w) + \sum\sum (k_{yz}a_y - k_{yy}a_z)(\alpha - \boldsymbol{\alpha}) + \sum\sum (k_{xy}a_z - k_{yz}a_x)(\beta - \boldsymbol{\beta}) + \sum\sum (k_{yy}a_x - k_{xy}a_y)(\gamma - \boldsymbol{\gamma}) = F_y$$

$$
\begin{aligned}
I_{yy}\ddot{\beta} - I_{xy}\ddot{\alpha} - I_{yz}\ddot{\gamma} &+ \sum (k_{xx}a_z - k_{xz}a_x)(x_g - u) \\
&+ \sum (k_{xy}a_z - k_{yz}a_x)(y_g - v) \\
&+ \sum (k_{xz}a_z - k_{zz}a_x)(z_g - w) \\
&+ \sum (k_{xz}a_y a_z + k_{yz}a_x a_z - k_{zz}a_x a_y \\
&- k_{xy}{a_z}^2)(\alpha - \boldsymbol{\alpha}) \\
&+ \sum (k_{xx}{a_z}^2 + k_{zz}{a_x}^2 - 2k_{xz}a_x a_z)(\beta \\
&- \boldsymbol{\beta}) \\
&+ \sum (k_{xy}a_x a_z + k_{xz}a_x a_y - k_{xx}a_y a_z \\
&- k_{yz}{a_x}^2)(\gamma - \boldsymbol{\gamma}) = M_y
\end{aligned}
$$

$$
\begin{aligned}
m\ddot{z}_g &+ \sum k_{xz}(x_g - u) + \sum k_{yz}(y_g - v) \\
&+ \sum k_{zz}(z_g - w) \\
&+ \sum (k_{zz}a_y - k_{yz}a_z)(\alpha - \boldsymbol{\alpha}) \\
&+ \sum (k_{xz}a_z - k_{zz}a_x)(\beta - \boldsymbol{\beta}) \\
&+ \sum (k_{yz}a_x - k_{xz}a_y)(\gamma - \boldsymbol{\gamma}) = F_z
\end{aligned}
$$

$$
\begin{aligned}
I_{zz}\ddot{\gamma} - I_{xz}\ddot{\alpha} - I_{yz}\ddot{\beta} &+ \sum (k_{xy}a_x - k_{xx}a_y)(x_g - u) \\
&+ \sum (k_{yy}a_x - k_{xz}a_y)(y_g - v) \\
&+ \sum (k_{yz}a_x - k_{xz}a_y)(z_g - w) \\
&+ \sum (k_{xy}a_x a_z + k_{yz}a_x a_y - k_{yy}a_x a_z \\
&- k_{xz}{a_y}^2)(\alpha - \boldsymbol{\alpha}) \\
&+ \sum (k_{xy}a_x a_z + k_{xz}a_x a_y - k_{xx}a_y a_z \\
&- k_{yz}{a_x}^2)(\beta - \boldsymbol{\beta}) \\
&+ \sum (k_{xx}{a_y}^2 + k_{yy}{a_x}^2 - 2k_{xy}a_x a_y)(\gamma \\
&- \boldsymbol{\gamma}) = M_z
\end{aligned}
$$

Though the terms used in the equations of motion are explained in the preceding paragraphs, it would be convenient to summarize them here. The mass of the rigid body is indicated by **m**. The mass moment of inertia with respect to $\bar{X}$, $\bar{Y}$ and $\bar{Z}$ axes are I_x, I_y and I_z, respectively. The mass product of inertia with respect to $\bar{X}$, $\bar{Y}$ and $\bar{Z}$ axes are $-I_{xy}$, $-I_{xz}$ and $-I_{yz}$, respectively. The displacements of the center of gravity of the rigid body are indicated by x_g, y_g and z_g in $\bar{X}$, $\bar{Y}$ and $\bar{Z}$ axes, respectively. The rotations of the rigid body about these axes are indicated by α, β and γ, respectively. In the same manner, the displacements of the center of gravity of the base are indicated by u, v and w in $\bar{X}$, $\bar{Y}$ and $\bar{Z}$ axes, respectively. The rotations of the rigid body about these axes are denoted by **α**, **β** and **γ**, respectively The distances of the center-of-gravity of the rigid body to the resilient element mounting position are indicated by a_x, a_y, and a_z in $\bar{X}$, $\bar{Y}$ and $\bar{Z}$ axes, respectively. Principal stiffness coefficients are indicated by k_{xx}, k_{yy} and k_{zz}. The rest of the stiffness coefficients are the coupling stiffness coefficient such as k_{xy}. Forces applied on the body are indicated by F_x, F_y, F_z in $\bar{X}$, $\bar{Y}$ and $\bar{Z}$directions, respectively. Moments applied on the body are indicated by M_x, M_y, M_z about $\bar{X}$, $\bar{Y}$ and $\bar{Z}$directions, respectively.

Simultaneous linear equations can be solved in a convenient mean by utilizing matrices. For this purpose, coefficients and unknowns in equations are to be separately gathered in rectangular matrix and column matrix, respectively.

Total rigid body mass matrix comprises of translational and rotational mass matrix terms. In other words, system mass matrix contains principal masses and mass moments of inertia as given by *Equation 3.3* [41].

$$[M] = \begin{bmatrix} m & 0 & 0 & 0 & 0 & 0 \\ 0 & m & 0 & 0 & 0 & 0 \\ 0 & 0 & m & 0 & 0 & 0 \\ 0 & 0 & 0 & I_{xx} & -I_{xy} & -I_{xz} \\ 0 & 0 & 0 & -I_{xy} & I_{yy} & -I_{yz} \\ 0 & 0 & 0 & -I_{xz} & -I_{yz} & I_{zz} \end{bmatrix} \qquad 3.3$$

Translational stiffness matrix of the resilient supporting element according to its principal elastic axes is given by *Equation 3.4*.

$$\left[\bar{k}^{tt}\right] = \begin{bmatrix} k_p & 0 & 0 \\ 0 & k_q & 0 \\ 0 & 0 & k_r \end{bmatrix} \qquad 3.4$$

Direction cosine matrix of *the principal elastic axes of resilient supporting element* (three mutually perpendicular members of resilient element) and *reference axes of rigid body motion* is given by *Equation 3.5*.

$$[\lambda] = \begin{bmatrix} \lambda_{xp} & \lambda_{xq} & \lambda_{xr} \\ \lambda_{yp} & \lambda_{yq} & \lambda_{yr} \\ \lambda_{zp} & \lambda_{zq} & \lambda_{zr} \end{bmatrix} \qquad 3.5$$

Translational stiffness matrix of the resilient supporting element transformed to the reference axes is given by *Equation 3.6*.

$$[k^{tt}] = [\lambda]\left[\bar{k}^{tt}\right][\lambda]^T \qquad 3.6$$

Translational stiffness matrix in explicit expression of matrices is given by *Equation 3.7*.

$$\begin{aligned} [k^{tt}] &= \begin{bmatrix} k_{xx} & k_{xy} & k_{xz} \\ k_{xy} & k_{yy} & k_{yz} \\ k_{xz} & k_{yz} & k_{zz} \end{bmatrix} \\ &= \begin{bmatrix} \lambda_{xp} & \lambda_{xq} & \lambda_{xr} \\ \lambda_{yp} & \lambda_{yq} & \lambda_{yr} \\ \lambda_{zp} & \lambda_{zq} & \lambda_{zr} \end{bmatrix} \begin{bmatrix} k_p & 0 & 0 \\ 0 & k_q & 0 \\ 0 & 0 & k_r \end{bmatrix} \begin{bmatrix} \lambda_{xp} & \lambda_{xq} & \lambda_{xr} \\ \lambda_{yp} & \lambda_{yq} & \lambda_{yr} \\ \lambda_{zp} & \lambda_{zq} & \lambda_{zr} \end{bmatrix}^T \end{aligned} \qquad 3.7$$

Translational stiffness matrix terms are expressed explicitly as given by *Equation 3.8*.

$$\begin{aligned} k_{xx} &= k_p{\lambda_{xp}}^2 + k_q{\lambda_{xq}}^2 + k_r{\lambda_{xr}}^2 \\ k_{yy} &= k_p{\lambda_{yp}}^2 + k_q{\lambda_{yq}}^2 + k_r{\lambda_{yr}}^2 \\ k_{zz} &= k_p{\lambda_{zp}}^2 + k_q{\lambda_{zq}}^2 + k_r{\lambda_{zr}}^2 \\ k_{xy} &= k_p\lambda_{xp}\lambda_{yp} + k_q\lambda_{xq}\lambda_{yq} + k_r\lambda_{xr}\lambda_{yr} \end{aligned} \qquad 3.8$$

$$k_{xz} = k_p\lambda_{xp}\lambda_{zp} + k_q\lambda_{xq}\lambda_{zq} + k_r\lambda_{xr}\lambda_{zr}$$

$$k_{yz} = k_p\lambda_{yp}\lambda_{zp} + k_q\lambda_{yq}\lambda_{zq} + k_r\lambda_{yr}\lambda_{zr}$$

Global stiffness matrix of the system for an isolator is calculated according to that isolator's stiffness terms and distance to the center of the rigid body motion. Hence, stiffness matrix of the resilient supporting element transformed to the reference axes and its distance components to the center of RBM are enough to create the stiffness contribution of this element to the entire system. It is given by *Equation 3.9*.

$$[k] = \begin{bmatrix} k_{xx} & k_{xy} & k_{xz} & k_{x\alpha} & k_{x\beta} & k_{x\gamma} \\ k_{yx} & k_{yy} & k_{yz} & k_{y\alpha} & k_{y\beta} & k_{y\gamma} \\ k_{zx} & k_{zy} & k_{zz} & k_{z\alpha} & k_{z\beta} & k_{z\gamma} \\ k_{\alpha x} & k_{\alpha y} & k_{\alpha z} & k_{\alpha\alpha} & k_{\alpha\beta} & k_{\alpha\gamma} \\ k_{\beta x} & k_{\beta y} & k_{\beta z} & k_{\beta\alpha} & k_{\beta\beta} & k_{\beta\gamma} \\ k_{\gamma x} & k_{\gamma y} & k_{\gamma z} & k_{\gamma\alpha} & k_{\gamma\beta} & k_{\gamma\gamma} \end{bmatrix} \qquad 3.9$$

Or with block matrices as given by *Equation 3.10*.

$$[k] = \begin{bmatrix} [k^{tt}] & [k^{tr}] \\ [k^{rt}] & [k^{rr}] \end{bmatrix} \qquad 3.10$$

Where, in compact form for unloaded configuration (*Equation 3.11*),

$$[k^{tr}] = [k^{tt}][A_0]^T$$

$$[k^{rt}] = [k^{tr}]^T \qquad 3.11$$

$$[k^{rr}] = [A_0][k^{tt}][A_0]^T$$

Where (*Equation 3.12*)

$$[A_0] = \begin{bmatrix} 0 & -a_z & a_y \\ a_z & 0 & a_x \\ -a_y & a_x & 0 \end{bmatrix} \qquad 3.12$$

Damping matrix can be written by adding the appropriate damping terms with analogous to the corresponding stiffness terms. Stiffness matrix is given explicitly by *Equation 3.13*.

$$k_{11} = k_{xx}$$

$$k_{12} = k_{xy}$$

$$k_{13} = k_{xz}$$

$$k_{14} = k_{xz}a_y - k_{xy}a_z$$

$$k_{15} = k_{xx}a_z - k_{xz}a_x$$

$$k_{16} = k_{xy}a_x - k_{xx}a_y$$

$$k_{21} = k_{xy}$$

$$k_{22} = k_{yy}$$

$$k_{23} = k_{yz}$$

$$k_{24} = k_{yz}a_y - k_{yy}a_z$$

$$k_{25} = k_{xy}a_z - k_{yz}a_x$$

$$k_{26} = k_{yy}a_x - k_{xy}a_y \qquad 3.13$$

$$k_{31} = k_{xz}$$

$$k_{32} = k_{yz}$$

$$k_{33} = k_{zz}$$

$$k_{34} = k_{zz}a_y - k_{yz}a_z$$

$$k_{35} = k_{xz}a_z - k_{zz}a_x$$

$$k_{36} = k_{yz}a_x - k_{xz}a_y$$

$$k_{41} = k_{xz}a_y - k_{xy}a_z$$

$$k_{42} = k_{yz}a_y - k_{yy}a_z$$

$$k_{43} = k_{zz}a_y - k_{yz}a_z$$

$$k_{44} = k_{yy}{a_z}^2 + k_{zz}{a_y}^2 - 2k_{yz}a_y a_z$$

$$k_{45} = k_{xz}a_y a_z + k_{yz}a_x a_z - k_{zz}a_x a_y - k_{xy}{a_z}^2$$

$$k_{46} = k_{xy}a_y a_z + k_{yz}a_x a_y - k_{yy}a_x a_z - k_{xz}{a_y}^2$$

$$k_{51} = k_{xx}a_z - k_{xz}a_x$$

$$k_{52} = k_{xy}a_z - k_{yz}a_x$$

$$k_{53} = k_{xz}a_z - k_{zz}a_x$$

$$k_{54} = k_{xz}a_y a_z + k_{yz}a_x a_z - k_{zz}a_x a_y - k_{xy}{a_z}^2$$

$$k_{55} = k_{xx}{a_z}^2 + k_{zz}{a_x}^2 - 2k_{xz}a_x a_z$$

$$k_{56} = k_{xy}a_x a_z + k_{xz}a_x a_y - k_{xx}a_y a_z - k_{yz}{a_x}^2$$

$$k_{61} = k_{xy}a_x - k_{xx}a_y$$

$$k_{62} = k_{yy}a_x - k_{xy}a_y$$

$$k_{63} = k_{yz}a_x - k_{xz}a_y$$

$$k_{64} = k_{xy}a_y a_z + k_{yz}a_x a_y - k_{yy}a_x a_z - k_{xz}{a_y}^2$$

$$k_{65} = k_{xy}a_x a_z + k_{xz}a_x a_y - k_{xx}a_y a_z - k_{yz}{a_x}^2$$

$$k_{66} = k_{xx}{a_y}^2 + k_{yy}{a_x}^2 - 2k_{xy}a_x a_y$$

System stiffness matrix is given by *Equation 3.14*.

$$[K] = \sum_{i=1}^{n} [k_i] \qquad 3.14$$

System viscous damping matrix is given by *Equation 3.15*.

$$[C] = \sum_{i=1}^{n} [c_i] \qquad 3.15$$

In the Equation 3.14, k_i refers to the stiffness matrix of the i^{th} resilient element as given in Equation 3.9. With analogy, c_i refers to the viscous damping matrix of the i^{th} resilient element. Besides, n is the number of resilient elements in the system.

If damping matrix is proportional to mass and stiffness, then it can be written as given by *Equation 3.16*.

$$[C] = A[M] + B[K] \tag{3.16}$$

In this study, damping is proportional to both stiffness and mass, so it is called proportional damping or Rayleigh damping.

Displacement vector consists of the unknowns of the equations of motion as given by *Equation 3.17*.

$$\{X\} = \{x_g - u \quad y_g - v \quad z_g - w \quad \alpha - \boldsymbol{\alpha} \quad \beta - \boldsymbol{\beta} \quad \gamma - \boldsymbol{\gamma}\}^T \tag{3.17}$$

In this study, foundation on which resilient elements are attached is assumed to have no rigid body motion. Thus, translational and rotational displacement terms of base motion in the system equations of motion will vanish and reduce to *Equation 3.18*.

$$\{X\} = \{x_g \quad y_g \quad z_g \quad \alpha \quad \beta \quad \gamma\}^T \tag{3.18}$$

In the same manner, acceleration vector is given in the reduced form by *Equation 3.19*.

$$\{\ddot{X}\} = \{\ddot{x}_g \quad \ddot{y}_g \quad \ddot{z}_g \quad \ddot{\alpha} \quad \ddot{\beta} \quad \ddot{\gamma}\}^T \tag{3.19}$$

Load vector is given by *Equation 3.20*.

$$\{L\} = \{F_x \quad F_y \quad F_z \quad M_x \quad M_y \quad M_z\}^T \tag{3.20}$$

Forces and moments are not directly applied to the body; however, the system has a random base excitation at a certain degrees-of-freedom.

The vibrational symmetry is touched on to advance the understanding of the underlying physics. Thus, the change in the coupling of modes as the vibrational symmetry differentiates might be recognized. Furthermore, various mounting arrangements are investigated regarding the effect on vibrational symmetry and the practicability.

3.3.1. Vibrational Symmetry

Vibrational symmetry brings about the simplification on the calculations of the natural frequencies. Although the present facilities readily serve the acceptable computational efforts, the ease of calculations will contribute to improve the comprehension of physical phenomenon of vibration analysis.

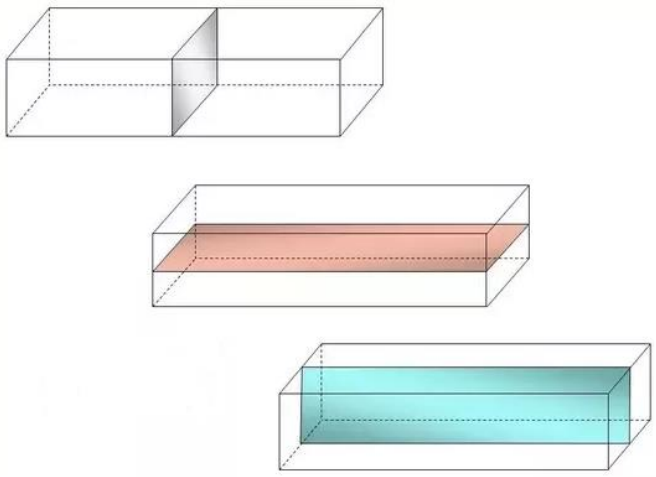

Figure 3.9. Vibrational Symmetry Planes of Homogeneous Rectangular Prism

One plane of symmetry may be achieved by adjusting one of the planes among XY, XZ and YZ planes as the plane of symmetry. Thus, following terms of the equations of motion become zero for each separate plane of symmetry, respectively as in [34][55].

For XY-plane of symmetry, following terms of equations of motion become zero (*Equation 3.21* through *3.23*):

$$\sum k_{xx}a_z = \sum k_{yy}a_z = \sum k_{xx}a_z a_y = \sum k_{yy}a_z a_x = 0 \qquad 3.21$$

For XZ-plane of symmetry, following terms of equations of motion become zero:

$$\sum k_{xx}a_y = \sum k_{zz}a_y = \sum k_{xx}a_y a_z = \sum k_{zz}a_y a_x = 0 \qquad 3.22$$

For XZ-plane of symmetry, following terms of equations of motion become zero:

$$\sum k_{yy}a_x = \sum k_{zz}a_x = \sum k_{yy}a_x a_z = \sum k_{zz}a_x a_y = 0 \qquad 3.23$$

For several planes of symmetry, corresponding reductions are implemented simultaneously.

Vibrational symmetry may be succeeded by various mounting arrangements of the resilient elements on the body.

3.3.1.1. Installation Arrangements

The most useful mounting or installation arrangements of the resilient elements are presented in this section by addressing the vibrational symmetry [55]. They are namely

- Center-of-gravity arrangement
- Bottom arrangement

In the center-of-gravity arrangement, the mounting plane becomes the symmetry plane if it contains two axes of body inertia. Three planes of symmetry can be achieved.

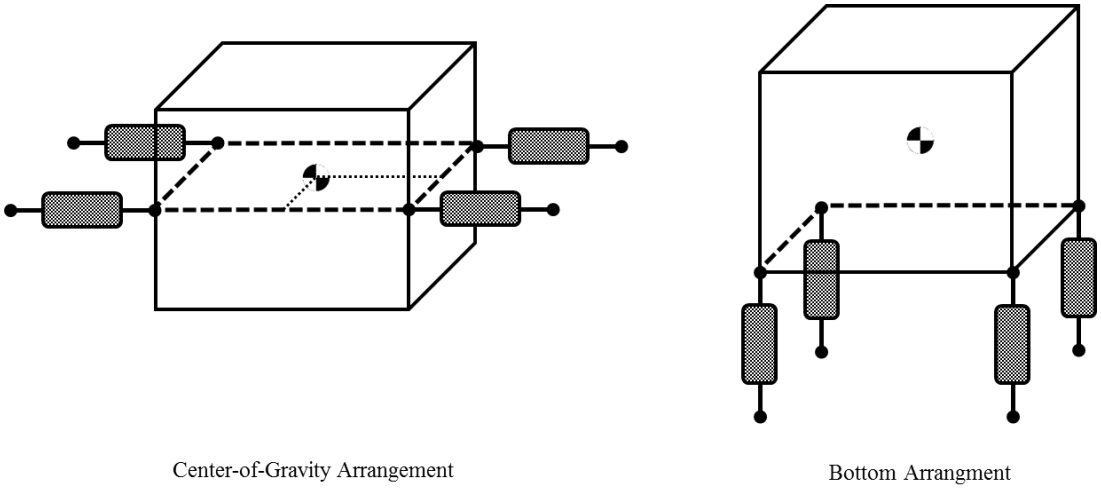

Figure 3.10. Common Installation Arrangements

In bottom arrangement, the resilient supports are usually installed under the body. A plane parallel to the foundation contains the attachment points. Two planes of symmetry can be achieved in this arrangement. Specifically, more than one parallel plane might be in question if the body has a stepped geometry. Only one plane of symmetry can be achieved with stepping installation.

In this study, attachment points can be anywhere in the space. Nevertheless, the exterior surface of the body must be accounted for being the limits of the available space to obtain a meaningful design.

CHAPTER 4

VIBRATION ANALYSIS

Vibration analysis will be summarized by indicating the identifiable aspects of the subject. It consists of two successive stages. They are namely the free vibration and forced vibration analyses. A free vibration analysis ends up with modal properties or the natural frequencies and mode shapes. Besides, frequency response characteristics are obtained by implementing a forced vibration analysis. To itemize, vibration analysis is achieved in three phases:

- Setting up the spatial properties i.e. the values of mass and inertia, stiffness and damping elements
- Performing a free vibration analysis to obtain modal properties i.e. natural frequencies, damping factors, and mode shapes vectors as many as the number of degrees of freedom.
- Performing a forced response analysis to obtain frequency response characteristics

In order to start with the first phase, the class of system model should be determined among three different categories:

- Undamped
- Viscously damped
- Hysteretically or structurally damped

Undamped system assumption is applicable for dynamic structures with negligible damping. This is not the case when the purpose of this study is considered. The system has a linear spring, and a sufficiently slow motion is assumed so that damping forces

applied by the dashpot on the rigid body is proportional to the velocity. Therefore, a linear set of equations of motion is of interest.

The off-diagonal terms of the damping matrix can be wiped out by the undamped mode shape matrix since the damping matrix is proportional to stiffness and mass matrices which are already diagonalizable.

4.1. Free Vibration Analysis

Details of matrix construction with spatial elements are presented in CHAPTER 3. Hence, free vibration analysis can be implemented by using the previously obtained coefficient matrices as given in *Equation 4.1*.

$$[M]\{\ddot{X}\} + [C]\{\dot{X}\} + [K]\{X\} = \{0\} \qquad 4.1$$

Or (*Equation 4.2*)

$$[M]\{\ddot{X}\} + (A[M] + B[K])\{\dot{X}\} + [K]\{X\} = \{0\} \qquad 4.2$$

Free vibration problem is solved for the undamped system with the equation of motion as given by *Equation 4.3*.

$$[M]\{\ddot{X}\} + [K]\{X\} = \{0\} \qquad 4.3$$

A solution is offered in the form of *Equation 4.4*.

$$\{x(t)\} = \{X\}e^{j\lambda t} \qquad 4.4$$

The eigenvalue problem in *Equation 4.5* is obtained.

$$([K] - \lambda^2[M])\{X\} = \{0\} \qquad 4.5$$

The solution to the eigenvalue problem yields the modal properties of the system. Eigenvalue and eigenvector matrices are denoted by $[\lambda^2]$ and $[\varphi]$, respectively. Solution of eigenvalue problem leads to damped natural frequency λ_r of the r^{th} mode. The eigenvalue λ_r^2 is related to the natural frequency or undamped natural frequency ω_r of the r^{th} mode and modal damping ratio ζ_r of the r^{th} mode of the system as given by *Equation 4.6* where $\zeta_r = c_r/2m_r\omega_r$.

$$\lambda_r{}^2 = \omega_r{}^2\left(1 - \zeta_r{}^2\right) \quad 4.6$$

Mode shape matrix is given by *Equation 4.7*.

$$[\varphi] = [\varphi_1 \quad \varphi_2 \quad \cdots \quad \varphi_n] \quad 4.7$$

Modal mass, stiffness, and damping matrices are obtained by applying the orthogonality properties as given in *Equation 4.8*.

$$\begin{aligned} [\varphi]^T[M][\varphi] &= [m_r] \\ [\varphi]^T[K][\varphi] &= [k_r] \\ [\varphi]^T[C][\varphi] &= [c_r] \end{aligned} \quad 4.8$$

Mode shapes are normalized to unit modal mass in keeping with the conventional approach as given in *Equation 4.9*.

$$[\phi]^T[M][\phi] = [I] \quad 4.9$$

Or (*Equation 4.10*)

$$[\phi] = [m_r]^{\frac{1}{2}}[\varphi] \quad 4.10$$

In which, ϕ_r is the mass-normalized mode shape of the r^{th} mode.

Modal matrix is treated with mass matrix to give diagonal identity matrix as given by *Equation 4.11*.

$$[\phi]^T[M][\phi] = [I] \quad 4.11$$

Modal matrix is treated with stiffness matrix to give diagonal eigenvalue matrix as given by *Equation 4.12*.

$$[\phi]^T[K][\phi] = [\omega_r{}^2] \quad 4.12$$

Modal matrix is treated with damping matrix as given by *Equation 4.13*.

$$[\phi]^T[C][\phi] = [2\zeta\omega_r] \quad 4.13$$

Thus, modal properties can be obtained by free vibration analysis [22].

4.2. Forced Vibration Analysis

At the third phase of the vibration analysis, system response is to be determined. Input and output variables of a system can be set among any type of force or motion variable. At first, the vibration environment of the aircraft is to be specified to continue with the response calculation.

4.2.1. Vibration Environment

Vibration exposure for military aircraft is available in military standards prepared by the Department of Defense of USA. Vibration profiles, each specific to a certain type of air vehicle construction, are generated by performing environmental tests. The Environmental Engineering Considerations and Laboratory Tests report of the USA Department of Defense, MIL-STD-810-G defines the vibration environment of the jet aircraft in [18] as shown in *Figure 4.1*. Power spectral density level of acceleration response for turbulent air flow which is the main source of interior noise problems in jet aircraft, which leads the upper limit of PSD level of the acceleration response $W_0 = 0.20\ g^2/Hz$ [15][20]. This vibration level is used in the vibration exposure offered by MIL-STD-810-G as presented in *Figure 4.1*.

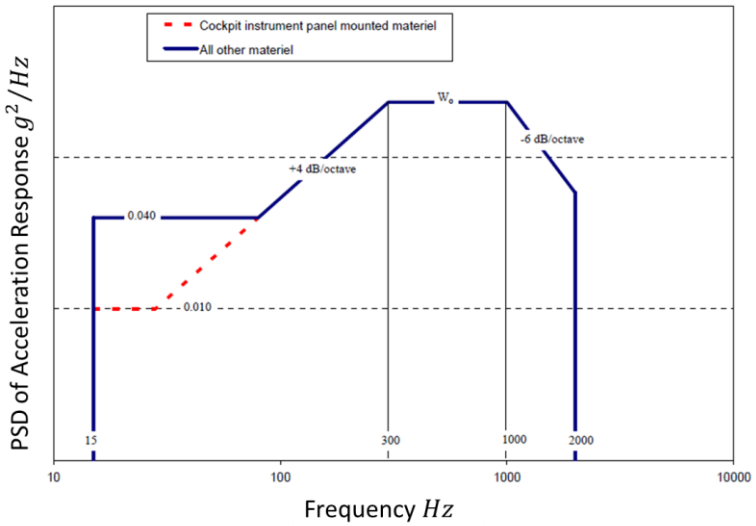

Figure 4.1. Jet Aircraft Vibration Exposure by MIL-STD-810-G

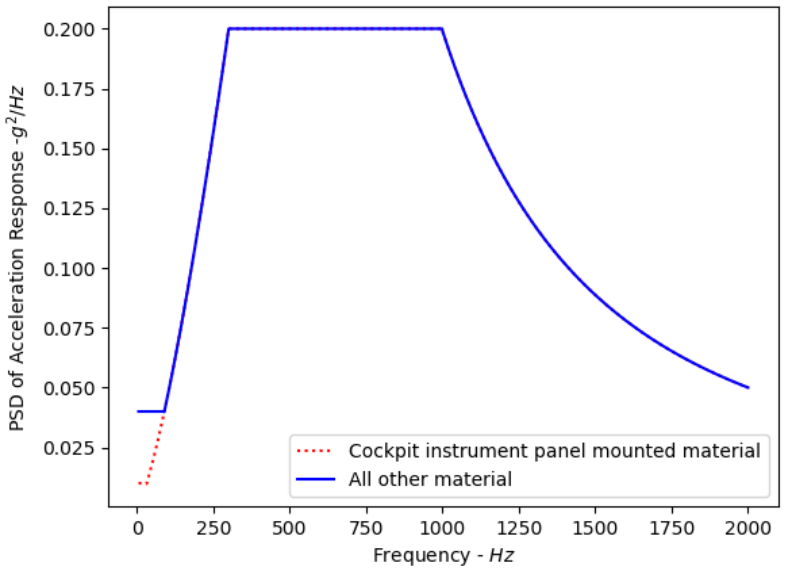

Figure 4.2. Jet Aircraft Vibration Exposure

Eventually, break points of the jet aircraft vibration exposure are given in *Table 4.1* and *Table 4.2* for cockpit instrument panel mounted material and all other material, respectively.

Table 4.1. *Jet Aircraft Vibration Exposure for Cockpit Instrument Panel Mounted Material*

Frequency [Hz]	*ASD [g^2/Hz]*
15	0.01
31	0.01
300	0.2
1000	0.2
2000	0.05

Table 4.2. *Jet Aircraft Vibration Exposure for All Other Material*

Frequency [Hz]	*ASD [g^2/Hz]*
15	0.04
89	0.04
300	0.2
1000	0.2
2000	0.05

4.2.2. Vibration Response

A transfer function must be defined for a given input to obtain a desired output.

Specifically, transfer function becomes frequency response function when only the imaginary part of the Laplace operator s is considered. Employing frequency response function (FRF) is the most effective mean to come up with system response in a vibration analysis. Three frequency response functions are

- Mobility
    - Input: Force & Output: Velocity
- Impedance
    - Input: Velocity & Output: Force
- Transmissibility
    - Input: Force & Output: Force or Input: Velocity & Output: Velocity

These functions can be varied to make it useful in the specific analysis. Those most commonly used are listed in *Table 4.3*.

Table 4.3. *Mechanical Frequency Response Functions*

FRF	*Definition (In the Frequency Domain) Output/Input*
Mobility	Velocity/Force
Impedance	Force/Velocity
Receptance, Dynamic Flexibility, Compliance	Displacement/Force
Dynamic Stiffness	Force/Displacement
Accelerance	Acceleration/Force
Dynamic Inertia, Apparent Mass	Force/Acceleration
Force Transmissibility	Transmitted Force/Applied Force
Motion Transmissibility	Transmitted Velocity/Applied Velocity

Harmonic or random vibration continuously excites the rigid body by the foundation-induced vibration or the body-induced vibration. In the foundation-induced vibration, the vibratory motion of the foundation excites the resiliently supported rigid body. In the body-induced vibration, the rigid body itself is directly loaded. In this study, foundation-induced vibration is considered.

Modal frequency response analysis is explained in chronological order regarding the practical implementation. At the beginning, damping is neglected for convenience. Mass and stiffness matrices are assembled to give a set of differential equations of motion as presented in *Equation 4.14*.

$$[M]\{\ddot{X}\} + [K]\{X\} = \{L(\omega)\} \qquad 4.14$$

Characteristic equation in *Equation 4.15* is solved for natural frequencies and mode shapes as previously mentioned. This procedure is simply repeated here for completeness.

$$det([K] - \omega^2[M]) = 0 \qquad 4.15$$

System is diagonalized by utilizing the orthogonality properties of mode shapes that are the constituents of the modal matrix. Thus, modal transformation is achieved by applying the separation approach as given by *Equation 4.16*.

$$\{X\} = [\varphi]\{q(\omega)\}$$
$$\{P\} = [\varphi]\{L(\omega)\} \qquad 4.16$$
$$[\varphi] = [\varphi_1 \quad \varphi_2 \quad \cdots \quad \varphi_n]$$

Herewith, the system of multiple degrees of freedom is decoupled to a system of single-mass oscillators as many as the number of degrees of freedom. Each single mass oscillator represents one of the eigenvectors of the system. Following the modal transformation, system is represented in general coordinates q as given by *Equation 4.17* [58].

$$m_r\ddot{x}_r + k_r x_r = l_r$$
$$m_r\varphi_r\ddot{x}_r + k_r\varphi_r x_r = \varphi_r l_r$$
$$m_r\ddot{q}_r(\omega) + k_r q_r(\omega) = p_r \qquad 4.17$$
$$\ddot{q}_r(\omega) + \frac{k_r}{m_r} q_r(\omega) = \frac{p_r(\omega)}{m_r}$$
$$\ddot{q}_r(\omega) + {\omega_r}^2 q_r(\omega) = \frac{p_r(\omega)}{m_r}$$

As of now, damping may be included in the equations by employing the modal damping ratio ζ by starting with *Equation 4.18*.

$$\ddot{q}_r(\omega) + 2j\zeta\omega_r q_r(\omega) + {\omega_r}^2 q_r(\omega) = \frac{p_r(\omega)}{m_r} \qquad 4.18$$

This differential equation can be solved easily and the solution for the displacement in general coordinates is obtained as given by *Equation 4.19*.

$$q_r(\omega) = \frac{\frac{p_r(\omega)}{m_r}}{{\omega_r}^2 - \omega^2 + 2j\zeta\omega_r\omega} \qquad 4.19$$

All the single mass oscillators are combined linearly to give the system solution by *Equation 4.20*.

$$X(\omega) = \sum_{r=1}^{N} \varphi_r q_r(\omega) \qquad 4.20$$

Frequency response function is obtained by dividing the response of the system by the excitation force. Response might be displacement, velocity or acceleration. Frequency response function for displacement i.e. receptance is given by *Equation 4.21*.

$$H(\omega) = \frac{X(\omega)}{L(\omega)} = \sum_{r=1}^{N} \frac{\varphi_r {\varphi_r}^T}{{\omega_r}^2 - \omega^2 + 2j\zeta_r\omega_r\omega} \frac{1}{m_r} \qquad 4.21$$

Frequency response function might also be written in terms of mass normalized modal matrix, and it comprises the contributions of all individual modes as given by *Equation 4.22*.

$$H(\omega) = \frac{X(\omega)}{L(\omega)} = \sum_{r=1}^{N} \frac{\phi_r {\phi_r}^T}{{\omega_r}^2 - \omega^2 + 2j\zeta_r\omega_r\omega} \qquad 4.22$$

Furthermore, the receptance for the i^{th} node (degree of freedom) with a single excitation force at k^{th} degree of freedom can be calculated by *Equation 4.23*.

$$H_{ik}(\omega) = \frac{X(\omega)}{L(\omega)} = \sum_{r=1}^{N} \frac{\phi_{ir}\phi_{kr}}{{\omega_r}^2 - \omega^2 + 2j\zeta_r\omega_r\omega} \qquad 4.23$$

Conversion from displacement to velocity and acceleration may be achieved through multiplication by ω and ω^2, respectively [58].

Damping may be indicated by various expressions. Commonly used representation manners are namely amplification or quality factor *Q*, viscous damping ratio or fraction of critical damping ζ and equivalent viscous damping *G*. They are related to each other as given by *Equation 4.24*.

$$Q = \frac{1}{2\zeta} = \frac{1}{G} \qquad 4.24$$

Isolation performance may be investigated in terms of maximum responses. In this study, maximum response of the system will be presented in terms of frequency response function.

Response at coordinate i of an MDOF system to a single stationary random excitation at coordinate k is calculated by *Equation 4.25* [58].

$$S_i(\omega) = |H_{ik}||H_{ik}|S_k(\omega) \qquad 4.25$$

The mean square of power spectral density of response may be calculated by *Equation 4.26* [58].

$$\sigma_i{}^2 = \int S_i(\omega)\, d\omega \qquad 4.26$$

CHAPTER 5

MODEL VERIFICATION

Mathematical model and vibration analysis method that are presented in CHAPTER 3 and CHAPTER 4, respectively are to be verified. Once the verification is achieved, optimization analysis and reliability analysis can be implemented.

Literature is reviewed for studies that perform free vibration analysis of isolation systems. An isolation system from literature, whose natural frequencies are shared out explicitly, is modeled in an FE environment. Natural frequencies of the reference study and FE model are compared to be sure of that the finite element model is created properly. Once the FE model is made certain of, frequency response analysis is conducted and response results for displacement, velocity and acceleration are obtained in the FE environment.

The reason to use an FE environment is the facility to simulate many different isolation systems. Furthermore, frequency response analysis data is not readily accessible in literature. This makes the complete verification of the developed tool difficult. However, it is relatively easier to reach modal properties of various isolation systems in literature, and this fact is utilized to verify whether the FE model is created correctly, which is required to continue with the frequency response analysis. Hereby, both the free vibration and forced vibration procedures of an entire vibration analysis are achieved through the FE model. Eventually, analysis results which are obtained from the FE model are used to verify the developed computer code (DCC).

There exist plenty of finite element software packages such as Femap®, SESAM®, Abaqus®, Hypermesh®, Ansys®, Nastran®, etc. Nastran® is developed by NASA and commonly employed in the aerospace industry. The finite element environment used in this study is MSC Patran/Nastran®. It is a multidisciplinary structural analysis

software which can perform static, dynamic, and thermal analysis in both linear and nonlinear domains.

MSC Patran/Nastran® has basically a workflow starting with pre-processing in MSC Patran®, continuing with solving process in MSC Nastran® and ending with post-processing in again MSC Patran®.

5.1. Sample Isolation System I

Center-of-gravity installation arrangement of four coplanar identical resilient elements with three planes of vibrational symmetry is considered in this example [55]. The isolation procedure is applied to a solid homogeneous rectangular body. The results are analytically obtained in [55]. Therefore, impeccable results can be and are found during the calculations.

System properties are obtained by using body dimensions and mass information which are provided in [55] beside the stiffness of isolators. Isolation system is shown in *Figure 5.1*. Isolation system properties are given in inertial axis system $\overline{XYZ}$, and center-of-gravity and mounting positions are given in global axis system xyz. Mounting orientations of resilient elements are also given with respect to the global axis system xyz.

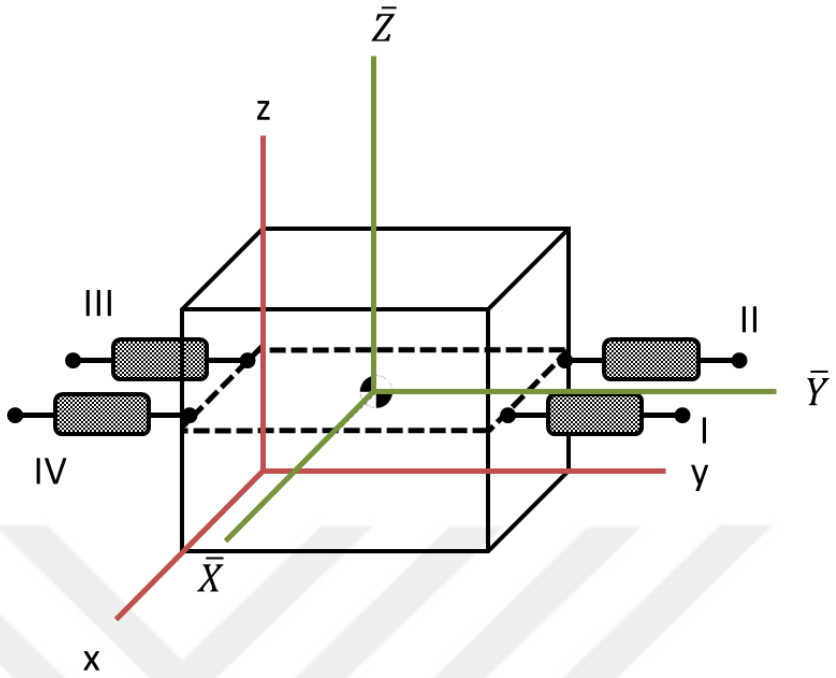

Figure 5.1. Representation of Sample Isolation System I

Positions of center-of-gravity and mounting points beside the directional cosines of mounts and body dimensions are presented in *Table 5.1*.

Table 5.1. *Geometric Texture of Sample Isolation System I*

Parameter	*x [mm]*	*y[mm]*	*z[mm]*	*Directional Cosine*
CG	635.0	406.4	254.0	N/A
Isolator I	1219.2	889.0	254.0	<0,0,1>
Isolator II	50.8	889.0	254.0	<0,0,1>
Isolator III	50.8	-76.2	254.0	<0,0,1>
Isolator IV	1219.2	-76.2	254.0	<0,0,1>
Body Dimension	1270.0	812.8	508.0	N/A

Inertial properties of the isolation system which comprise of mass and mass moments of inertia in principal directions are given in *Table 5.2*.

Table 5.2. *Inertial Properties of Sample Isolation System I*

Component	$m\ [Mg]$	$I_{\bar{X}}\ [Mgmm^4]$	$I_{\bar{Y}}[Mgmm^4]$	$I_{\bar{Z}}[Mgmm^4]$
Body	1.8144	138906.2888	282884.9983	343754.0462

Elastic properties of resilient elements of the isolation system are presented in *Table 5.3*. In all the isolators, the same damping ratio of 0.05 has been assumed to be existed.

Table 5.3. *Elastic Properties of Sample Isolation System I*

Parameter	K_{axial} *[N/mm]*	K_{radial} *[N/mm]*	ζ_r
Isolator I	4027.92	4027.92	0.05
Isolator II	4027.92	4027.92	
Isolator III	4027.92	4027.92	
Isolator IV	4027.92	4027.92	

In so far, all the parameters required for a complete definition of the isolation system are provided. Based on these parameters, FE model is created in the MSC Patran/Nastran® software.

5.1.1. System FE Model

FE Model contains "CBUSH" elements to represent resilient mounts in the system. Besides, "CONM2" element to represent the rigid body by introducing mass and inertia properties is rigidly connected to the "CBUSH" elements with "RBE2" elements in all degrees of freedom. Model generation is performed in the MSC Patran® pre-processor environment.

"CBUSH" is used to define a structural element comprising of spring and damper. "CONM2" is used to define a concentrated mass at a single node. "RBE2" is used to define a rigid element between a single node of independent degrees-of-freedom and an arbitrary number of nodes of dependent degrees-of-freedom.

As the solution sequence, "SOL 111" included in the MSC Nastran® analysis solver is employed as the frequency response solution sequence. Excitation is introduced to the system from the fixed ends of "CBUSH" elements, which represent the rigid connection points of resilient mounts to the base. Response is measured from the center-of-gravity of the isolated body which corresponds to the position of the "CONM2" element. Detailed information of MSC Nastran® entries can be reached in [31].

FE model is shown in *Figure 5.2*.

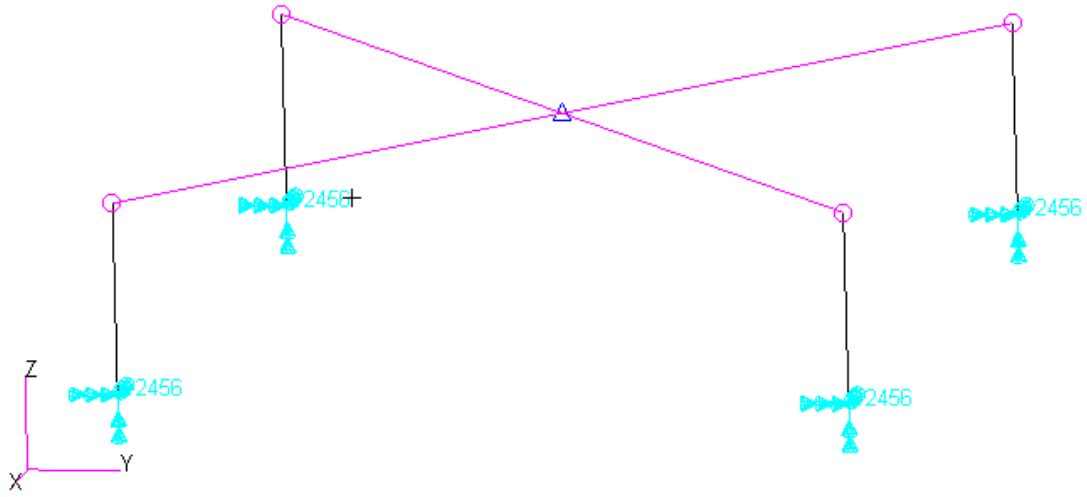

Figure 5.2. Representation of the FE Model for Sample Isolation System I

According to the free vibration analysis results of both the FE model and reference application natural frequencies are compared in *Table 5.4*. The results are demonstrated to be in good agreement.

Table 5.4. *Natural Frequency Comparison of Reference [55] & FE Models for Sample Isolation System I*

	Natural Frequency [Hz]		
DOF	*FE Model*	*Reference [55]*	*Difference [%]*
1	14.998~15.0	15.0	0.0
2	14.998~15.0	15.0	0.0
3	14.998~15.0	15.0	0.0
4	22.189~22.2	22.3	0.4
5	26.109~26.1	26.1	0.0
6	26.159~26.2	26.1	0.4

Following the confirmation of that the FE model is created properly by correct definition of mass and stiffness terms, modal property results of the FE model are compared with those of the mathematical model. According to the free vibration analysis results of both the FE model and mathematical model, modal properties are compared in *Table 5.5* and in *Table 5.6* terms of natural frequencies and mode shapes, respectively.

Table 5.5. *Natural Frequency Comparison of Mathematical & FE Models for Sample Isolation System I*

	Natural Frequency [Hz]		
DOF	*FE Model*	*Mathematical Model*	*Difference [%]*
1	14.998	14.998	0.0
2	14.998	14.998	0.0
3	14.998	14.998	0.0

Table 5.5 Continued.

4	22.189	22.189	0.0
5	26.109	26.109	0.0
6	26.159	26.159	0.0

Table 5.6. *Mode Shapes Comparison of Mathematical & FE Models for Sample Isolation System I*

Natural Frequency [Hz]		*Mode Shapes Constituent*					
		1	*2*	*3*	*4*	*5*	*6*
	FEM	-0.7424	0.0	0.0	0.0	0.0	0.0
14.998	DCC	-0.7424	0.0	0.0	0.0	0.0	0.0
	DIFF [%]	0.0	0.0	0.0	0.0	0.0	0.0
	FEM	0.0	0.7424	0.0	0.0	0.0	0.0
14.998	DCC	0.0	0.7424	0.0	0.0	0.0	0.0
	DIFF [%]	0.0	0.0	0.0	0.0	0.0	0.0
	FEM	0.0	0.0	0.7424	0.0	0.0	0.0
14.998	DCC	0.0	0.0	0.7424	0.0	0.0	0.0
	DIFF [%]	0.0	0.0	0.0	0.0	0.0	0.0
	FEM	0.0	0.0	0.0	0.0	0.00188	0.0
22.189	DCC	0.0	0.0	0.0	0.0	0.00188	0.0
	DIFF [%]	0.0	0.0	0.0	0.0	0.0	0.0
	FEM	0.0	0.0	0.0	0.0	0.0	0.00170
26.109	DCC	0.0	0.0	0.0	0.0	0.0	0.00171
	DIFF [%]	0.0	0.0	0.0	0.0	0.0	0.6
	FEM	0.0	0.0	0.0	-0.00268	0.0	0.0
26.159	DCC	0.0	0.0	0.0	-0.00268	0.0	0.0
	DIFF [%]	0.0	0.0	0.0	0.0	0.0	0.0

Result of modal properties show that mathematical model is created properly by correct definition and formulation of mass and stiffness elements. Mode shapes obtained from the FE model and mathematical model are illustrated in *Figure 5.3* and *Figure 5.4*, respectively. These figures of the FE model and mathematical model give

the opportunity to observe the mode shapes in three-dimensional and two-dimensional views, respectively.

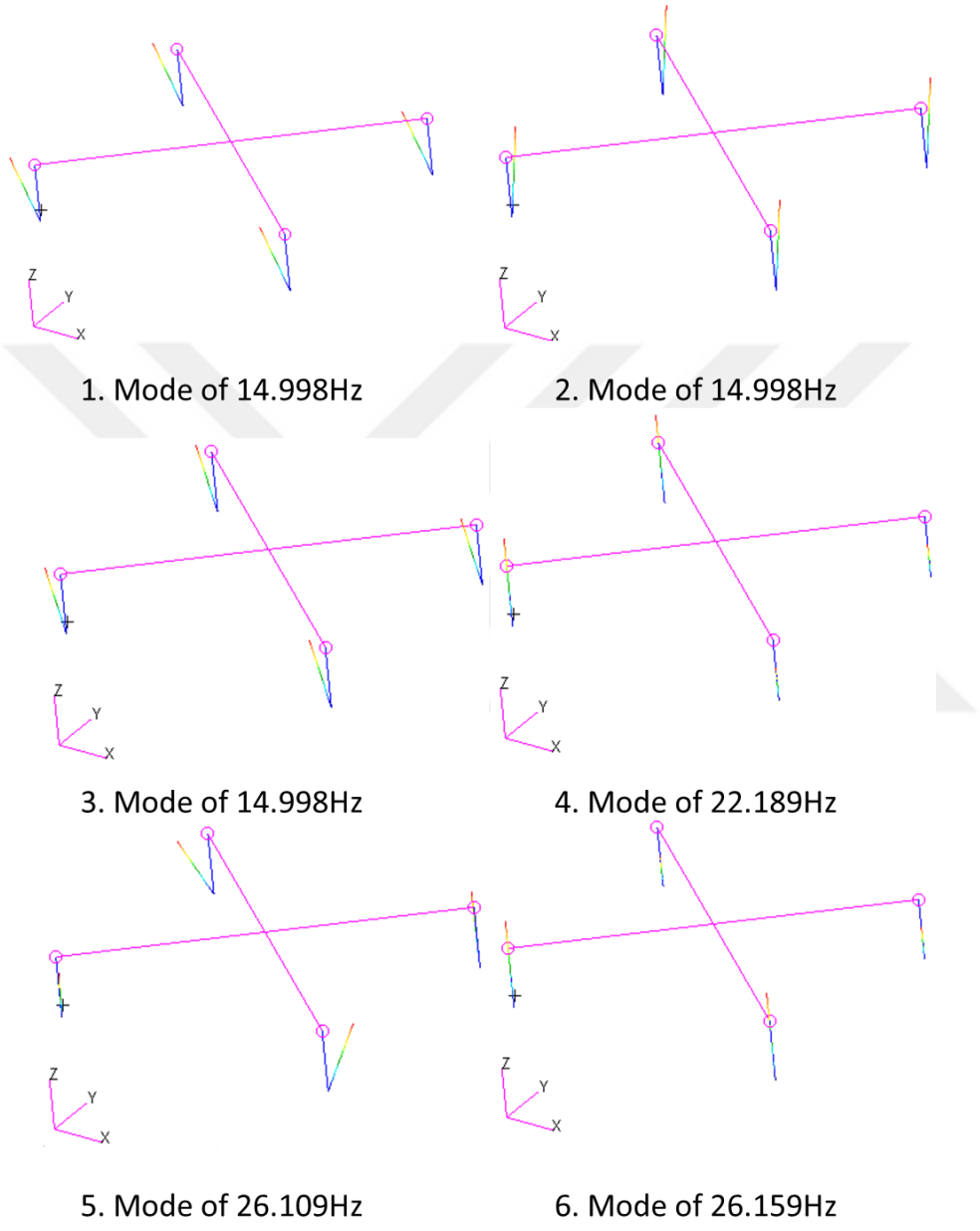

Figure 5.3. Mode Shapes of the FE Model for Sample Isolation System I

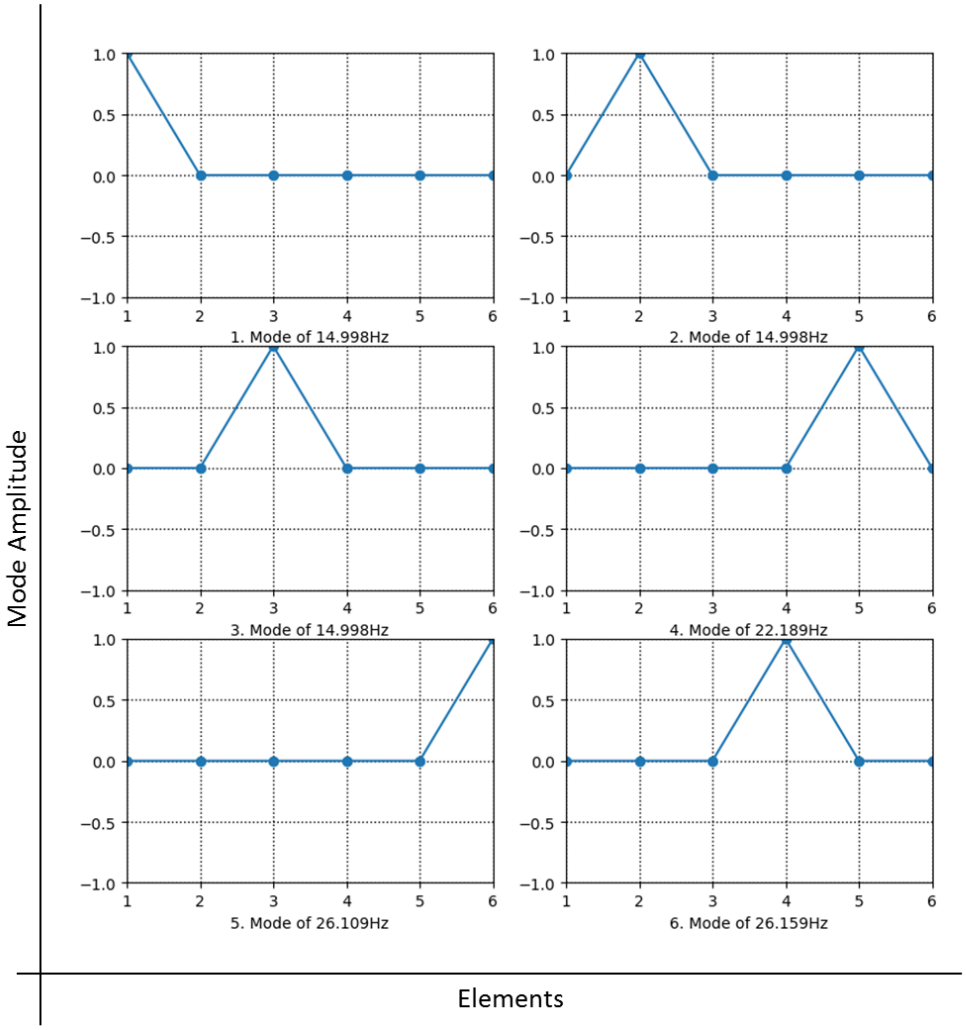

Figure 5.4. Normalized Mode Shapes of the Mathematical Model for Sample Isolation System I

Mode shapes obtained through the mathematical model, which are represented in *Figure 5.4*, are normalized with respect to the maximum mode amplitude. As seen from *Figure 5.4*, mode shapes of the system are completely decoupled. That is, a motion in a certain degrees-of-freedom does not induce the motion in another degrees-of-freedom. Therefore, mode amplitude become maximum at a single DOF and zero at all the other DOFs.

Modal assurance criterion is also applied to visualize the identity extent of the mode sets. Yellow and purples boxes in *Figure 5.5* correspond 1 and 0, respectively. This indicates that MAC values are 100% or that the mode sets of the FE model and mathematical model are identical.

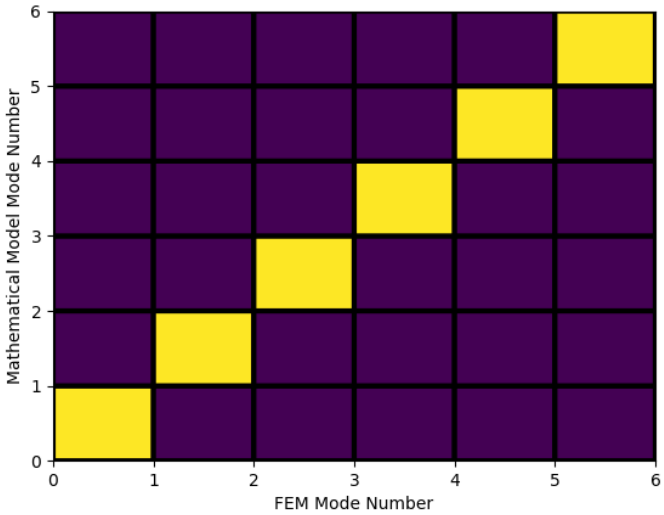

Figure 5.5. Modal Assurance Criterion for Sample Isolation System I

Frequency response analysis of the mathematical model is also to be verified. A random excitation of acceleration spectrum is considered to demonstrate the capability of the theoretical model to execute a frequency response analysis. Acceleration power spectral density function has units of acceleration $\mathbf{g^2/Hz}$ versus frequency **Hz**. In the meantime, acceleration may be expressed in metric units as $\mathbf{(mm/s^2)^2/Hz}$. System is subjected to the constant acceleration of 0.01 g^2/Hz over the entire frequency range as shown in *Figure 5.6*.

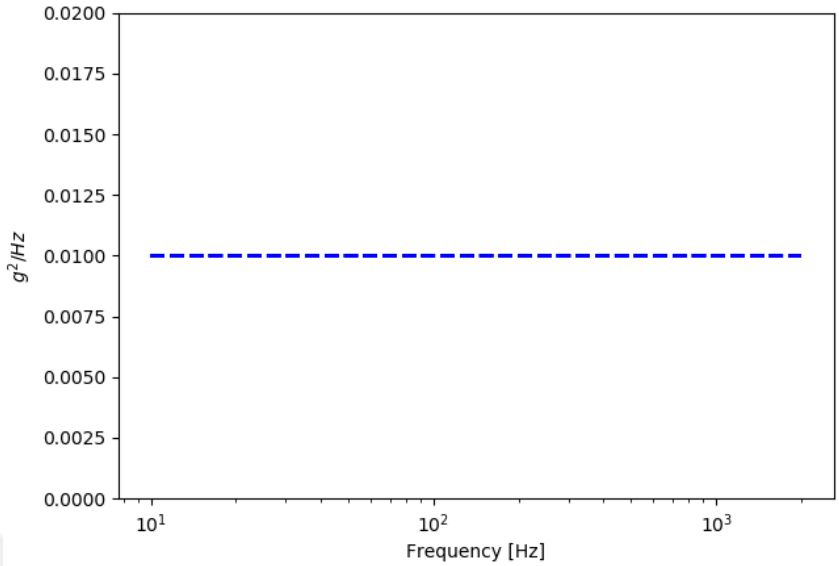

Figure 5.6. ASD Input in Z-Direction for Sample Isolation System I

System response is obtained as acceleration response, velocity response and displacement response for comparison. Frequency response graphs are presented in *Figure 5.7* through *Figure 5.9.*

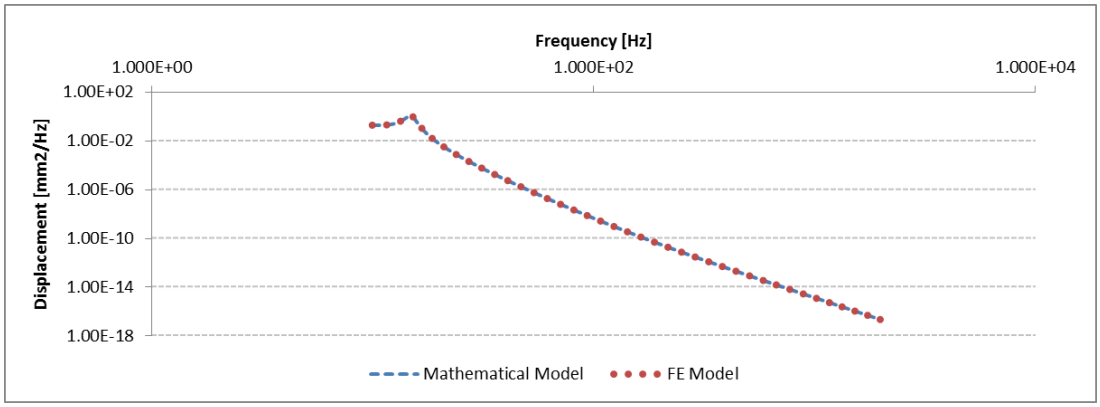

Figure 5.7. Random Frequency Response Comparison for Displacement in Z-Direction for Sample Isolation System I

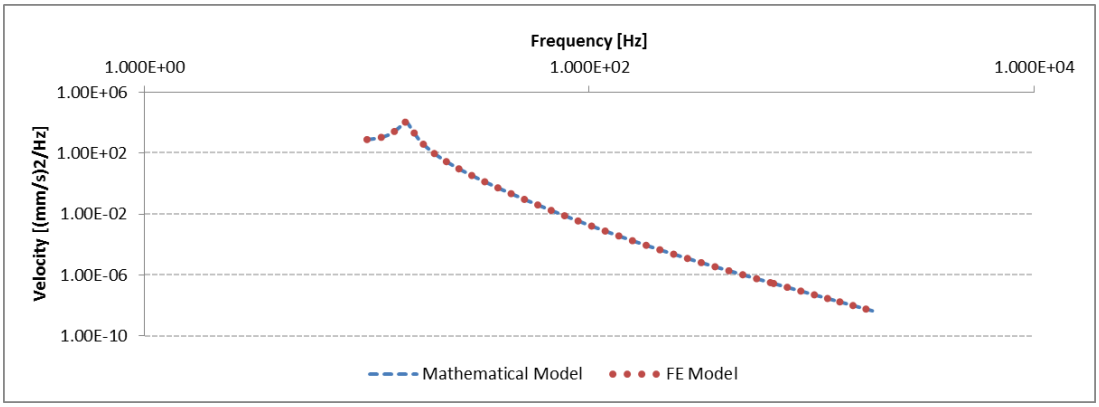

Figure 5.8. Random Frequency Response Comparison for Velocity in Z-Direction for Sample Isolation System I

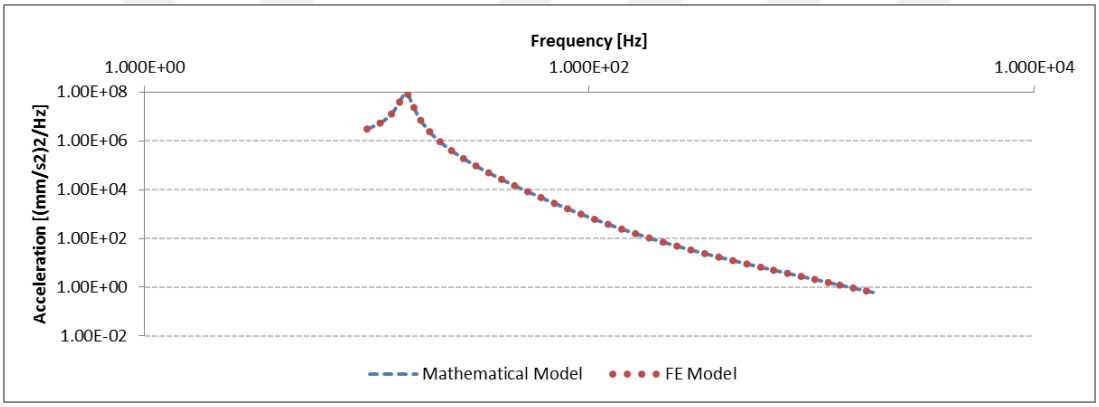

Figure 5.9. Random Frequency Response Comparison for Acceleration in Z-Direction for Sample Isolation System I

Root mean square (RMS) values of response spectrums are compared in *Table 5.7.*

Table 5.7. *RMS Comparison for Sample Isolation System I*

Response		*Degree-of-Freedom*
		Z
Displacement RMS	FEM [mm]	1.774
	DCC [mm]	1.774
	DIFF [%]	0.0

Table *5.7 Continued.*

Velocity RMS	FEM [mm/s]	159.592
	DCC [mm/s]	159.592
	DIFF [%]	0.0
Acceleration RMS	FEM [mm/s2]	14779.08
	DCC [mm/s2]	14779.11
	DIFF [%]	0.0

5.2. Sample Isolation System II

Non-center-of-gravity installation arrangement of pair of two coplanar identical resilient elements with two planes of vibrational symmetry is considered in this example [5]. Isolation subjects to a solid homogeneous rectangular body. Results are obtained through analytical calculations in [5].

Isolation system is shown in *Figure 5.10*. Isolation system properties are given in inertial axis system $\bar{X}\bar{Y}\bar{Z}$, and center-of-gravity and mounting positions are given in global axis system xyz. Mounting orientations of resilient elements are also given with respect to the global axis system xyz.

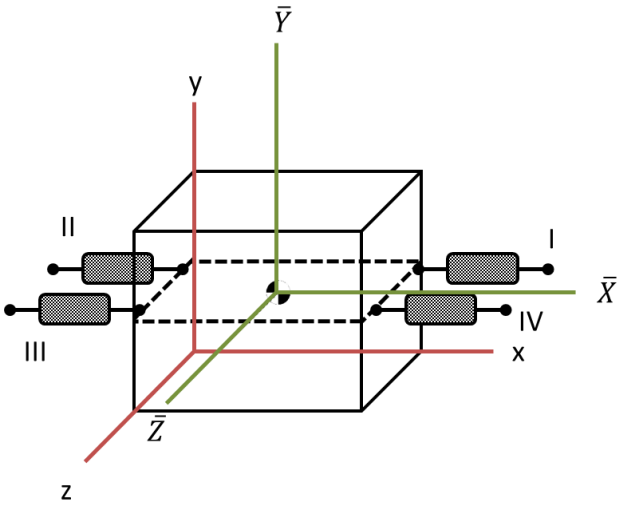

Figure 5.10. Representation of Sample Isolation System II

Positions of center-of-gravity and mounting points beside the directional cosines of mounts and body dimensions are presented in *Table 5.8*.

Table 5.8. *Geometric Texture of Sample Isolation System II*

Parameter	*x [mm]*	*y[mm]*	*z[mm]*	*Directional Cosine*
CG	100.0	25.0	50.0	N/A
Isolator I	135.0	20.0	-5.0	<0,1,0>
Isolator II	45.0	20.0	-5.0	<0,1,0>
Isolator III	15.0	20.0	105.0	<0,1,0>
Isolator IV	185.0	20.0	105.0	<0,1,0>
Body Dimension	200.0	50.0	100.0	N/A

Inertial properties of the isolation system that comprise of mass and mass moments of inertia in principal directions are given in *Table 5.9*.

Table 5.9. *Inertial Properties of Sample Isolation System II*

Component	$m\ [Mg]$	$I_{\bar{X}}\ [Mgmm^4]$	$I_{\bar{Y}}[Mgmm^4]$	$I_{\bar{Z}}[Mgmm^4]$
Body	0.0022271	2.162	9.304	7.719

Elastic properties of resilient elements of the isolation system are presented in *Table 5.10*.

Table 5.10. *Elastic Properties of Sample Isolation System II*

Parameter	K_{axial} *[N/mm]*	K_{radial} *[N/mm]*	ζ_r
Isolator I	4.0	6.0	0.05
Isolator II	4.0	6.0	
Isolator III	8.0	6.0	
Isolator IV	8.0	6.0	

Insofar, all the parameters required for a complete definition of the isolation system are provided. Based on these parameters, FE model is created in the MSC Patran/Nastran® software.

5.2.1. System FE Model

FE Model contains CBUSH elements to represent resilient mounts in the system. Besides, CONM2 element to represent the rigid body by introducing mass and inertia properties is rigidly connected to the CBUSH elements with RBE2 elements in all degrees of freedom. Model generation is performed in the MSC Patran® pre-processor environment.

As the solution sequence, SOL 111 included in the MSC Nastran® analysis solver is employed. Excitation is introduced to the system from the fixed ends of CBUSH elements, which represent the rigid connection points of resilient mounts to the base. Response is measured from the center-of-gravity of the isolated body that corresponds to the position of the CONM2 element.

FE model is shown in *Figure 5.11*.

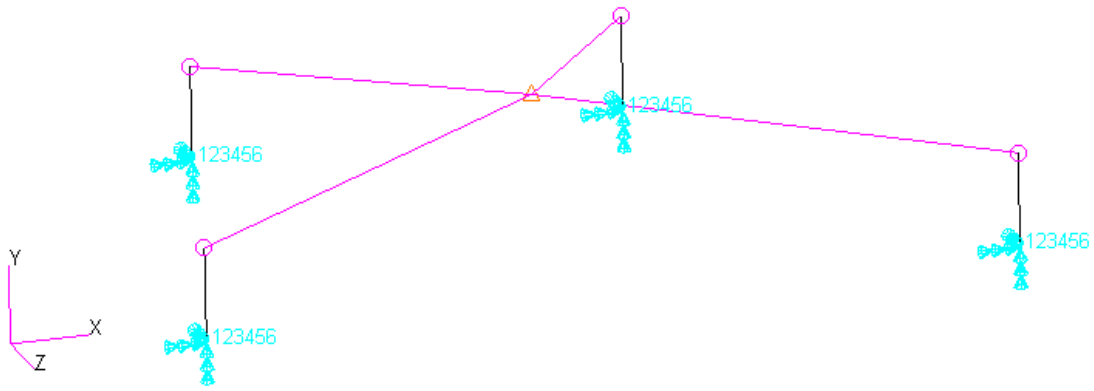

Figure 5.11. Representation of the FE Model for Sample Isolation System II

According to the free vibration analysis results of both FE model and reference application natural frequencies are compared in *Table 5.11*. The results are demonstrated to be in good agreement.

Table 5.11. *Natural Frequency Comparison of Reference [5] & FE Models for Sample Isolation System II*

	Natural Frequency [Hz]		
DOF	*FE Model*	*Reference [5]*	*Difference [%]*
1	15.050	15.050	0.0
2	16.423	16.423	0.0
3	16.471	16.471	0.0
4	21.010	21.010	0.0
5	22.471	22.471	0.0
6	30.048	30.048	0.0

Following the confirmation of that the FE model is created properly by correct definition of mass and stiffness terms, modal property results of the FE model are compared with those of the mathematical model. According to the free vibration analysis results of both the FE model and mathematical model, modal properties are compared in Table 5.12 and Table 5.13.

Table 5.12. *Natural Frequency Comparison of Mathematical & FE Models for Sample Isolation System II*

	Natural Frequency [Hz]		
DOF	*FE Model*	*Mathematical Model*	*Difference [%]*
1	15.050	15.050	0.0
2	16.423	16.423	0.0
3	16.471	16.471	0.0
4	21.010	21.010	0.0
5	22.471	22.471	0.0
6	30.048	30.048	0.0

Table 5.13. *Mode Shapes Comparison of Mathematical & FE Models for Sample Isolation System II*

Natural Frequency [Hz]		*Mode Shapes Constituent*					
		1	*2*	*3*	*4*	*5*	*6*
	FEM	1.1329	-19.6125	-5.2962	-0.1751	0.0052	-0.0386
15.050	DCC	1.1330	-19.6100	-5.2960	-0.1751	0.0052	-0.0386
	DIFF [%]	0.0	0.0	0.0	0.0	0.0	0.0
	FEM	-19.4112	0.7978	-7.9748	-0.0079	0.0111	0.0462
16.423	DCC	19.4100	-0.7978	7.9750	0.0079	-0.0111	-0.0462
	DIFF [%]	0.0	0.0	0.0	0.0	0.0	0.0
	FEM	-7.9181	5.5867	-18.7576	0.0036	0.0265	-0.0096
16.471	DCC	7.9180	-5.5870	18.7600	-0.0036	-0.0265	0.0096
	DIFF [%]	0.0	0.0	0.0	0.0	0.0	0.0
	FEM	2.8703	-2.3441	-0.1096	0.0145	0.0010	0.3543
21.010	DCC	2.8700	-2.3440	-0.1096	0.0145	0.0010	0.3543
	DIFF [%]	0.0	0.0	0.0	0.0	0.0	0.0
	FEM	-0.0084	-0.2206	1.8595	0.0105	0.3265	-0.0014
22.471	DCC	0.0084	0.2206	-1.8600	-0.0105	-0.3265	0.0014
	DIFF [%]	0.0	0.0	0.0	0.0	0.0	0.6
	FEM	-0.0379	-5.1936	-1.4317	0.6569	-0.0039	-0.0175
30.048	DCC	0.0379	5.1940	1.4320	-0.6569	0.0039	0.0175
	DIFF [%]	0.0	0.0	0.0	0.0	0.0	0.0

Result of modal properties show that mathematical model is created properly by correct definition and formulation of mass and stiffness elements. Mode shapes obtained from the FE model and mathematical model are illustrated in *Figure 5.12* and *Figure 5.13*, respectively.

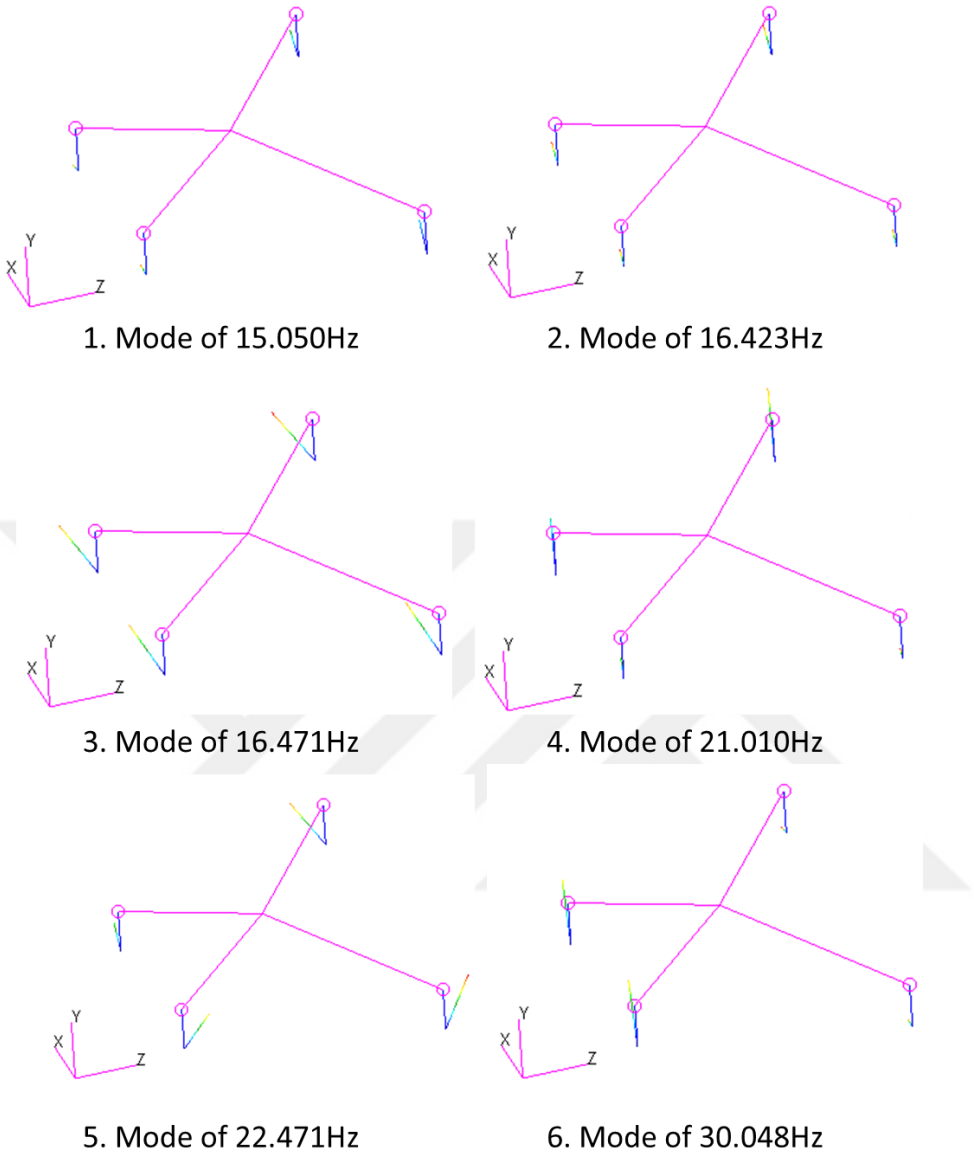

Figure 5.12. Mode Shapes of the FE Model for Sample Isolation System II

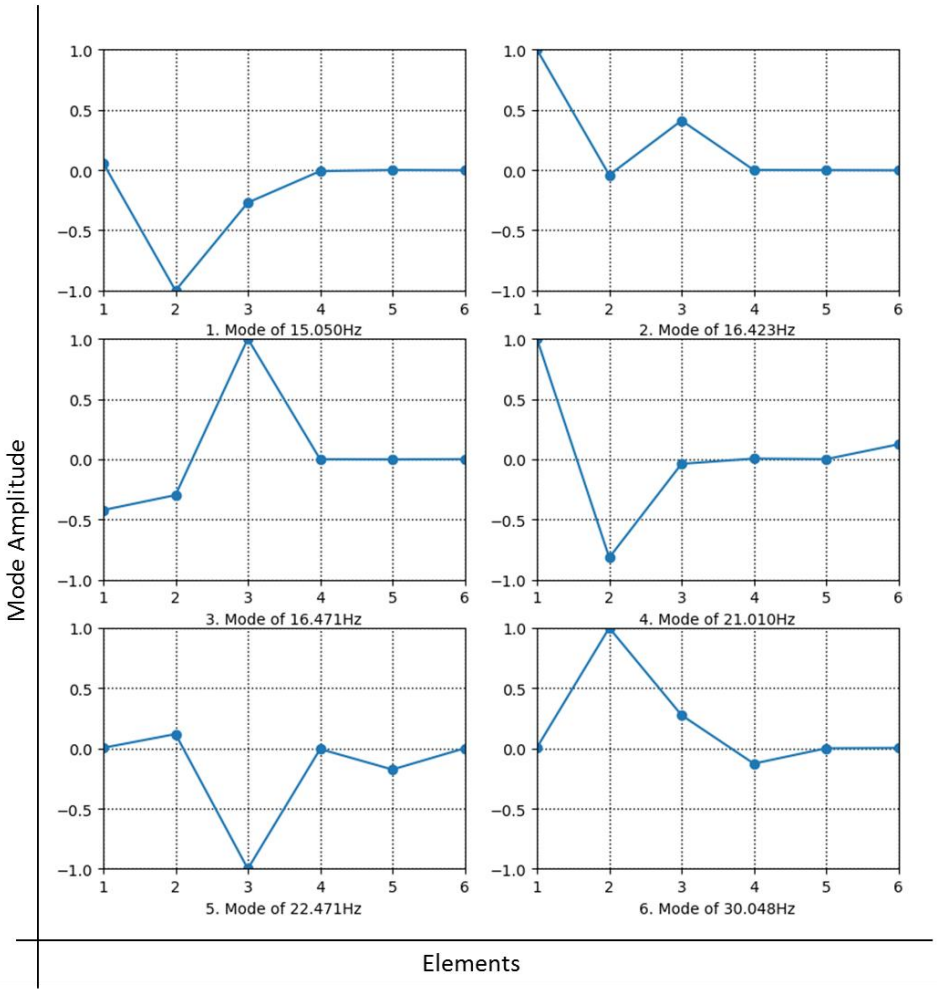

Figure 5.13. Normalized Mode Shapes of the Mathematical Model for Sample Isolation System II

Mode Shapes obtained through the mathematical model, which are represented in *Figure 5.13* are normalized with respect to the maximum mode amplitude. In this system, modes are not completely decoupled. In other words, some modes are coupled; that is, motion in a certain direction induces the motion in another direction. For example, there exist relatively small coupling between the 2nd and 3rd DOFs of the system for the 1st mode. On the other hand, a significant coupling occurs between the

1st and 2nd DOFs of the system for the 4th mode. These couplings appear due to the lack of vibrational symmetry in the system.

Modal assurance criterion is also applied to visualize the identity extent of the mode sets. Yellow and purples boxes in Figure 5.14 correspond 1.0 and 0.0, respectively. Others refers to the intermediate values. This indicates that MAC values are not 100% but the mode sets are nearly similar as already implied in Table *5.13*.

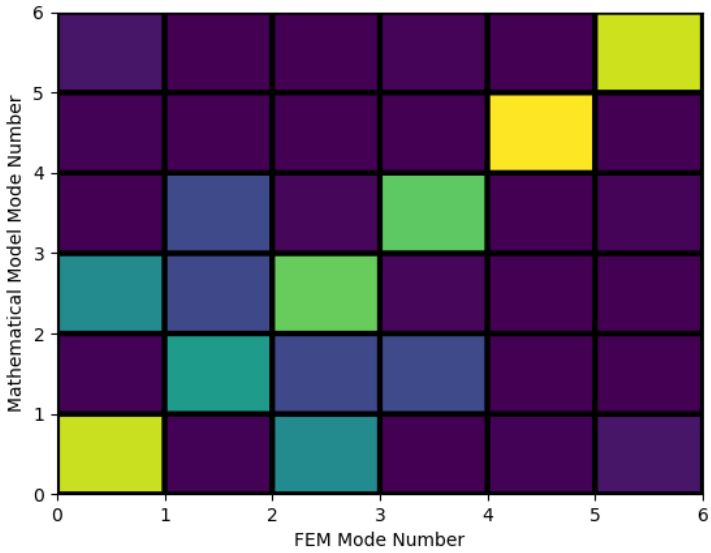

Figure 5.14. Modal Assurance Criterion for Sample Isolation System II

Frequency response analysis of the mathematical model is also to be verified. A random excitation of acceleration spectrum is considered to demonstrate the capability of the theoretical model to execute a frequency response analysis. Power spectral density function of acceleration response has units of acceleration $\mathbf{g^2/Hz}$ versus frequency **Hz**. In the meantime, acceleration may be expressed in metric units as $\mathbf{(mm/s^2)^2/Hz}$. System is subjected to the constant acceleration over the entire frequency range as shown in *Figure 5.15*.

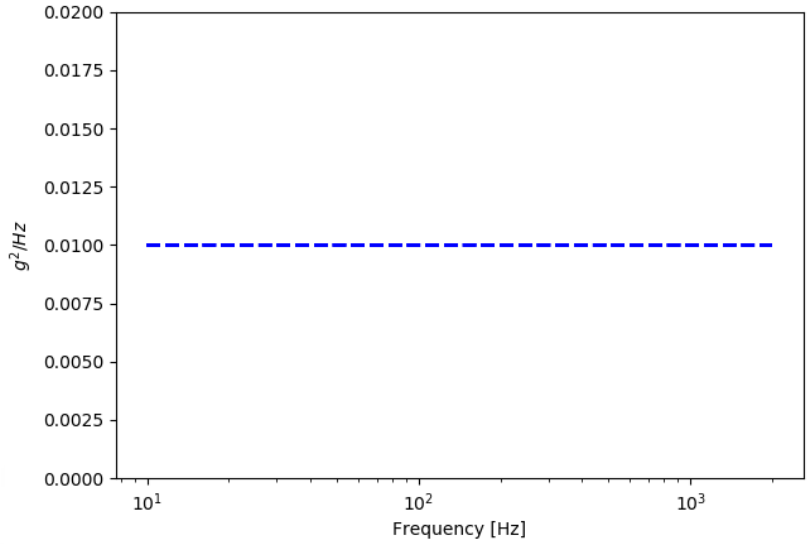

Figure 5.15. ASD Input in Y-Direction for Sample Isolation System II

System response is obtained as acceleration response, velocity response and displacement response for comparison. Frequency response graphs are presented from *Figure 5.16* to *Figure 5.24*.

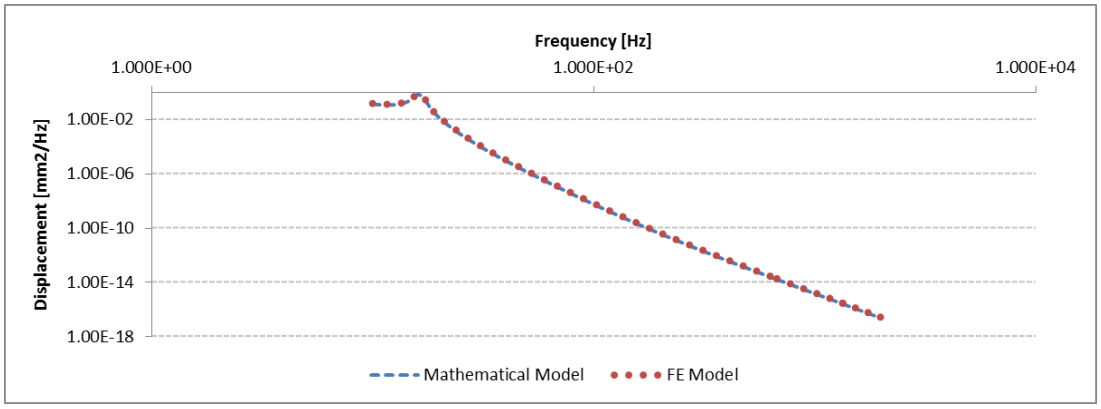

Figure 5.16. Frequency Response Comparison for Displacement in X-Direction for Sample Isolation System II

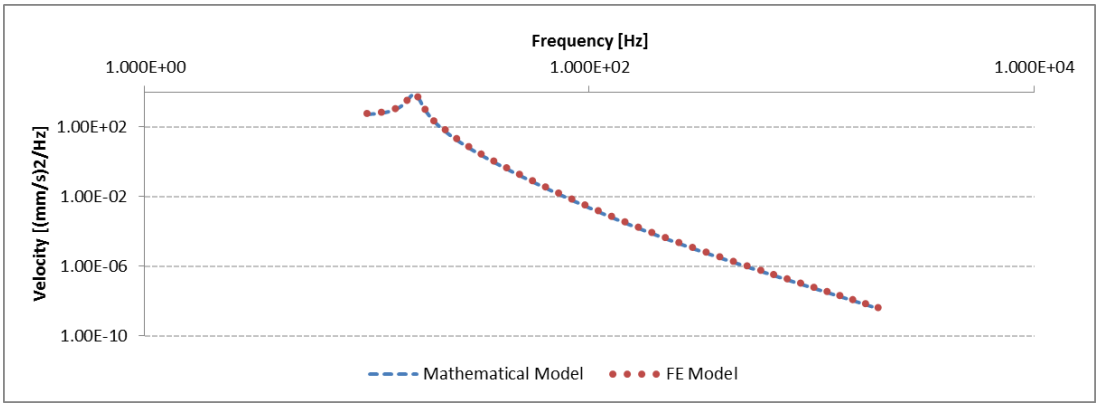

Figure 5.17. Frequency Response Comparison for Velocity in X-Direction for Sample Isolation System II

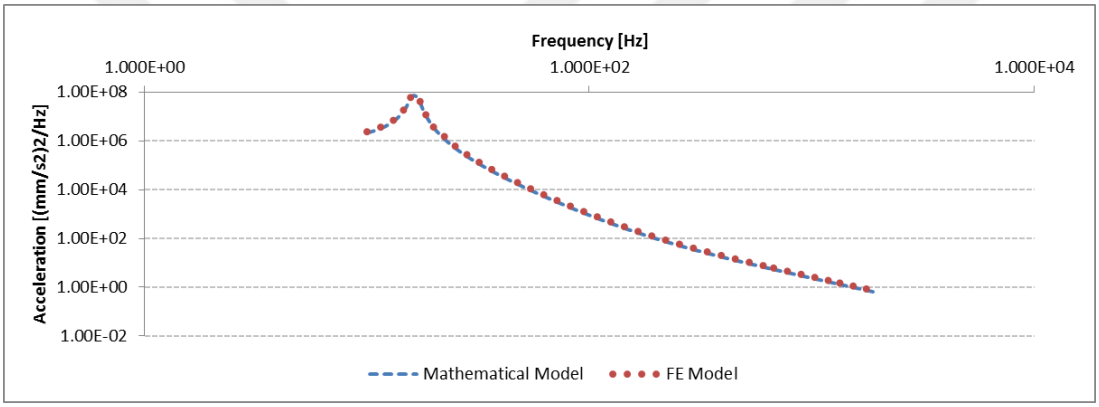

Figure 5.18. Frequency Response Comparison for Acceleration in X-Direction for Sample Isolation System II

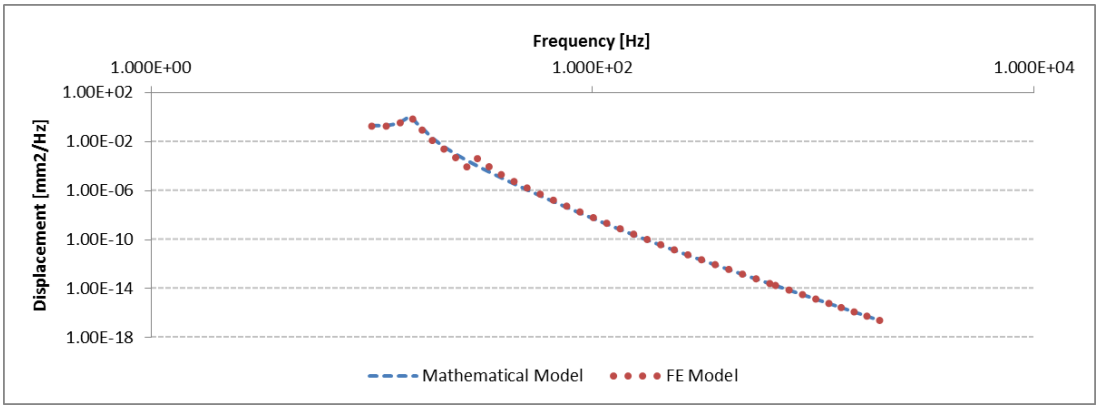

Figure 5.19. Frequency Response Comparison for Displacement in Y-Direction for Sample Isolation System II

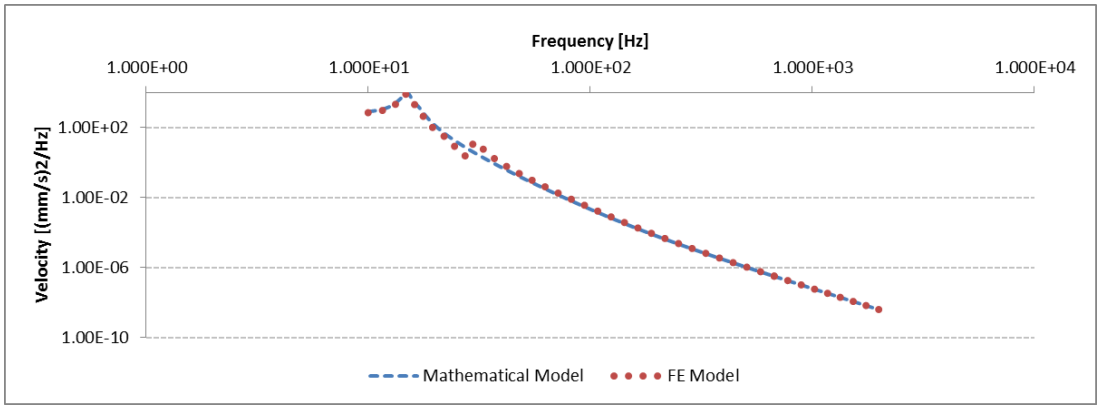

Figure 5.20. Frequency Response Comparison for Velocity in Y-Direction for Sample Isolation System II

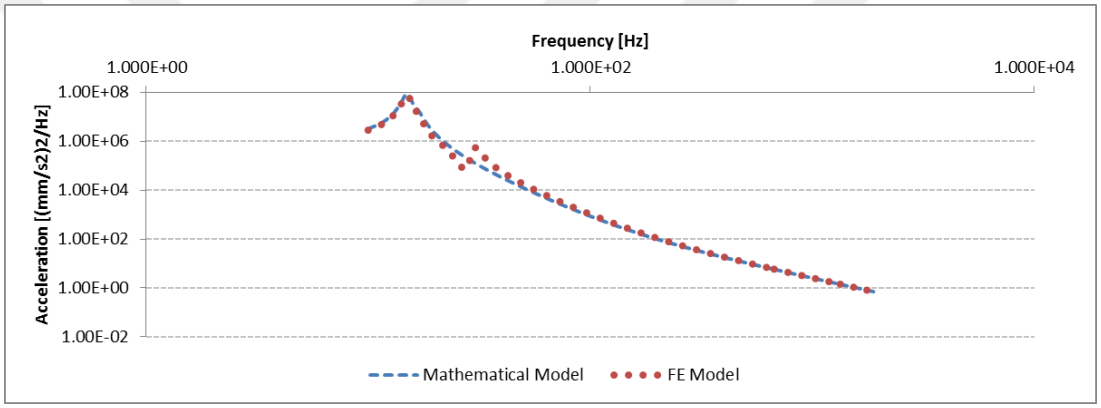

Figure 5.21. Frequency Response Comparison for Acceleration in Y-Direction for Sample Isolation System II

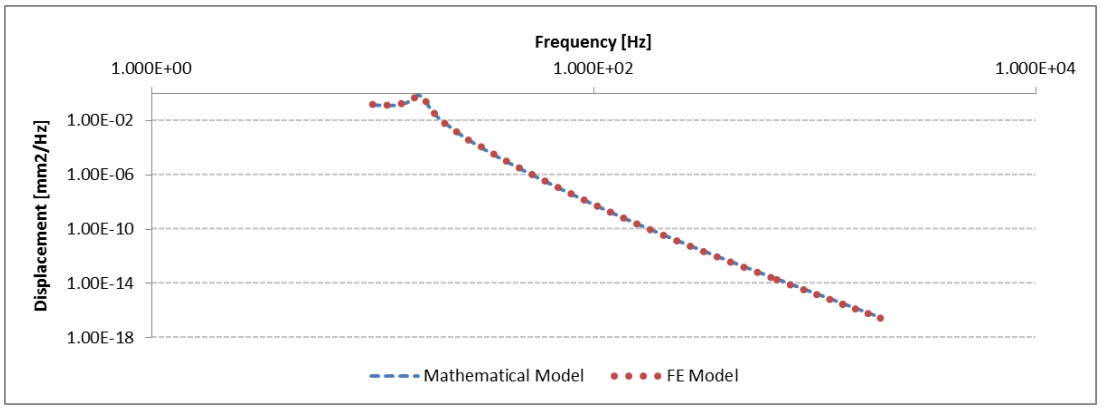

Figure 5.22. Frequency Response Comparison for Displacement in Z-Direction for Sample Isolation System II

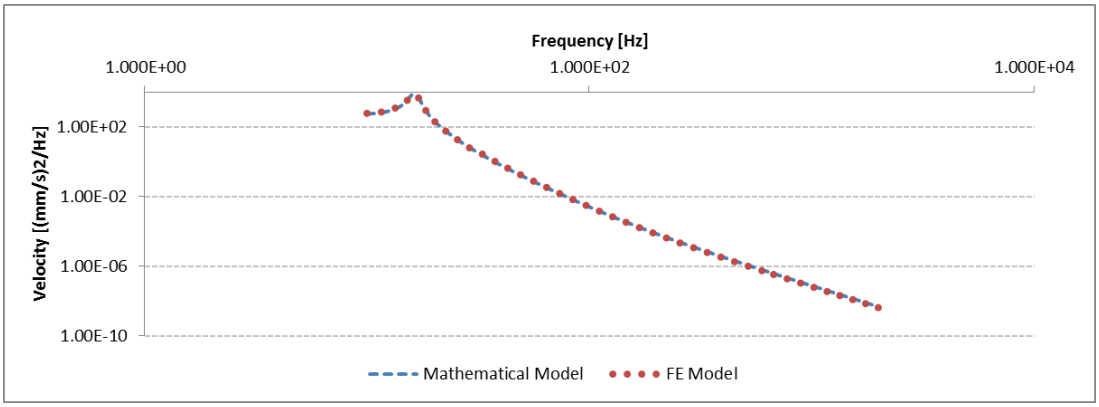

Figure 5.23. Frequency Response Comparison for Velocity in Z-Direction for Sample Isolation System II

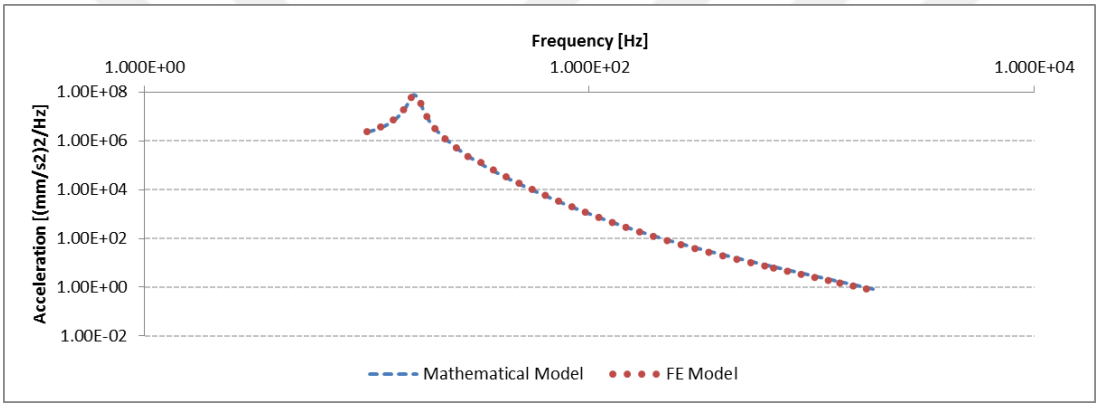

Figure 5.24. Frequency Response Comparison for Acceleration in Z-Direction for Sample Isolation System II

Root mean square (RMS) values of response spectrums are also compared in *Table 5.14.*

Table 5.14. *RMS Comparison for Sample Isolation System II*

Response		*Degree-of-Freedom*		
		X	*Y*	*Z*
Displacement RMS	FEM [mm]	1.551	1.600	1.524
	DCC [mm]	1.481	1.740	1.525
	DIFF [%]	4.5	8.7	0.0

Table *5.14 Continued.*

Velocity RMS	FEM [mm/s]	149.915	143.633	146.745
	DCC [mm/s]	142.903	158.188	146.095
	DIFF [%]	4.3	9.3	0.4
Acceleration RMS	FEM [mm/s2]	15069.180	13355.220	14715.290
	DCC [mm/s2]	14436.930	14763.779	14508.529
	DIFF [%]	4.2	9.7	1.4

In brief, FE models are created to verify the mathematical model by comparing results of vibration analysis. At the very beginning, it is demonstrated that mass and stiffness properties of the FE model are defined properly by comparing natural frequency results of the FE model and a reference study from literature. Once it is ensured that the FE model works properly, modal property results and frequency response results are obtained from the FE model and mathematical model by implementing free vibration and forced vibration analyses. Eventually, it is shown that modal property results are in well agreement such that the mathematical model gives almost the same results with the FE model. Furthermore, frequency response results show some difference up to approximately 10% as the coupling between different modes increase as presented in *Table 5.14* for Y degree-of-freedom. This differentiation can better be observed from *Figure 5.19* to *Figure 5.21*. A discrepancy occurs about the second resonant frequency. On the other hand, frequency response results are almost the same with those of the FE model when there is no coupling between modes.

Hereby, optimization analysis and reliability simulations can be conducted relying on the created mathematical model.

CHAPTER 6

DESIGN OPTIMIZATION AND UNCERTAINTY SIMULATION

6.1. Design Optimization

Optimization is defined as the deal to achieve best results under present conditions. Knowing that structure is to sustain loads so to maintain the structural integrity, structural optimization is defined as a subject of design to maintain the structural integrity in the best means. This best possible way refers to the design objective. Weight, stiffness, critical load, stress, displacement and geometry are the structural performance parameters whose maximization or minimization determines the design objective for structural optimization. Structural performance parameters other than what is specified as design objective are used as design constraints. These constraints bound the design in an intended way for some reasons e.g. manufacturability, affordability, sustainability, practicality, etc. [9][30]

Decision of which optimization method to use is based on the following aspects:

- Whether the final design is of the real optimum or not.
- Rapidity and safety of the convergence
- Amount of computational costs
- Possibilities to extend the method to additional boundary conditions and design variables

Mathematical programming methods rely on gradient information. Gradient-based algorithms are efficient at finding local minima for high-dimensional, nonlinearly constrained, convex problems; however, they are not proper for dealing with noisy and discontinuous functions beside that they are not designed to handle multi-modal problems or discrete and mixed discrete-continuous design variables.

Gradient-based methods (Hill-climbing methods) can be used in the optimization of too many variables and constraints during computers serve. Efficiency in structural optimization is achieved by using approximation techniques.

Optimality criteria methods are heuristic. Heuristic methods are good at dealing with local optima without getting stuck in them while searching for the global optimum unlike the gradient-based methods. However, they come up not necessarily with the real optimum, yet they are able to get many good solutions. Heuristics need high computational time.

Gradient-based algorithms are good in optimizing a small number of continuous parameters. On the other hand, heuristic algorithms are good in optimizing large number of discrete parameters. Historically, it has been argued that mathematical programming methods are unable to solve real (large) problems while optimality criteria methods lack the theory. However, the earlier claim loses its validity as the number of available optimization tools increases [21][14].

Knowledge-based methods are also used in optimization process. Engineer's knowledge and experience can be applied to guide the search for optimum if there is a struggle due to the limited time and so it is not possible to consider many design evaluations. Number of design variables may be diminished taking the most influential design variables into account. Besides, constraints may be rearranged to narrow the design space.

In a successful optimization process, knowledge-based methods should be applied before the local search for optimum. Besides, a global search for optimum, which is based on heuristic methods, should intervene the local search for optimum, which is based on the gradient-based methods. Following the intervention, local search is re-implemented in a different starting point that is determined based on heuristic approach. That is, the strategy to achieve a practical goal is obtaining an approximation to the global optimum with an acceptable amount of computer resources and time.

In this study, an existing optimization algorithm is applied, and no optimization algorithm development methodology is attempted. The "**minimize**" module in the optimization library of "**SciPy**" software of Python is employed as the formal optimization algorithm. Since the problem is relatively basic in the sense of property relations and system connections, mathematical programming methods are applicable and adequate for converging to an optimum which is close to the global optimum result.

6.1.1. Optimization Problem

Optimization problem basically comprises of design variables, design constraints and objective function to be minimized. Each argument of an optimization problem should be determined carefully to obtain a properly designed system. A diagram is shown in *Figure 6.1* for the designated parameters of the optimization problem of this study.

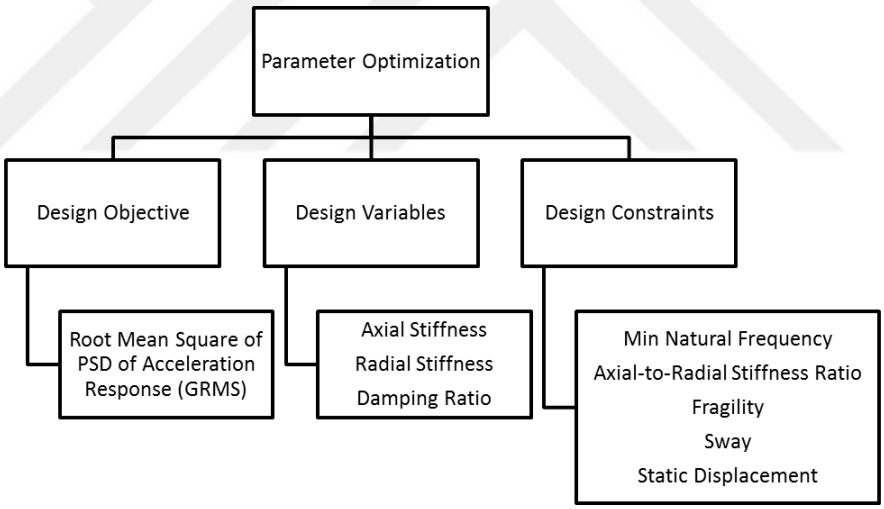

Figure 6.1. Diagram of the Optimization Problem

Mathematically speaking, the optimization problem might be defined by *Equation 6.1*.

$$\begin{aligned} &minimize\ f(x) \\ &subject\ to\ h_i(x) = 0\ i = 1,2,\dots,m \\ &\qquad g_j(x) \leq 0\ j = 1,2,\dots,n \\ &\qquad x_l \leq x \leq x_u \end{aligned} \tag{6.1}$$

6.1.1.1. Objective Function

The objective function is primarily responsible for the performance of an optimization problem. The definition of the objective function and its functional links to the other arguments of the optimization problem decide to the accomplishment of the optimization process [23][32].

The response of the system may be obtained as the mean square of the power spectral density σ^2 as given in Equation 4.26. The objective function is the equally weighted as sum of the root mean square values of the power spectral density of the responses through the body center of gravity in the translational directions. This approach relies on that the objective is settled as a linear function. The root mean square value $\sqrt{\sigma^2}$ refers to the displacement, velocity or acceleration. It can be mathematically stated as in *Equation 6.2* [10].

$$f(x) = \frac{\sqrt{{\sigma_1}^2} + \sqrt{{\sigma_2}^2} + \sqrt{{\sigma_3}^2}}{3} \qquad 6.2$$

6.1.1.2. Design Variables

Design variables may be any among all the parameters that are involved in the system definition. In a vibration isolation problem, isolator properties are the identifying system parameters. They directly affect the isolation performance. Therefore, design variables of the optimization problem are selected as the mount properties in each direction as

- Axial Stiffness
- Radial Stiffness
- Fractional damping ratio

Each design variable is bounded at some lower and upper value. It can be mathematically stated as in *Equation 6.3*.

$$x_i = k_p, k_q, \zeta \qquad 6.3$$

6.1.1.3. Design Constraints

Design constraints have importance in terms of an acceptable design. In other words, design constraints are designated to eventually come up with a plausible and sustainable design. Design constraints are

- Minimum natural frequency to provide for stability
  - $f_{n1} \geq UB$
- Isolator axial to radial stiffness ratio to provide for manufacturability
  - $LB \leq k_1/k_2 \leq UB$
- Maximum load on the isolator to provide for mount strength or fragility
  - $\sqrt{S_i(\omega)} \leq UB$ where S is the acceleration PSD response
- Maximum dynamic displacement or sway to provide for allowable space
  - $\sqrt{S_i(\omega)} \leq UB$ where S is the displacement PSD response
- Maximum static displacement under standard gravitational acceleration to provide for allowable space
  - $\delta_z = [K]^{-1}[M]\{0. \quad 0. \quad 9807. \quad 0. \quad 0. \quad 0.\}^T$ where z is the direction of gravity.

It can be mathematically stated in a more compact form as in *Equation 6.4*.

$$\begin{matrix} h_i(x) = 0 \; i = 1,2, \dots, m \\ g_j(x) \leq 0 \; j = 1,2, \dots, n \end{matrix} \qquad 6.4$$

6.2. Uncertainty Simulation

Reliability is defined as the probability of a product to be satisfactory in the sense of its intended function. In other words, reliability guarantees the prevention of failure in a stochastic base. Traditionally, a design safety factor is chosen to provide for the possible uncertainties. However, it is not adequate unless the variability is not accounted for. That is, the uncertainty should be quantified. It is significantly important to provide for the possible uncertainties and variability. Thus, the essence

of reliability can be understood by quantifying the uncertainty with probabilistic approach.

In this study, reliability is considered to the extent of the determination of the variations of system input parameters. In this way, the effect of the deviations in input parameters on output parameters are investigated. No failure criteria methodology to predict failure is used in this study.

The uncertainty quantification might be realized by characterizing the variable quantities in a collection of identical samples of sufficient amount. Random variables are created to form such a collection to represent the possible outcomes of a measurement. Each variable takes its numerical value depending on the chance of occurrence.

Arithmetic methods are useful for the computation of data values. Measures of central tendency and dispersion are the arguments of the arithmetic methods. The arithmetic mean, the median and the mode are the measures of central tendency. The range, the average deviation, and the variance are the measures of dispersion. There exists a variety of probability distribution models to generate random variables to be used in simulation analyses. These models are basically classified into two main categories which are namely the continuous and discrete distributions. In this study, continuous distribution is considered for convenience in the sense of the comprehension of basic concepts. Most common continuous distributions are normal distribution, uniform distribution, Cauchy distribution, exponential distribution, Weibull distribution, lognormal distribution, gamma distribution, etc.

Central limit theorem states that the distribution of random variables is close to the normal distribution if adequate number of measurements is provided. In this way, this theorem explains that many physical events can be approximately represented by normal distribution. Based on this, normal or Gaussian distribution is employed in this study.

The uncertainty quantification process is completed by specifying statistical interval (SI) to contain the margin of error. Among statistical intervals, confidence interval is appropriate for this study as it contains the proportion of each specimen that exceeds an indicated threshold value for the sampled population [37].

6.2.1. Markov Chain Monte Carlo Simulation

Monte Carlo simulation method for the system reliability analysis is based on the sets of random variables for the system parameters. Basic steps in the Monte Carlo simulation might be itemized as follows:

- Designate the definitive system parameters
- Determine the reference probability distribution model for each designated parameter
- Build probability density function (PDF) for each designated parameter
- Assign random values to the random variables of each designated parameter according to the determined PDFs
- Execute a deterministic analysis with the simulated model

Reliability analysis is implemented through the simulation of random variables with a certain type of distribution function. As previously mentioned, a normal distribution is assumed for all parameters as many physical phenomena can be described by this type of distribution according to the central limit theorem Normal distribution function requires two sample characteristics, namely the mean and standard deviation.

For reliability analysis, deviating parameters of the system model are primarily determined. Deviation amounts are specified for each parameter separately to find the upper and lower limits. Besides, a statistical interval should be designated for the system parameters to quantify the uncertainty as previously mentioned. Two-sided value of standard deviations of 3.29, 3.92 and 5.15 corresponding to the confidence interval (**CI**) levels of 90%, 95% and 99% are provided as options in this study [26].

Mean (**μ**) is calculated as the average of the upper and lower limits, which are indicated as p_{upper} and p_{lower}, respectively. Standard deviation (**SD**) can be selected among previously defined standard deviation values corresponding to specific confidence interval levels. Therefore, normal distribution parameters are completely defined.

$$\mu = \frac{p_{upper} + p_{lower}}{2} \qquad 6.5$$

Simulation results of response parameters are also manipulated before statistical inference. They are quantified in terms of uncertainty by stating a confidence level. Thus, outliers of sample data are removed. The confidence intervals correspond to 3-sigma rule of the normal distribution as shown in *Figure 6.2*. Two-sided standard deviations of 1, 2 and 3 corresponding to the two-sided confidence interval levels of 68.27%, 95.45% and 99.73% are provided as options in this study depending on the 3-sigma rule [26].

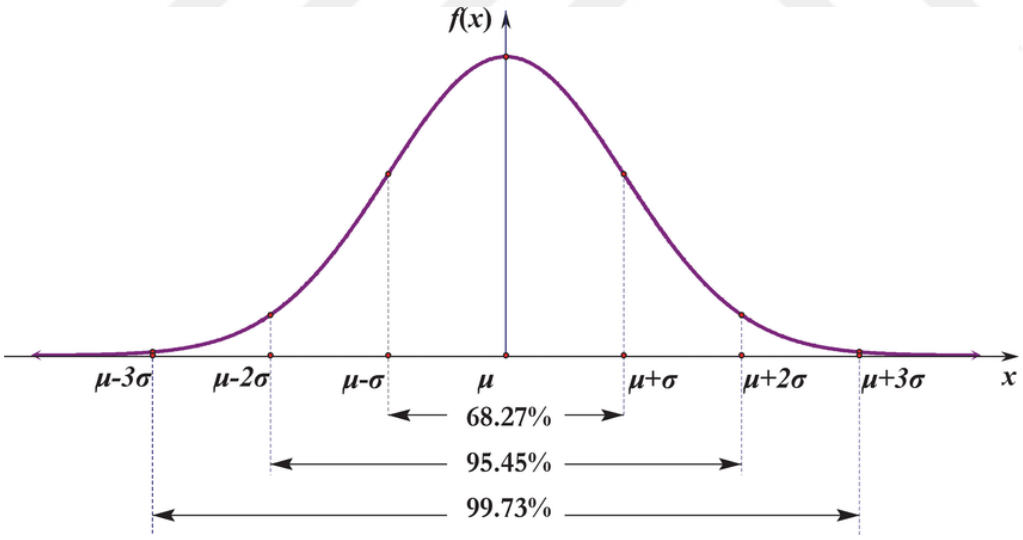

Figure 6.2. 3-Sigma Rule

In this study, followings are selected as the illustrative system parameters to be considered as the input variables of the simulation process, which are also presented in *Figure 6.3*:

- Stiffness coefficient
- Damping ratio
- Mounting position
- Mounting orientation

Besides, response parameters to be investigated depending on the deviating system parameters are

- Natural frequency
- Static deflection
- Dynamic response

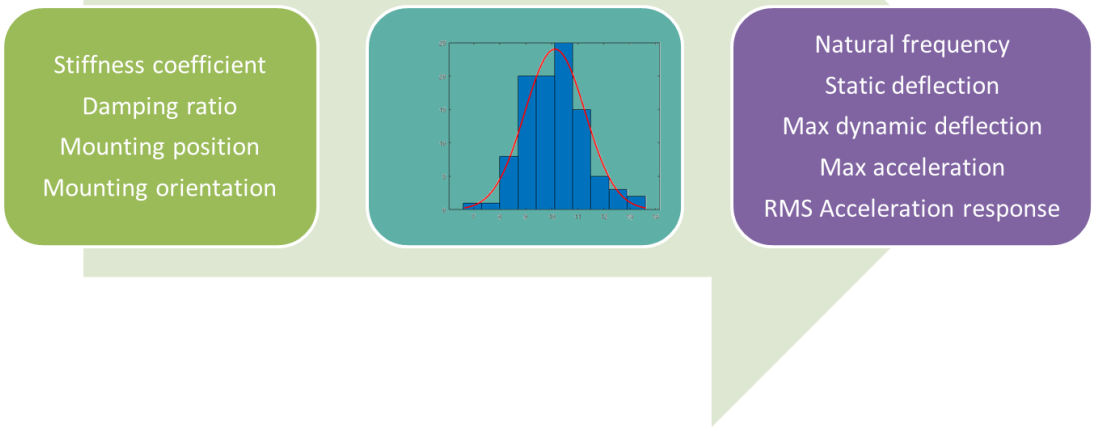

Figure 6.3. Simulation Parameters

CHAPTER 7

CASE STUDY

In this chapter, a complete analysis of airborne electronic equipment which is placed on isolator mounts will be implemented. This entire process comprises of vibration analysis, optimization analysis and reliability analysis. In the case study, bottom installation of mounts as one of the mostly applied mounting arrangements is considered. Root-mean-square of transmitted acceleration obtained through frequency response analysis is tried to be minimized during the optimization analysis. Eventually, deviation of system input parameters from their nominal values is simulated via reliability analysis, and parameters with violated design limits are determined. This study demonstrates the capability of the developed tool to design a safe isolation system at optimum.

7.1. Isolation System Definition

A fictitious case study is created through fabricated equipment properties and design constraints. Purpose of the case study is proving the entire analysis process by suggested methods through the developed computer code. A random avionics line-replaceable-unit (LRU) situated in the avionics bay of front fuselage of a fighter aircraft is assumed to be isolated from the harsh environment during mission flight. An avionics LRU is exemplified in *Figure 7.1*.

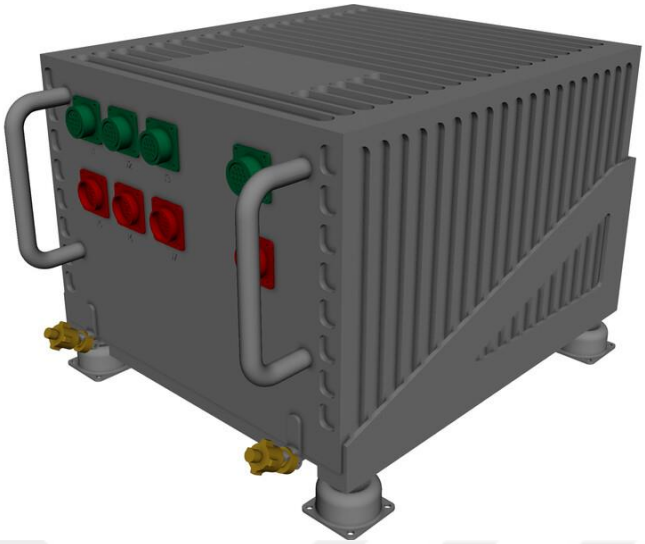

Figure 7.1. Representative CAD Model of Avionics LRU

Bottom installation arrangement of four coplanar identical resilient elements with no vibrational symmetry is considered in this case study. Isolation subjects to a solid non-homogeneous body.

Isolation system is shown in *Figure 7.2*. Isolation system properties are given in inertial axis system $\bar{X}\bar{Y}\bar{Z}$, and center-of-gravity and mounting positions are given in global axis system xyz. Mounting orientations of resilient elements are also given with respect to the global axis system xyz.

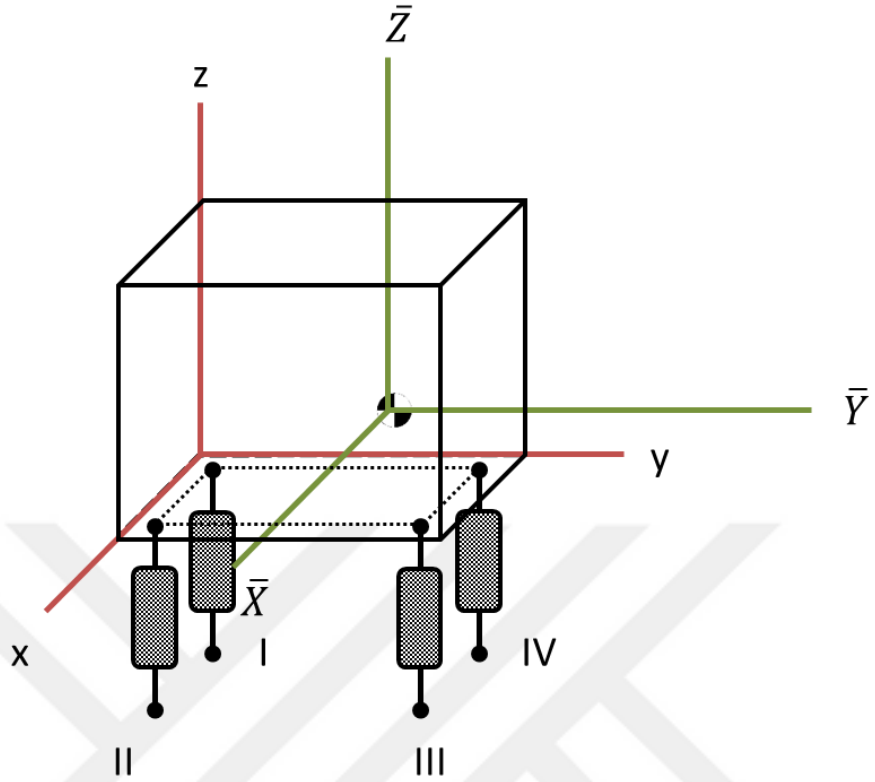

Figure 7.2. Representation of the Isolation System for Case Study

Positions of center-of-gravity and mounting points beside the directional cosines of mounts and body dimensions are presented in *Table 7.1* and in *Figure 7.3*.

Table 7.1. *Geometric Texture of the Isolation System for Case Study*

Parameter	*x [mm]*	*y[mm]*	*z[mm]*	*Directional Cosine*
CG	79.50	85.68	179.92	N/A
Isolator I	3.0	3.0	0.0	<0,0,1>
Isolator II	315.0	3.0	0.0	<0,0,1>
Isolator III	315.0	272.05	0.0	<0,0,1>
Isolator IV	3.0	272.05	0.0	<0,0,1>
Body Dimension	318.00	257.05	269.88	N/A

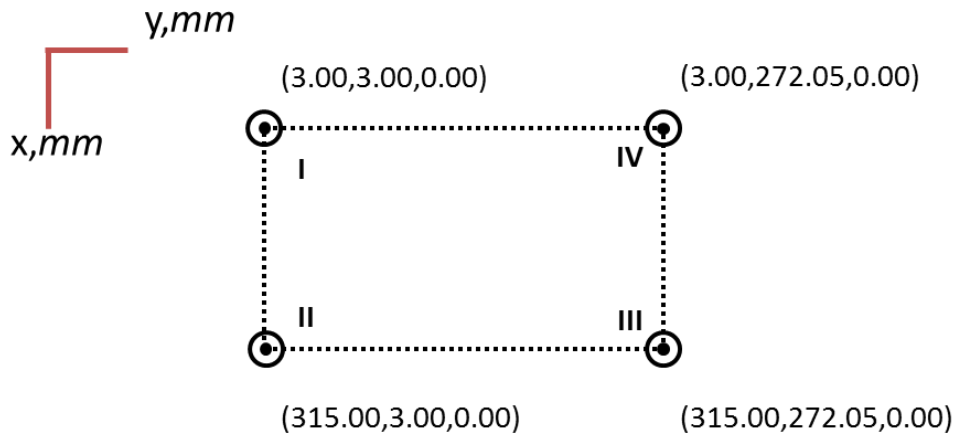

Figure 7.3. Geometric Texture of the Isolation System for Case Study

Inertial properties of the isolation system that comprise of mass and mass moments of inertia in principal directions are given in *Table 7.2*.

Table 7.2. *Inertial Properties of the Isolation Systems for Case Study*

Component	$m\ [Mg]$	$I_{\bar{X}}\ [Mgmm^4]$	$I_{\bar{Y}}[Mgmm^4]$	$I_{\bar{Z}}[Mgmm^4]$
Body	0.040	617.3888	913.6021	883.5668

Elastic properties of resilient elements of the isolation system are presented in *Table 7.3*.

Table 7.3. *Elastic Properties of the Isolation System for Case Study*

Parameter	K_{axial} *[N/mm]*	K_{radial} *[N/mm]*	ζ_r
Isolator I	30.0	25.0	0.05
Isolator II	30.0	25.0	
Isolator III	30.0	25.0	
Isolator IV	30.0	25.0	

In so far, all the parameters required for a complete definition of the isolation system are provided.

7.2. Vibration Analysis

Normal modes analysis gives the system natural frequencies as presented in *Table 7.4*.

Table 7.4. *Natural Frequencies*

DOF	*Natural Frequency [Hz]*
1	8.016
2	8.536
3	15.505
4	19.203
5	28.277
6	31.272

Mode shapes of the isolation system are presented in *Figure 7.4*. Modes are coupled such that motions in different degrees-of-freedom come out simultaneously. Especially, translational motions in 1st and 2nd degrees-of-freedom seem to be highly coupled in the 4th mode shape. Modes coupling develops due to the any missing vibrational symmetry. Figure coincides the expected results since the created model has no vibrational symmetry.

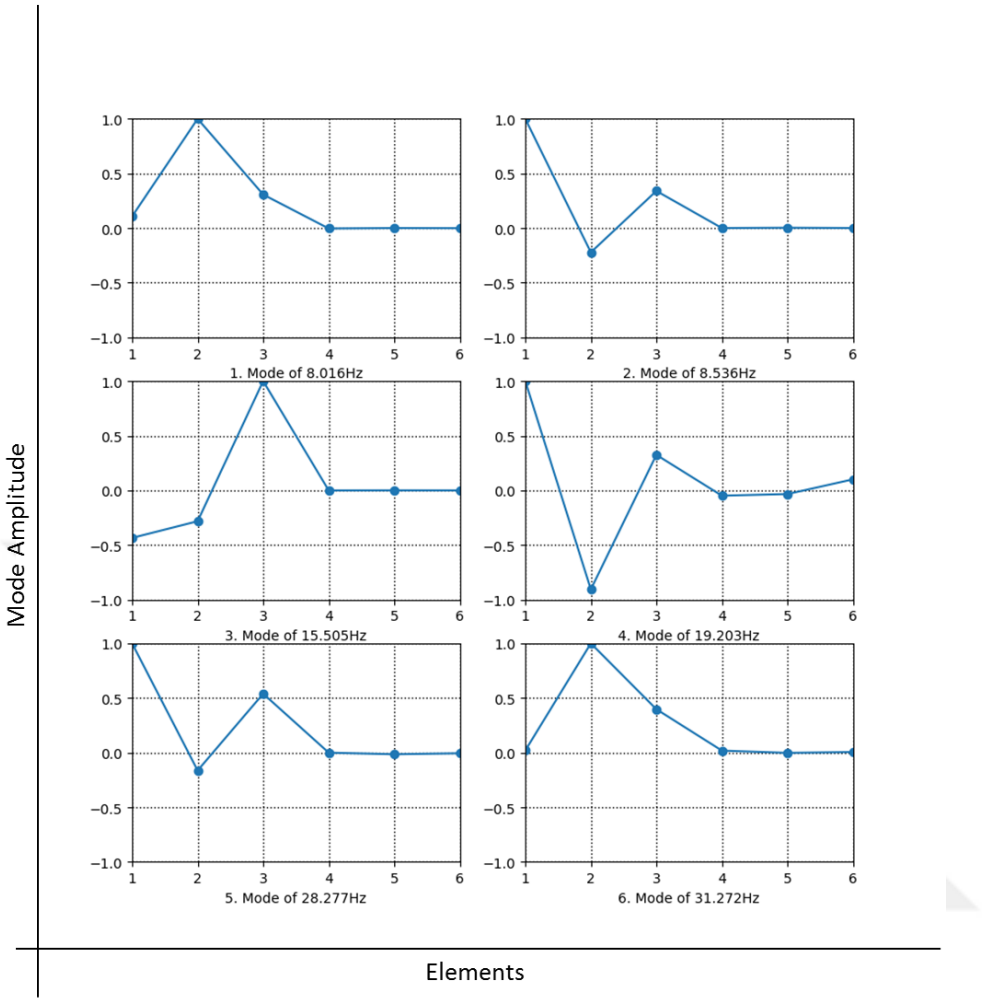

Figure 7.4. Mode Shapes

Transmissibility functions for all degrees-of-freedom are shown in *Figure 7.5*. As expected, transmissibility peaks in translational directions are far greater than those in rotational directions. T_{11}, T_{22} and T_{33} refer to the transmissibility functions in translational degrees-of-freedom, and T_{44}, T_{55} and T_{66} refer to the transmissibility functions in rotational degrees-of-freedom.

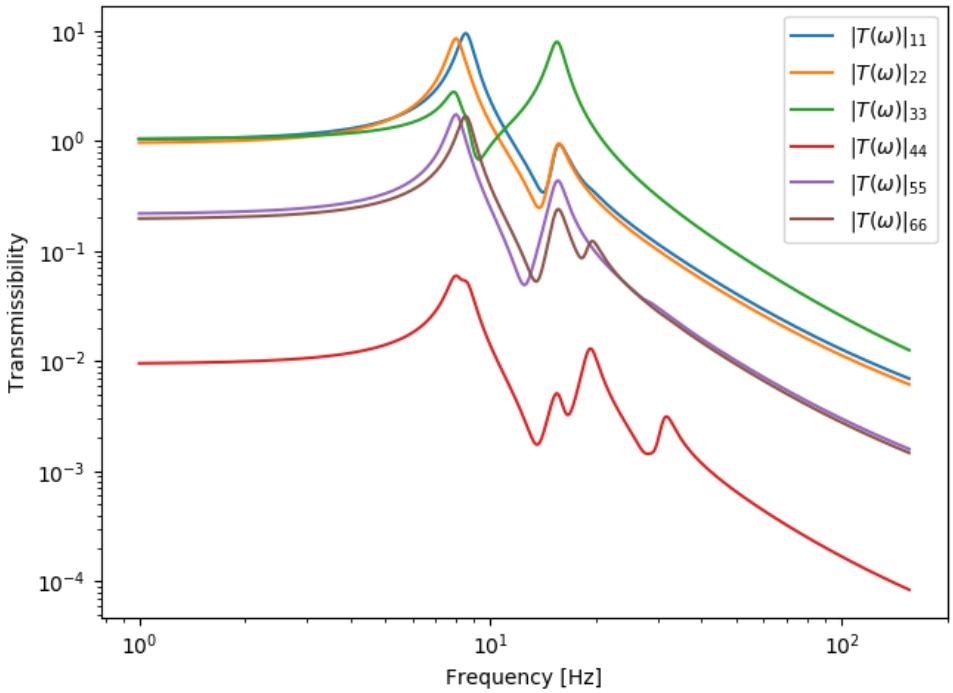

Figure 7.5. Transmissibility Functions

Acceleration response of the system to the base excitation given in *Table 4.2*, which represents the vibration exposure of jet aircrafts, is presented in *Figure 7.6*. Power spectral density of acceleration response in three translational degrees-of-freedom, which refer to the maximum amplitudes, are shown in this figure. The trends in the curves in *Figure 7.6* agrees with those in *Figure 7.5* as expected. Maximum acceleration response values exist at resonant points. Root mean square value of the area under the power spectral density of acceleration response curve is also presented in *Figure 7.7* for translational degrees-of-freedom. Power spectral densities of acceleration responses in 1st and 2nd degrees-of-freedom are close to each other as seen in *Figure 7.6*. The blue line for the 1st degree-of-freedom is slightly above the orange line for the 2nd degree-of-freedom. On the other hand, the green line for the 3rd degree-of-freedom follows considerably a superior course. Therefore, the root mean square

values of areas under the power spectral density curves of acceleration responses ensue from these trends.

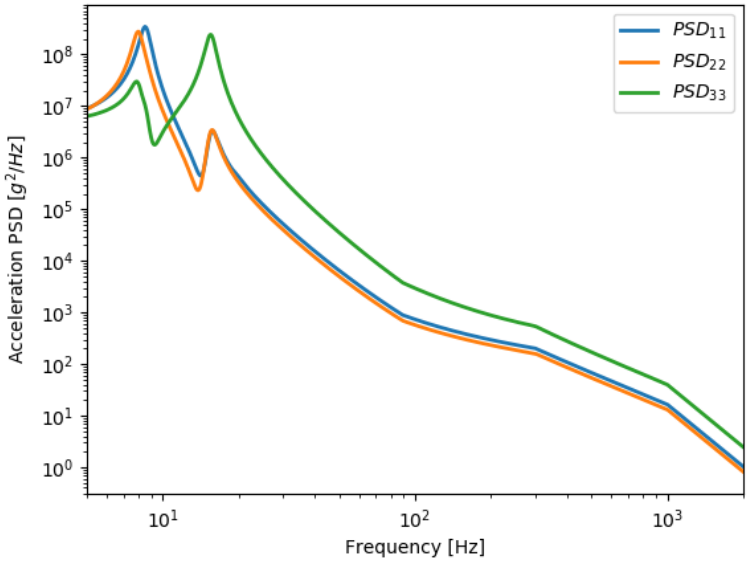

Figure 7.6. Power Spectral Density of Acceleration Response

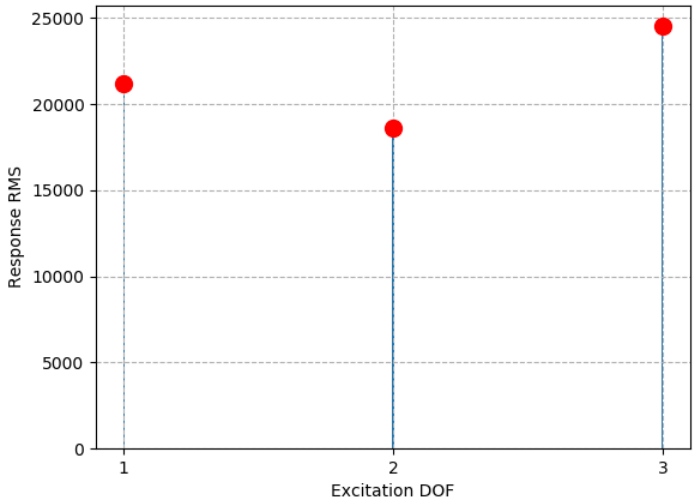

Figure 7.7. RMS of the Power Spectral Density of Acceleration Response

In the same manner, power spectral density of velocity response is obtained. Velocity response of the system to the base excitation, which represents the vibration exposure of jet aircrafts, is presented in *Figure 7.8*. The root mean square value of the area under the power spectral density of velocity response curve is also presented in *Figure 7.9* for translational degrees-of-freedom. It is worth emphasizing that the response rms value in 1st and 2nd degrees-of-freedom become higher than that in 3rd degree-of-freedom. According to *Figure 7.5*, the resonant point in 3rd degree-of-freedom appear at higher excitation frequency compared to the first two degrees-of-freedom. Recalling that the velocity response can be derived from the acceleration response by dividing the acceleration term by corresponding excitation frequency, amplification at higher-frequency resonance will be reduced more than amplification at lower-frequency resonance. Therefore, even the trends are more similar within a specific degree-of-freedom for different response parameters, it exhibits significant changes between different degrees of freedom for the same response parameter.

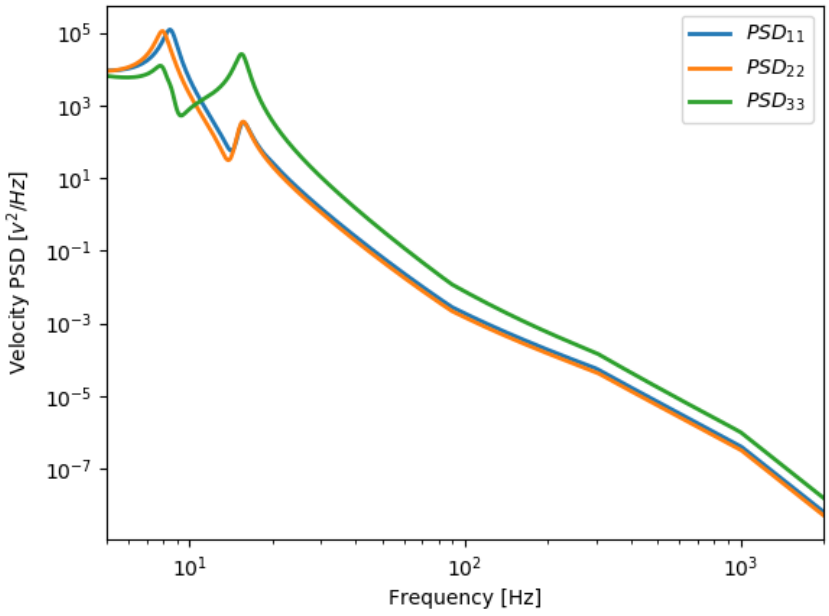

Figure 7.8. Power Spectral Density of Velocity Response

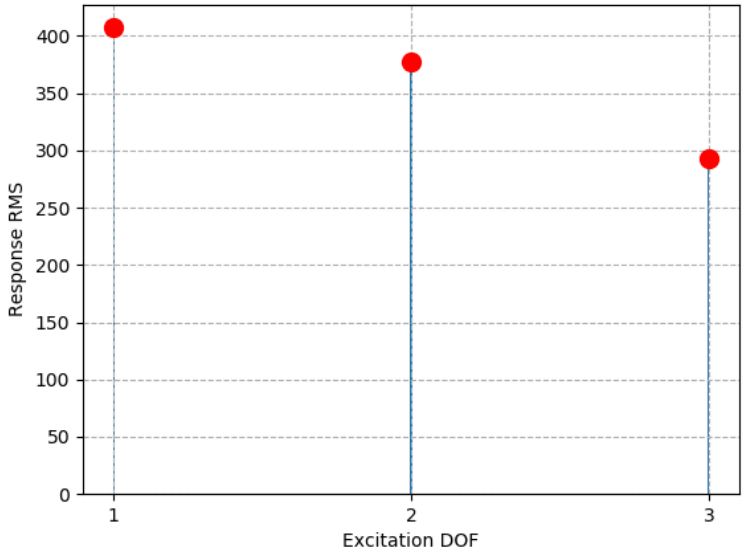

Figure 7.9. RMS of the Power Spectral Density of Velocity Response

Displacement response of the system to the base excitation, which represents the vibration exposure of jet aircrafts, is presented in *Figure 7.10*. The root mean square value of the area under the power spectral density response of displacement curve is also presented in *Figure 7.11* for translational degrees-of-freedom. The order of magnitude of first two degrees-of-freedom does not change but becomes closer since the superior one has slightly higher excitation frequencies at resonant points. On the other hand, the rms value for the 3rd degree-of-freedom becomes further smaller since displacement response is obtained by dividing the acceleration by square of the corresponding excitation frequency.

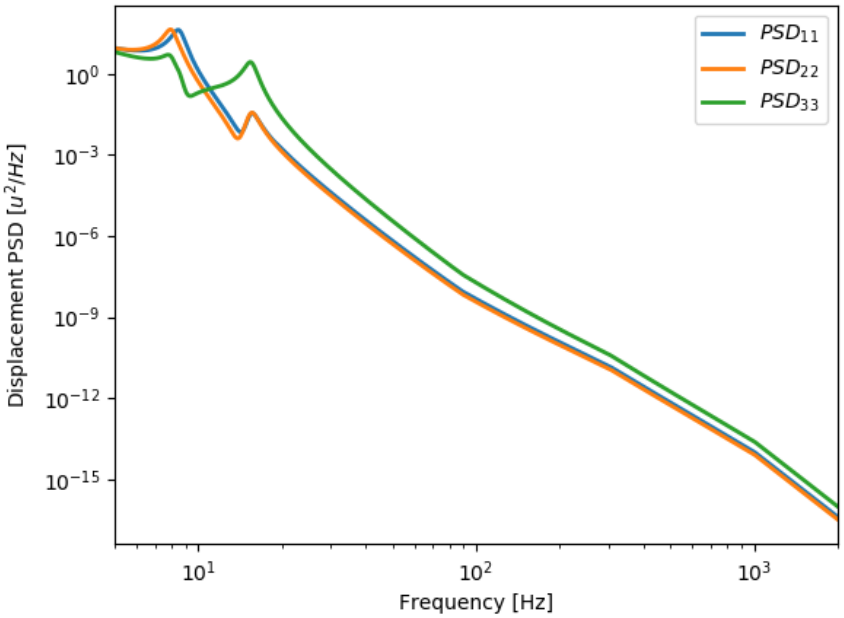

Figure 7.10. Power Spectral Density of Displacement Response

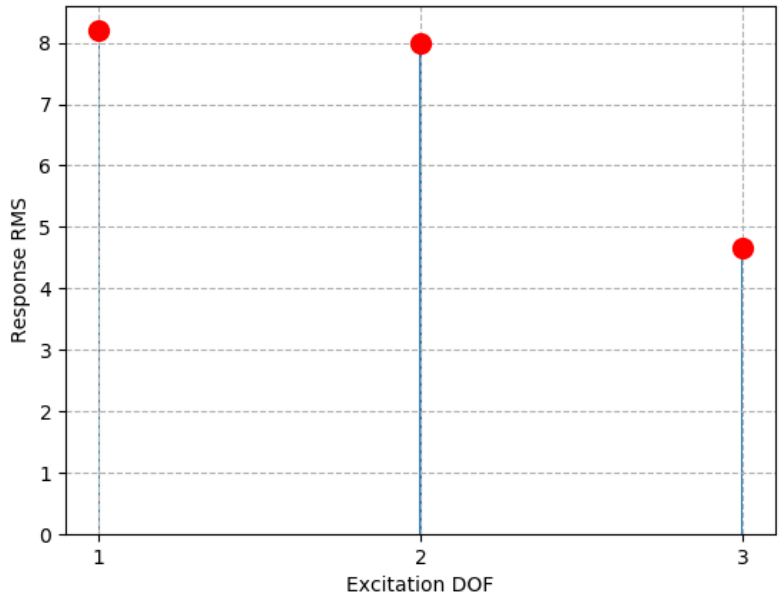

Figure 7.11. RMS of the Power Spectral Density of Displacement Response

7.3. Optimization Analysis

Stiffness and damping of the system are varied to minimize the transferred acceleration from base to the equipment. During the optimization process, constraints are applied to the system to create a physically meaningful and reasonable model. Formal definition of the optimization problem is provided in *Table 7.5* and *Table 7.6*.

Table 7.5. *Design Variables*

Variable	*Initial Value*	*Lower Bound*	*Upper Bound*
Axial Stiffness k_1 [N/mm]	100	50	240
Radial Stiffness k_2 [N/mm]	80	50	240
Damping Ratio ζ [-]	0.05	0.005	0.3

Table 7.6. *Design Constraints*

Constraint	*Lower Bound*	*Upper Bound*
Axial-to-Radial Stiffness Ratio [-]	1.2	1.6
Minimum Natural Frequency [Hz]	5	-
Maximum Acceleration [mm/s^2] in X,Y and Z directions	-	29421. (3g)
Maximum Dynamic Displacement [mm] in X,Y and Z directions	-	3
Maximum Static Displacement [mm] in X,Y and Z directions	-	2

Final values obtained from optimization analysis are presented in *Table 7.7*.

Table 7.7. *Final Values from Optimization Analysis*

Parameter	*Initial*	*Final*	*% Change*
Axial Stiffness k_1 [N/mm]	100.0	70.74	29.3
Radial Stiffness k_2 [N/mm]	80.0	58.95	26.3
Damping Ratio ζ [-]	0.05	0.3	500.0
Axial-to-Radial Stiffness Ratio [-]	1.25	1.20	4.0
Minimum Natural Frequency [Hz]	8.016	6.781	15.5
Maximum Acceleration [$mm/s^2/Hz$]	18637.06	3840.06	79.4
Maximum Dynamic Displacement [mm/Hz]	6.62	2.649	60.1
Maximum Static Displacement [mm]	1.381	1.952	41.3
RMS ASD [mm/s^2]	**21431.86**	**9132.62**	**57.4**

Considerable reduction in the transferred acceleration is obtained through the optimization analysis. Basically, system resilient elements are tried to be made softer to reduce the transferred vibration to the equipment to isolate it from the harsh environment. The stiffness variable and damping ratio variable are supposed to be enforced to get lower and upper bounds, respectively. However, the constraints on the system because of several reasons such as the system stability, design space limits, etc. interfere with this fact. Therefore, optimization analysis gives a great chance to determine to the optimum properties of the system. It is also worth noting that system constraints to be provided to the optimization problem should be determined properly. Otherwise, results might be fallacious. Transmissibility functions of the optimized system are shown in *Figure 7.12*. The peaks in the curves seem to reduce significantly at the resonant points. In this way, the overall value of the response rms is considerably reduced.

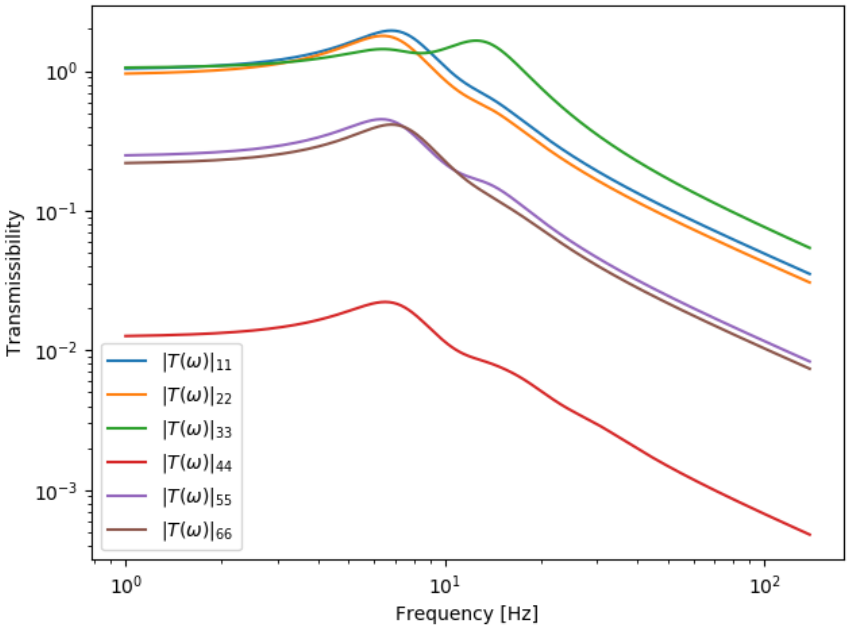

Figure 7.12. Transmissibility Functions of the Optimized System

Acceleration spectral density responses for initial and optimum systems are given in *Figure 7.13* through *Figure 7.15*. The reduction of the peak amplitude can be easily recognizable. As a fact of passive isolation theory, an effective isolation at the entire frequency range cannot be achieved. This can be observed from the response figures such that the response curve of the optimized system is above the response curve of the initial system on contrary to the relative course at resonant frequencies.

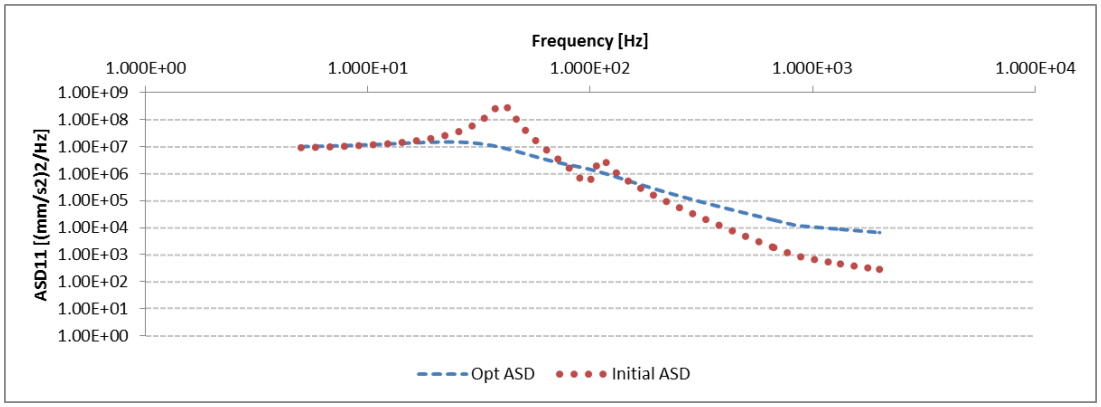

Figure 7.13. ASD_{11} Response for Initial & Optimum System

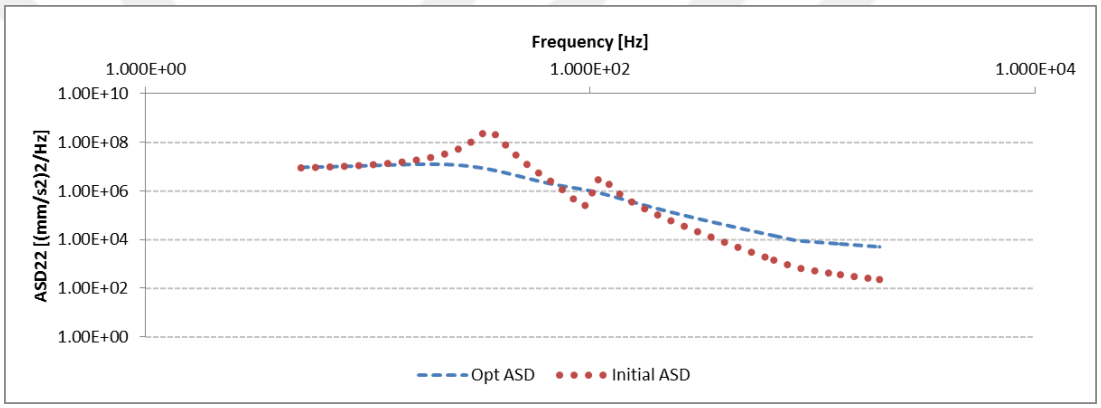

Figure 7.14. ASD_{22} Response for Initial & Optimum System

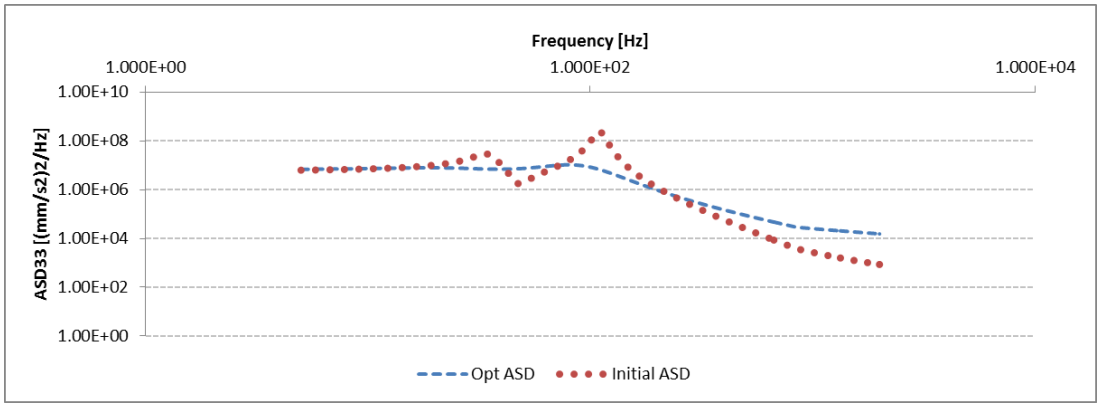

Figure 7.15. ASD_{33} Response for Initial & Optimum System

7.4. Monte Carlo Simulation

Following the optimization analysis, system parameters are simulated considering both input and output values. Simulation is based on the possible deviations of the input parameters from their nominal values as previously mentioned. At first, simulation setup for the input parameters is presented in *Table 7.8*.

Table 7.8. *Simulation Inputs*

Type of Travel	*Deviation*	*Distribution*	*Confidence Interval [%]*	*Simulation Number*
Stiffness *[%]*	5.0	Normal	95	1000
Damping Ratio *[%]*	10.0	Normal	95	
Mounting Position [mm]	3	Normal	95	
Mounting Orientation [Cosine]	0.035	Normal	95	

Axial stiffness, radial stiffness and damping ratio are common for all the mounts in the system. On the other hand, mount installation position and location may differ for each single one. Therefore, system parameters of stiffness and damping are simulated for each mount commonly while mounting position and orientation parameters are simulated for each resilient element separately. Simulation results of input parameters are presented in *Figure 7.16* through *Figure 7.25*. The occurrence numbers are normalized in these figures such that the area under the distribution fit curve with dashed red line becomes unit.

In these figures, mean values can be recognized to be the assumed nominal values for each parameter. The fit curves in red bring the normal distribution forward. Since the resilient elements of the system are assumed to have common axial stiffness, radial stiffness and damping ratio, these parameters are simulated once as seen in *Figure 7.16* and *Figure 7.17*. On the other hand, installation positions in three translational

directions are respectively simulated for each resilient element as seen from *Figure 7.18* to *Figure 7.21*. In the same manner, each member of directional cosine vectors for installation orientation are respectively simulated for each resilient element as seen from *Figure 7.22* to *Figure 7.25*.

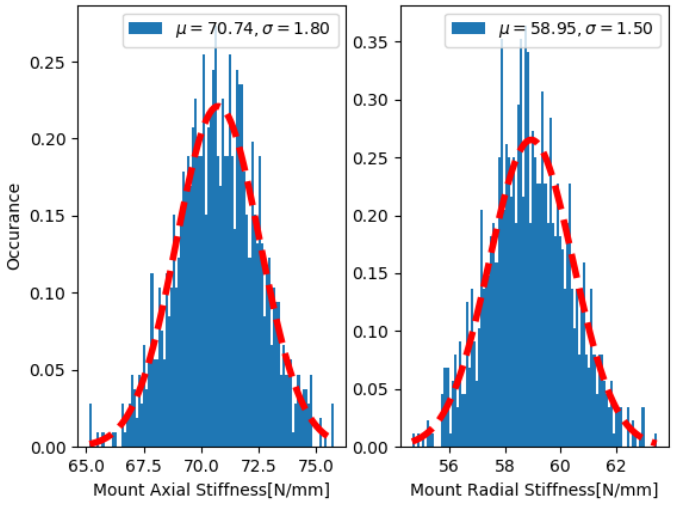

Figure 7.16. Mount Stiffness Simulation

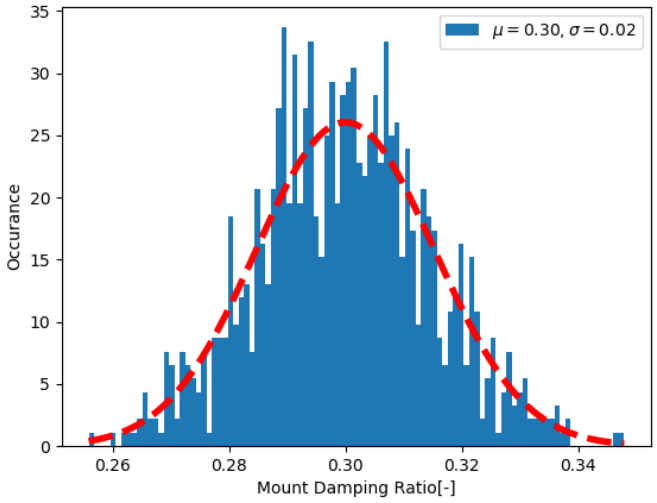

Figure 7.17 Mount Damping Ratio Simulation

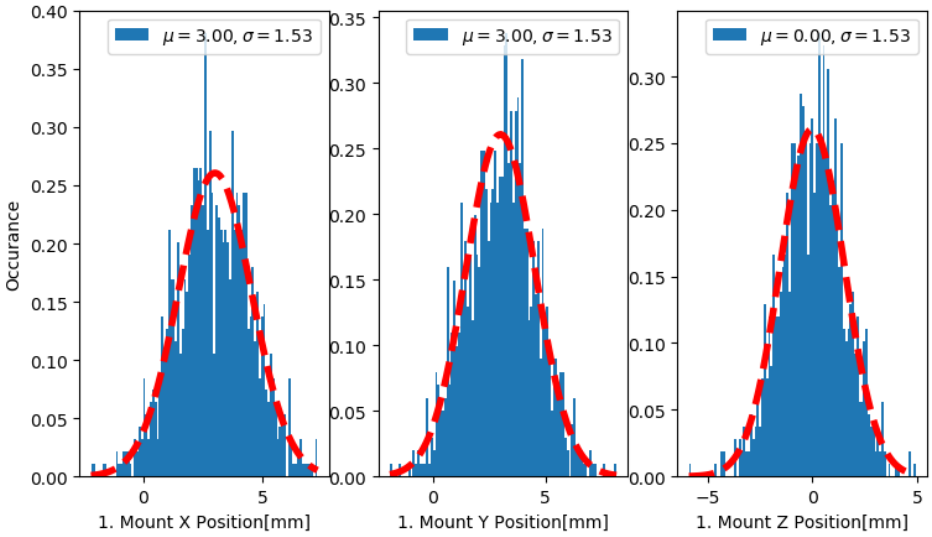

Figure 7.18. 1st Mount Installation Position Simulation

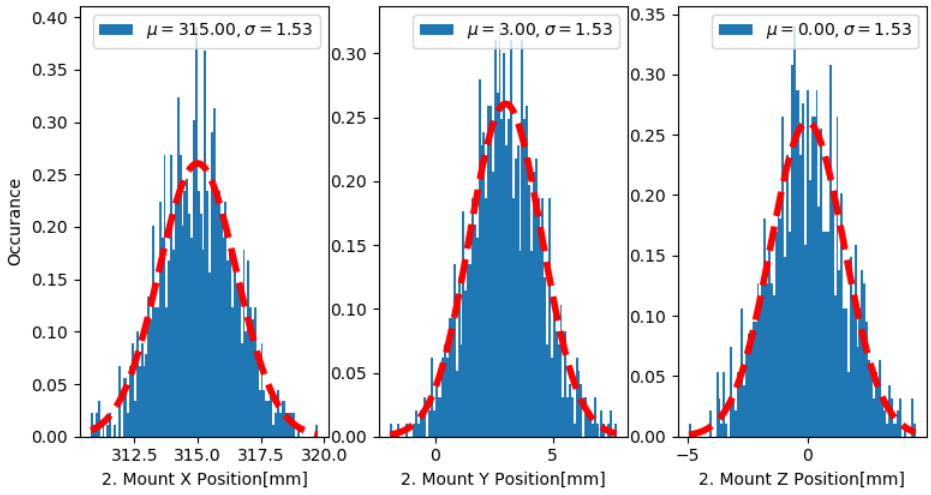

Figure 7.19. 2nd Mount Installation Position Simulation

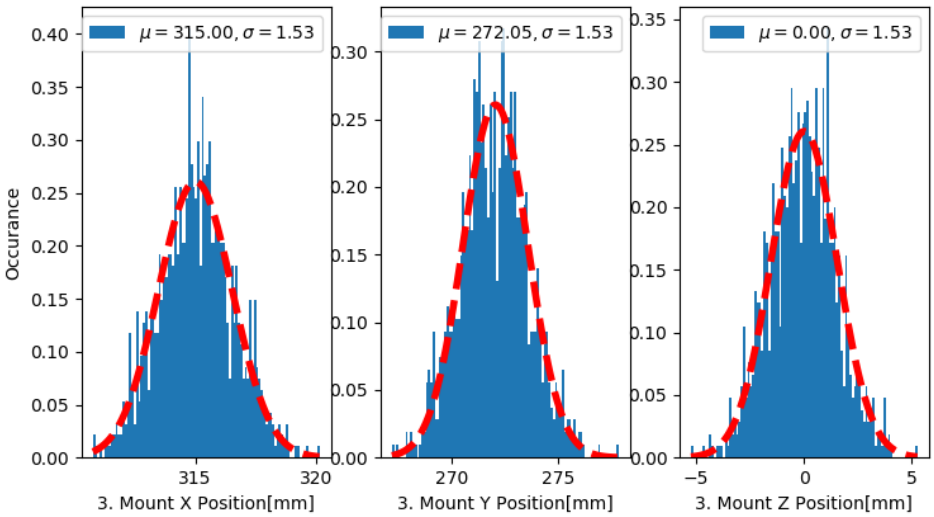

Figure 7.20. 3rd Mount Installation Position Simulation

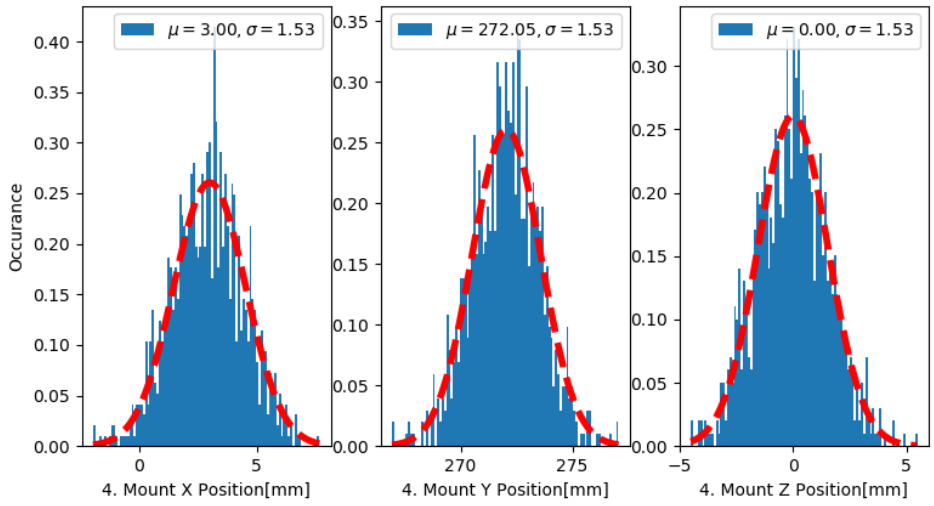

Figure 7.21. 4th Mount Installation Position Simulation

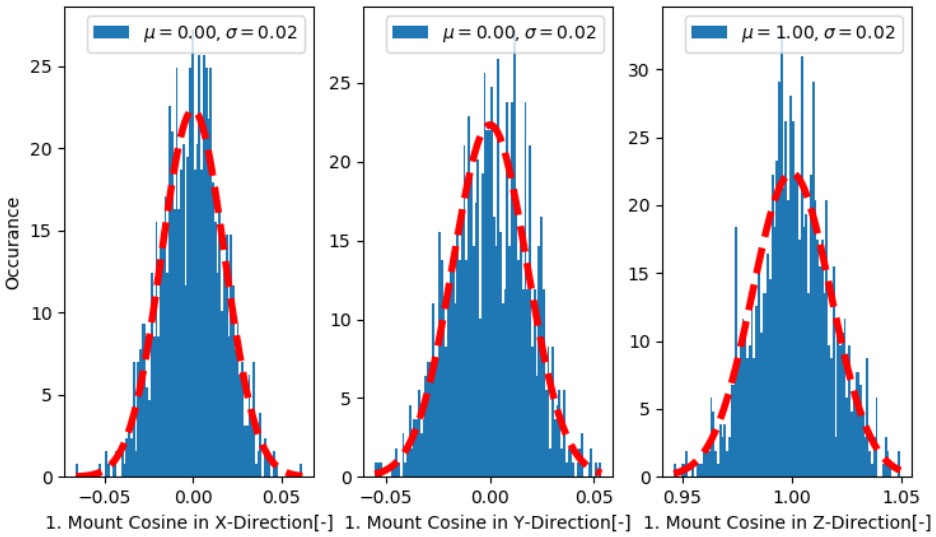

Figure 7.22. 1st Mount Installation Orientation Simulation

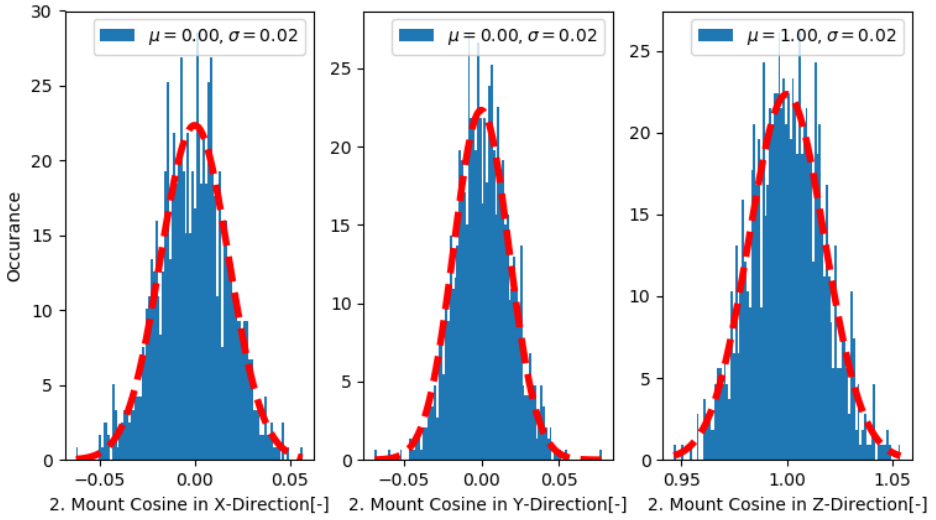

Figure 7.23. 2nd Mount Installation Orientation Simulation

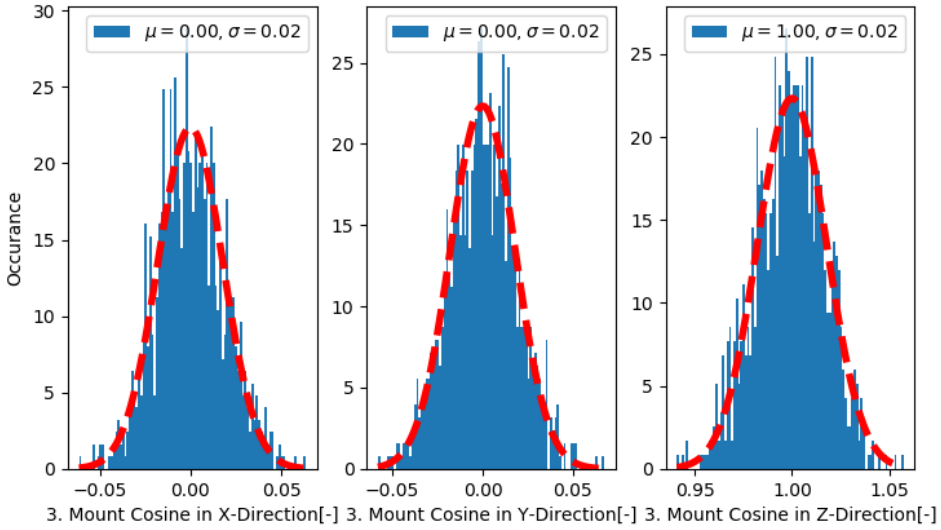

Figure 7.24. 3rd Mount Installation Orientation Simulation

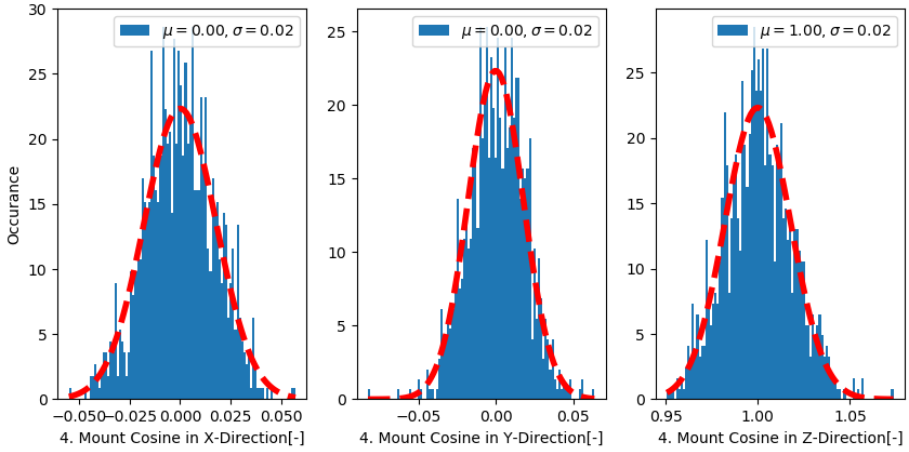

Figure 7.25. 4th Mount Installation Orientation Simulation

Simulation results for the first three natural frequencies, static deflection, dynamic deflection and equivalent acceleration responses are presented in *Table 7.9.*

Minimum and maximum values of each parameter are calculated by removing outliers of the random data according to 2-σ approach. In other words, random values within the probability of 95.45% are considered for each parameter.

Table 7.9. *Simulation of Response Parameters*

Type of Travel	*Nominal*	*Minimum*	*Maximum*
1^{st} f_n *[Hz]*	6.781	6.596	6.949
2^{nd} f_n *[Hz]*	7.224	7.029	7.430
3^{rd} f_n *[Hz]*	13.106	12.781	13.435
Static Deflection *[mm]*	1.952	1.872	**2.052**
Dynamic Deflection *[mm/Hz]*	2.649	2.598	2.699
Maximum Acceleration *[mm/s²/Hz]*	3840.06	3505.80	4103.89
Equivalent Acceleration RMS *[mm/s²]*	9132.62	8908.584	9349.353

Simulation histories of parameters are shown from *Figure 7.26* to *Figure 7.30*. The random data that is observed in the figures are handled by calculating the mean and standard deviation values. Once the outliers are removed from the system response data, the rest offers reasonable results and signifies a robust solution sequence.

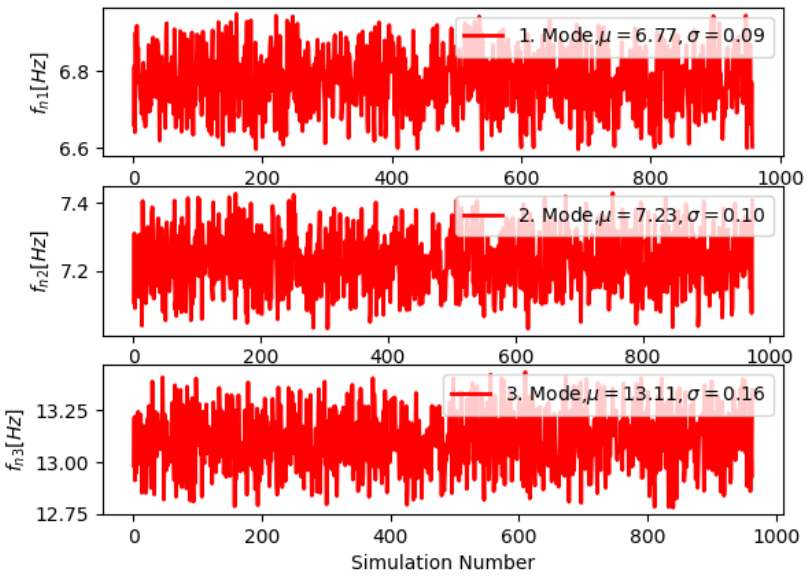

Figure 7.26. Simulation History of Natural Frequencies

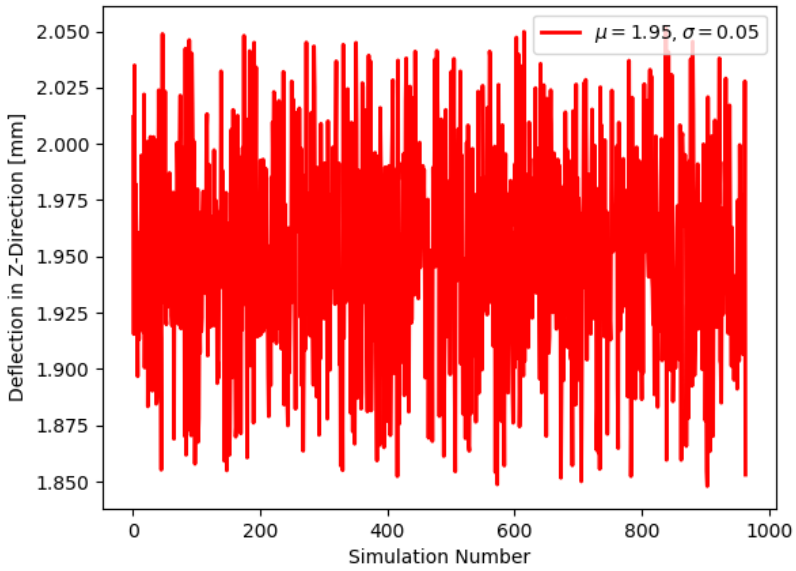

Figure 7.27. Simulation History of Static Deflection

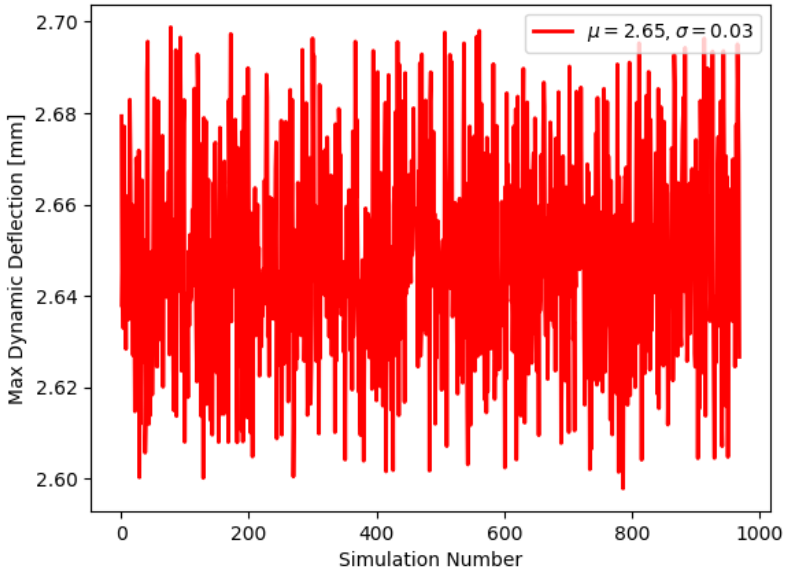

Figure 7.28. Simulation History of Maximum Dynamic Deflection

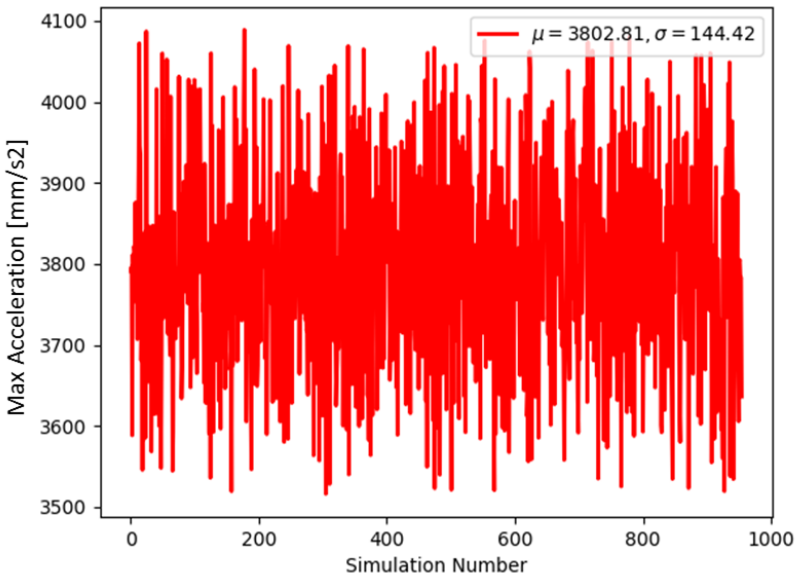

Figure 7.29. Simulation History of Maximum Acceleration

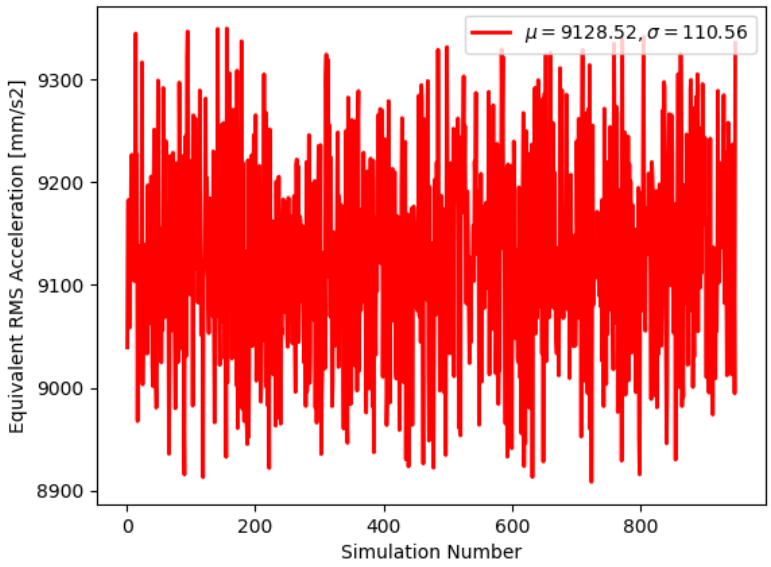

Figure 7.30. Simulation History of Equivalent RMS Acceleration Response

Simulation results show that lower and upper limits of the response parameters, which are provided in the optimization problem, are satisfied except the maximum static displacement. These results have been obtained for pre-determined deviation amounts of system spatial properties. The designer must consider the violation of the design limits according to the simulation results. Therefore, provided bounds to the optimization problem may be stricter than the desired limits to tolerate the extension of results due to the possible deviations.

CHAPTER 8

CONCLUSION

Protection of airborne electronics from severe vibration environment has been a critical issue over years. It has an importance to sustain the functionality of these avionics to ensure the safety of the flight. For this purpose, isolation system design has been drawing attention. During the design of isolation system high performance is intended by taking all essential considerations into account.

In this thesis, literature is reviewed for isolation system design studies after discussing different types of isolation practices. Design studies of isolation system involves a wide range of issues. Namely, the mount characterization, flexibility effects of foundation, mount representation, different degrees-of-freedom are some of these issues. Thus, isolation system design has been considered in distinctive aspects and requirements throughout the years.

In this study, a computer code in an open-software environment Python is aimed to be developed to consist all the required analyses for the isolation system design. At the very beginning, a mathematical model is created with pre-determined spatial values. Vibration analysis, optimization analysis and uncertainty simulation are performed by using the mathematical model to achieve a complete theoretical design. Developed computer code is composed of these analysis procedures and a GUI is also developed to give the opportunity of convenient use.

Mathematical model is verified through created FE model in Nastran®. Results of normal modes analysis and frequency response analysis are compared to verify the theoretical model. It is also worth noting that FE model is previously checked if the model is created properly by comparing its natural frequency results with those from a referred study in the literature. After demonstrating the agreement with the FE model

and theoretical model results, optimization and uncertainty simulation analyses are implemented subsequently.

In the optimization analysis, design objective is selected as the equivalent acceleration response of the system at the center-of-gravity. Equivalent acceleration is calculated by considering that the effect of the response in each translational direction is equally weighted. Design variables are selected as the damping ratio, axial and radial stiffness of the resilient elements. Acceleration response is tried to be minimized by varying these design variables. During the search for optimum, design constraints are also considered. They are imposed to the optimization problem to end up with a reasonable design. For this purpose, minimum natural frequency, maximum static and dynamic displacement, maximum acceleration, minimum and maximum axial-to-radial stiffness ratio are enforced to the optimization process.

Spatial properties as results of the optimization problem become the recent nominal values for the system design. However, all the spatial properties of resilient elements are simulated in terms of possible deviations from nominal values. Output parameters of the simulation are determined as the limiting parameters of the optimization problem. Hence, they may be controlled if the pre-employed limits are violated according to the simulation results. Designer should take the necessary measures considering the violations e.g. by repeating the analyses with stricter limits.

A case study is implemented to demonstrate the application of the analysis processes on an isolation system of common installation arrangement. All the steps of the isolation system design from the generation of spatial properties to the elimination of outliers in the uncertainty simulation results are applied during the demonstration study.

As feature studies, it is possible to mention variety of improvements. Some prominent improvements will be mentioned here. Considering the order of steps in the design process, representation of the mathematical model is touched on at first. In this study, the Voight model is employed to represent the resilient element behavior. Beside the

type of the elastic model, the characterization of the resilient element is also significant. Dependence of the stiffness and damping on the temperature, frequency and pre-loading may be investigated. In this way, more representative models may be used for improved design. Only the mass of the isolated equipment is considered in this study. Mass values of the resilient elements may be involved in the system equations of motion.

In the optimization problem, stiffness and damping are taken as the design variables. Installation position and orientation may be included in the optimization process. Thereby, all the spatial properties of the resilient elements are covered during the search for optimum. Constraint parameters may also be improved or varied depending on the application.

REFERENCES

[1] Agnes, G. S., Whitehouse, S. R. and Mackaman, J. R. 1993. Vibration attenuation of aircraft structures utilizing active materials. SPIE, 1917 Smart Structures and Intelligent Systems.

[2] Ahmadian, M. and Ahn, Y. K. 1999. Performance analysis of magneto-rheological mounts. Journal of Intelligent Material Systems and Structures. 10(3), 248-256.

[3] Alkhatip, F. 2013. Techniques for engine mount modeling and optimization. Theses and Dissertations (344). Mechanical Engineering Department, University of Wisconsin-Milwaukee, Wisconsin.

[4] Ashrafiuon, H. 1993. Design optimization of aircraft engine-mount systems. Journal of Vibration and Acoustics. 115(4), 463-467.

[5] Baytemir, O. Y. 2013. Development of a passive vibration isolation analysis and optimization software for mechanical systems. Mechanical Engineering Department, METU, Ankara.

[6] Belegundu, A. D. and Tirupathi, R. 1999. Optimization concepts and applications in engineering. Prentice Hall.

[7] Chen, Y., Fang, B., Yang, T. and Huang, W. 2009. Study of whole-spacecraft vibration isolators based on reliability method. Chinese Journal of Aeronautics. 22(2), 153-159.

[8] Cho, S. 2000. Configuration and sizing design optimization of powertrain mounting systems. International Journal of Vehicle Design. 24(1), 34-47.

[9] Christensen, P. W. and Klarbring, A. 2008. An introduction to structural optimization. Springer, Berlin.

[10] Cinarel, D. 2012.Vibration isolation of inertial measurement unit. Mechanical Engineering Department, METU, Ankara.

[11] Daley, S., Hätönen, J. and Owens, D. H. 2006. Active vibration isolation in a smart spring mount using a repetitive control approach. Control Engineering Practice. 14(9), 991-997.

[12] De Silva, C. W. 2005. Vibration and Shock Handbook. Taylor & Francis.

[13] De Pasquale, G. and Somà, A. 2010. Reliability testing procedure for MEMS IMUs applied to vibrating environments. Sensors. 10, 456-474.

[14] De Weck, O. 2005. Engineering design and rapid prototyping-design optimization. Lecture Notes. MIT, Massachusetts.

[15] Dreher, J. 1982. Aircraft equipment random vibration test criteria based on vibrations induced by turbulent airflow across aircraft external surfaces. DTIC.

[16] Du, Y. 2003. Internal resonances in vibration isolators and their control using passive and hybrid dynamic vibration absorbers. Mechanical Engineering, Virginia Tech, Blacksburg.

[17] Ellison, J., Ahmadi, G. and Kehoe, M. 2001. Passive vibration control of airborne equipment using a circular steel ring. Journal of Sound and Vibration. 246(1), 1-28.

[18] Environmental Engineering Considerations and Laboratory Tests 2008. MIL-STD-810G. The US Department of Defense.

[19] Harmoko, H., Yap, F. F., Vahdati, N. and Li, C. 2009. Design and analysis of shock and random vibration isolation of operating hard disk drive in harsh environment. Shock and Vibration. 16, 143-154.

[20] Hall, P. S. 1980. Vibration test level criteria for aircraft equipment. DTIC.

[21] Haupt, R. 1995. Comparison between genetic and gradient-based optimization algorithms for solving electromagnetics problems. IEEE Transactions on Magnetics. 31(3).

[22] He, J. 2001. Modal analysis. Butterworth Heinemann.

[23] Hilgers, A. and Boersma, BJ. 2001. Optimization of turbulent jet mixing. Fluid. Dynamics Research. 29(6), 345-368.

[24] Hosseinloo, A. H., and Yap, F. F. 2011. A new passive vibration isolator design for random base excitations in zero and non-zero g-loading situations. Defense Science Research Conference and Expo.

[25] John, R. A. and Straneva, E. J. 1966. A new generation of general aircraft engine mountings. SAE Technical Paper 840259.

[26] Kenney, J. F. and Keeping, E. S. 1939. Mathematics of statistics Part I. Chapman & Hall. 225-227.

[27] Mainardi, F. and Spada, G. 2011. Creep, Relaxation and Viscosity Properties for Basic Fractional Models in Rheology. The European Physical Journal Special Topics.

[28] Miller, L. R., Ahmadian, M., Nobles, C. M. and Swanson, D. A. 1995. Modeling and performance of an experimental active vibration isolator. Journal of Vibration and Acoustics. 117(3), 272-278.

[29] Nack, W. V. 1984. Optimization for vibration isolation. DTIC.

[30] MSC Nastran 2017, Design sensitivity and optimization user's guide. MSC Software Corporation, Los Angeles.

[31] MSC Nastran 2018, Quick reference guide. MSC Software Corporation, Los Angeles.

[32] Otamendi J. 2004. The importance of the objective function definition and evaluation in the performance of the search algorithms. Proceedings of the 16th European Simulation Symposium. Budapest, Hungary.

[33] Peng, Z. K. and Lang, Z. Q. 2008. The effects of nonlinearity on the output frequency response of a passive engine mount. Journal of Sound and Vibration. 318(1-2), 313-328.

[34] Piersol, A. G. and Paez, T. L. 2010. Harris' shock and vibration handbook. McGraw-Hill.

[35] Ponslet, E. R. and Eldred, M. S. 1996. Report SAND96-1169: Discrete optimization of isolator locations for vibration isolation systems: An analytical and experimental investigation. Sandia National Laboratories.

[36] Rivin, E. I. 2003. Passive vibration isolation. ASME Press.

[37] Roush, M. L. and Webb, W. 2006. Applied reliability engineering Volume I, Center for Reliability Engineering, University of Maryland, Maryland.

[38] Roylance, D. 2001. Report: Engineering Viscoelasticity, Department of Material Science and Engineering, Massachusetts Institute of Technology, Cambridge.

[39] Royston, T. J. and Singh, R. 1996. Optimization of passive and active non-linear vibration mounting systems based on vibratory power transmission. Journal of Sound and Vibration. 194(3), 295-316.

[40] Sciulli, D. 1997. Dynamics and control for vibration isolation design. Engineering Mechanics, Virginia Tech, Blacksburg.

[41] Sen, D. T. and Vinh, T. C. 2016. Determination of added mass and inertia moment of marine ships moving in 6 degrees of freedom. International Journal of Transportation Engineering and Technology. 2(1), 8-4.

[42] Smollen, L. E. 1966. Generalized matrix method for the design and analysis of vibration-isolation systems. The Journal of the Acoustical Society of America. 40(1), 195.

[43] Song, C. Y. 2006. Design optimization and development of vibration analysis program for engine mount system.

[44] Southern, B. M. 2008. Design and characterization of tunable magneto-rheological design and characterization of tunable magneto-rheological fluid-elastic mounts. Mechanical Engineering, Virginia Tech, Blacksburg.

[45] Spiller, W. R. and MacBain, K. M. 2009. Structural optimization. Springer, Berlin.

[46] Steinberg, D. S. 2000. Vibration analysis for electronic equipment. John Wiley and Sons, Inc.

[47] Swanson, D. A. and Wu, H. T. 1993. Optimization of aircraft engine suspension systems. Journal of Aircraft. 30(6), 979-984.

[48] Swanson, D. A. 1993. Active engine mounts for vehicles. SAE Technical Paper 932432.

[49] Snyman, J. A., Heyns, P. S. and Vermeulen, P. J. 1995. Vibration Isolation of a mounted engine through optimization. Mechanism and Machine Theory. 30(1), 109-118.

[50] Sjöberg, M. 2002. On dynamic properties of rubber isolators. Vehicle Engineering, KTH, Stockholm.

[51] Tao, J. S., Liu, G. R. and Lam, K. Y. 2000. Design optimization of marine engine-mount system. Journal of Sound and Vibration. 235(3), 477-494.

[52] Tarrago, M. J. G., Negrete, N. G. and Vinolas, J. 2009. Viscoelastic models for rubber mounts: Influence on the dynamic behaviour of an elastomeric isolated system. International Journal of Vehicle Design. 49(4), 303.

[53] Turkucu, T. 2013. Manyeto-reolojik akışkanlı motor takozu tasarımı ve karakteristiğinin belirlenmesi. Mechanical Engineering, Gazi University, Ankara.

[54] UNITRONIX, Military and Maritime - Aircraft Systems, https://www.unitronix.com.au/product-fit/military-and-maritime/aircraft-systems/#. [Date accessed August 18, 2019].

[55] Vane, F. F. 1958. Report 880 NAVSHIPS-713-017: A guide for the selection and application of resilient mountings to shipboard equipment. U.S. Navy.

[56] Veprik, A. M. 2002. Vibration protection of critical components of electronic equipment in harsh environmental conditions. Journal of Sound and Vibration. 259(1), 161-175.

[57] Vijayakumar, M. P., Ashwin, U. and Raja, S. 2014. Active vibration control of engine mount system of transport aircraft using PZT stack actuators. Journal of Mechatronics. 2(3), 226-23.

[58] Yang, C. Y. 1985. Random vibration of structures. John Wiley & Sons.

[59] Zhang, J. and Richards, C. M. 2007. Parameter identification of analytical and experimental rubber isolators represented by Maxwell models. Mechanical Systems and Signal Processing. 21(7), 2814-2832.

[60] Zhang, Y. W., Fang, B. and Zang, J. 2015. Dynamic features of passive whole-spacecraft vibration isolation platform based on non-probabilistic reliability. Journal of Vibration and Control. 2(1), 60-67.

APPENDICES

A. GUI of Developed Computer Code

GUI is composed of three main sections:

Section for the definition of spatial properties
Section for the preparation of the optimization problem
Section for the setup of the uncertainty simulation parameters

In the first section, job name and description are optionally required for convenience. Furthermore

i **Mass**
ii **Geometric Shape** may be either point or other basic shapes such as cube. This option is provided for automatic calculation of mass moment of inertia.
iii **Geometric Dimensions** if (ii) exists.
iv **CG**
    a. *At Centroid* is available if (ii) exists
v **Inertia Tensor**
    a. *Automatic Calculation* is available if (ii) exists
vi **Isolator Connection** requires position and orientation of each single isolator.
    a. *Natural Coord* option is available if (ii) exists
    b. List button enables checking and modifying added isolators
vii **Elastic Properties** can be entered separately for each single isolator previously added.

History window at the bottom enables following the taken actions on the window.

Figure A.1. GUI Overview I

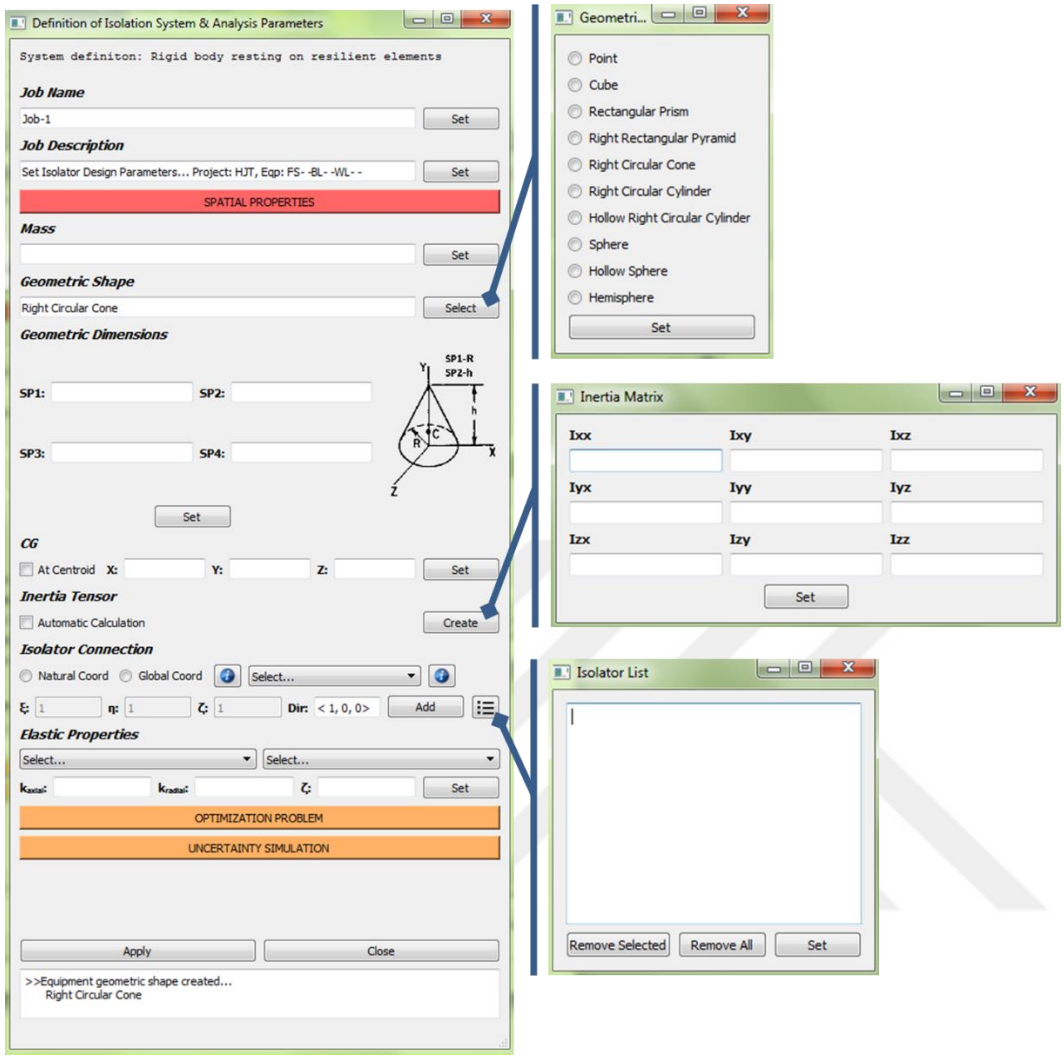

Side window for **Optimization Problem** requires initial value, lower bound and upper bound values of the design variables. Besides, minimum and maximum limits of the design constraints are also requested. Design objective has three options as acceleration, velocity and displacement to be selected.

Figure A.2. GUI Overview II

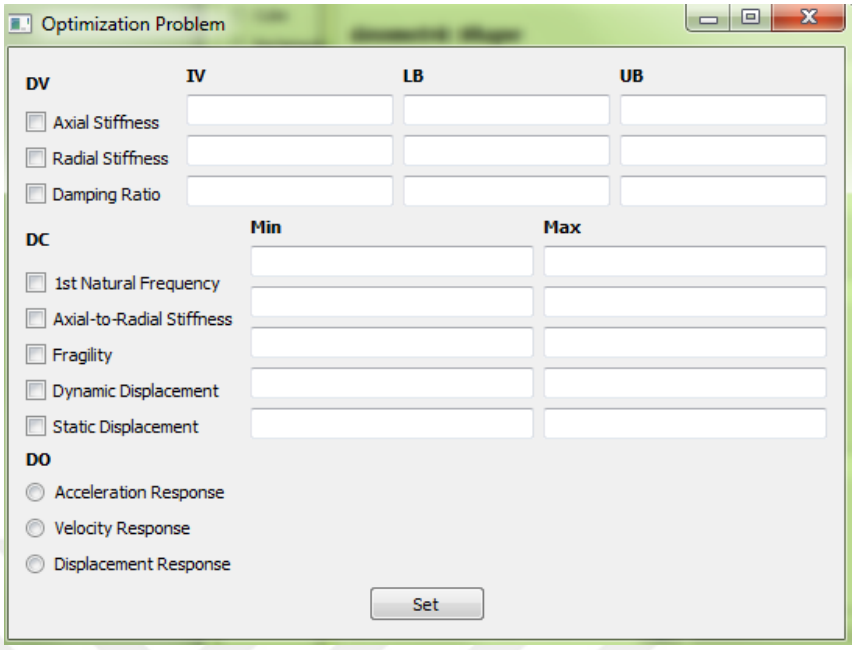

Side window for **Uncertainty Simulation** requires deviation amount, distribution type and confidence interval for each single input parameters. For output parameters, extraction method e.g. 1-Sigma, etc. is requested separately.

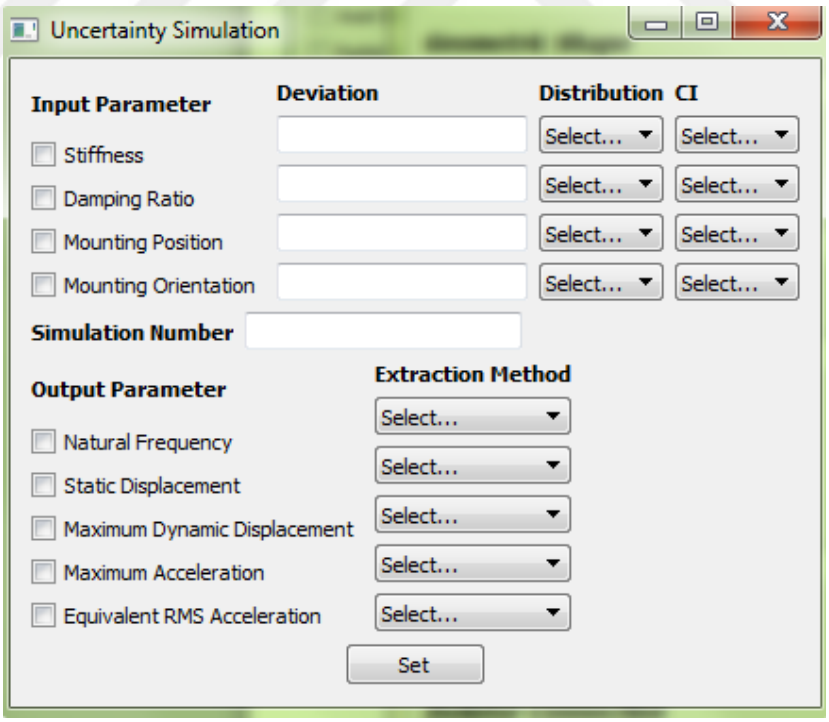

Figure A.3. GUI Overview III